ISBN 978-83-68188-49-3

Mirian Getsadze

# THE ROLE OF MODERN RADIOLOGICAL IMAGING

## IN THE DIAGNOSIS OF ORBITAL TUMORS

iScience
Warsaw, Poland - 2026

**Mirian Getsadze**

# THE ROLE OF MODERN RADIOLOGICAL IMAGING IN THE DIAGNOSIS OF ORBITAL TUMORS

**MONOGRAPH**

**iScience**
**Warsaw, Poland - 2026**

This work is devoted to studying the enhancement of diagnostic and differential diagnostic effectiveness of orbital and ocular neoplasms through the complex application of modern instrumental-diagnostic methods.

The monograph discusses the main instrumental methods of research – orbital ultrasonography, computed tomography (CT), and magnetic resonance imaging (MRI) – which make it possible to determine the size and spread of tumors, as well as to assess the soft tissues and bony structures of the orbit.

The monograph is intended for physicians working in the field of radiology, as well as medical Bachelor and Master students.

**Reviewer**: Sofio Chedia, Doctor of Medicine

**ISBN 978-83-68188-49-3**

## INTRODUCTION

Ophthalmo-oncology is one of the most complex and challenging directions in ophthalmology. Recently, there has been a confirmed increasing frequency in the diagnosis of eye socket and orbital neoplasms, which is undoubtedly due to the accessibility of primary healthcare sector and the growing availability of instrumental diagnostic capabilities. The active clinical integration of high-tech radiological methods has largely contributed to the timely diagnosis of these types of pathologies and highlighted their role both in treatment planning and monitoring outcomes. Considering the above, the study of functional and radiological anatomy of the eye socket and orbit, and the importance of interpreting ultrasound, computed tomography, and magnetic resonance imaging has gained even higher relevance in ophthalmo-oncology.

The difficulty in diagnosing orbital tumors is caused by the diversity of pathological processes in the orbit and the significant polymorphism of tumor types. The term “orbital tumor” is understood as a conditional clinical-anatomical combination of tumor tissue components that differ in structure, histogenesis, and function.

Among the variety of orbital tumors, two main groups are distinguished: primary and secondary neoplasms. Primary tumors include vascular maltumors, various types of cystic tumors, melanomas, retinoblastomas, carcinomas, sarcomas, neurogenic type tumors, and others. The main source of secondary tumors is hematogenous spread from the primary focus or direct extension from adjacent anatomical regions.

The complex arrangement and diversity of anatomical structures in the orbit (eye socket, optic nerve, muscular apparatus, major blood vessels and their branches), as well as close anatomical connection with the nasal cavity and paranasal sinuses, often complicates diagnosis and correct interpretation of results.

The spread of a tumor in the orbit, especially in its central parts, can cause significant and in some cases irreversible consequences for the patient - from cosmetic defects to complete blindness. The close anatomical connection with brain structures makes it possible for the process to spread to the structures of the central nervous system, disrupting its function and anatomical integrity. In cases of infiltrative growth of malignant orbital tumors, the spread of the process, both direct and hematogenous or perineural growth, makes the importance of early diagnosis of these types of pathologies even more evident. The difficulties in differential diagnosis of orbital tumors are due to the large number of nosological forms and their variants, similarity of clinical picture, and difficulty in interpreting instrumental research

methods, which necessitates a comprehensive examination of the patient for final diagnosis.

The development of radiological diagnosis for orbital tumors has led to the sequential use of methods such as X-ray diagnostics (including angiography), ultrasound examination, computed tomography (CT), and magnetic resonance imaging (MRI). The advantage of ultrasound diagnostic method is its minimal invasiveness, financial accessibility, and limited list of contraindications. The results of ultrasonographic studies of orbital tumors are mainly found in publications dedicated to using gray-scale scanning in differential diagnosis of orbital space-occupying processes; individual studies reflect the acoustic semiotics of benign and malignant orbital tumors.

The main instrumental research methods are orbital computed tomography (CT) and magnetic resonance imaging (MRI), which make it possible to determine the size and extent of the tumor, as well as assess the soft tissues and bone structures of the orbit. Computed tomography is associated with radiation exposure and has specific contraindications, which in rare cases limits the use of this modality.

Computed tomography visualizes changes in bone structure in detail and characterizes inclusions of different densities in the tumor with high specificity. However, the boundaries of the soft tissue component, especially in cases of infiltrative growth, are not always clearly defined.

Magnetic resonance imaging (MRI), due to its high contrast resolution, allows visualization of the tumor's soft tissue and cystic components. In addition to the absence of ionizing radiation and the ability to obtain images in different planes, MRI can show the condition of the optic nerve, extraocular muscles, orbital tissue, and eye socket, as well as extraorbital spread of the process and the presence of associated vascular pathology. It is worth considering MRI's capabilities in imaging cellular matrix and morpho-chemical features of the tumor, which emphasizes the uniqueness of this research method. The disadvantages of the method can be considered the duration of the examination and relatively low accessibility, as MRI remains an expensive examination method and is unavailable in some medical institutions.

Thus, the above has determined the relevance of the problem and the expediency of studying the possibilities of complex use of radiological diagnostic methods in the diagnosis, differential diagnosis, and assessment of the extent of orbital tumors.

The aim of the presented work is to increase the effectiveness of diagnosis and differential diagnosis of eye socket and orbital neoplasms based on the complex use of modern instrumental diagnostic research methods.

## CHAPTER 1. SOME FEATURES OF EYE AND EYELID TUMORS

Ophthalmo-oncology remains one of the most challenging directions in ophthalmology. Recent years have shown a trend toward increasing incidence, largely due to the wide growth in availability and accessibility of early instrumental diagnostic capabilities. Statistical data from various literary sources are, in some cases, contradictory. According to 2007 data, tumors of the visual organ account for 0.1% of all oncological diseases and 18% of all orbital diseases [160]. A census conducted in the United States population between 1973-2009 showed a total of 2802 patients with malignant orbital tumors, with an overall rate of 3.39 cases per 1 million inhabitants. Taking into account age groups, the highest proportion of malignant tumors—9.51 cases per 1 million inhabitants—occurs in the population aged ≥50 years. In patients aged 0-19 years, the corresponding rate is 0.56 cases per 1 million inhabitants. The growth and diversity of oncological pathologies in ophthalmo-oncology have created a demand for differential diagnostics aimed at early detection of individual types of tumors and selection of appropriate treatment tactics [134].

The anatomical and topographical features of the orbital structure stem from its close connection with cranial structures and paranasal sinuses, which creates a risk of possible spread of inflammatory and tumor processes from these areas to the orbit and retrograde. The difficulty in diagnosing orbital pathology is related not only to its anatomical structure but also to the similarity of clinical symptoms of many diseases of different etiologies (tumor, inflammatory, vascular, endocrine). Considering the aforementioned reasons, early detection and differentiation of orbital tumors and tumor- like tumors remains one of the significant challenges in diagnostic radiology [122, 145].

Tumors of the visual organ are characterized by pronounced polymorphism, which is due to the histological diversity of structures present in the orbit. Almost all types of neoplasms described in humans can be found in the orbit [57]. A retrospective study involving 2,480 patients with orbital tumors morphologically and histologically verified a 68% prevalence of benign tumors, among which dermoid cysts (14%) and cavernous hemangiomas (9%) occupied leading positions [153].

Eye socket tumors rank second among visual organ neoplasms (after eyelid neoplasms), with more than 2/3 being choroidal tumors. One of the most common malignant tumors of the eye socket, which is dangerous not only for visual functions but also for the patient's life, is uveal or intraocular melanoma. Intraocular melanoma accounts for up to 3-5% of all melanomas

and predominantly originates from choroidal melanocytes (85-90%). The peak of diagnosis occurs in the 70-79 age group. From a gender perspective, choroidal melanoma is 30% more common in men than in the opposite sex. In the United States, the overall rate of orbital melanomas is approximately 5 cases per 1 million inhabitants. Statistical data in Europe are somewhat different. In Italy and Spain, this number equals 2 per 1 million inhabitants, 6 in Central Europe, and 8 in Denmark and Norway [13, 37, 61, 124, 22].

There is global statistics on errors in the diagnosis of intraocular tumors, which is especially numerous for uveal melanomas, testifying to significant difficulties facing ophthalmology. According to some authors, the frequency of undiagnosed cases of choroidal melanoma, detected by histological examination of the enucleated eye, ranges from 3.6 to 12% [103, 144]. Such a large percentage of diagnosed melanomas is explained by the diversity of clinical symptoms of the disease and, in some cases (especially in unpigmented melanomas), an atypical radiological picture.

In ophthalmological practice, differential diagnosis of orbital tumors, as well as intraocular neoplasms, remains one of the most responsible procedures. Regardless of the nature of the pathological process, orbital neoplasms often cause loss of visual function and patient disability. Loss of visual function during benign tumors and the threat to the patient's life in cases of malignant tumors of the orbit and eye socket explain the medical and social importance of early diagnosis and timely treatment measures.

Visual examination of the patient is of great importance in diagnosing many diseases of the visual organ to establish the correct diagnosis. However, this way it is only possible to assess the condition of the eyelids, conjunctiva, anterior segment of the eye, and fundus. Determining changes in the inner membranes of the eye, as well as in the orbital structures behind the eye socket, is usually impossible.

The main group of orbital tumors consists of benign neoplasms. In the adult population, gender polymorphism of the total cases of benign tumors is not observed, although some subtypes, such as cavernous hemangioma, meningiomas of the optic nerve and the main bone wing, are more common in women. Geography and race are not currently considered risk factors for benign orbital tumors [155, 136, 119].

Benign tumors are predominantly localized in the upper lateral quadrant. Various authors believe that the proportion of malignant tumors is highest in tumors localized in the inner lower quadrant. Additionally, it should be noted that dermoid cysts are predominantly found in the upper lateral quadrant, while mucoceles are found in the upper-medial quadrant.

Cavernous hemangiomas are most often localized in the lower outer quadrant, and basal cell epitheliomas in the lower inner quadrant [22].

Another group that does not represent true neoplasms, but clinically and radiologically often presents signs similar to orbital tumors, is known as pseudotumorous diseases. These nosologies can be conditionally divided into two main groups: inflammatory and infectious pathologies. Among infectious diseases, orbital cellulitis, orbital tuberculosis, orbital sarcoidosis, histoplasmosis, mucormycosis, and others are notable. Equally diverse is the group of inflammatory diseases, which includes the relatively common thyroid ophthalmopathy, idiopathic orbital inflammation, IgG4-associated inflammation, giant cell myositis, optic neuritis, and others. These diseases unconditionally present a differential diagnostic dilemma, both at the clinical and instrumental examination stages. It is important to consider the use of specific diagnostic algorithms for these pathological conditions, which fundamentally differ from the diagnosis of true neoplasms and therefore necessarily require correct pre-interventional diagnostics [79, 80].

Dermoid cyst is a congenital, benign tumor whose development is associated with disruption of blasto- and embryogenesis. Considering the etiological factor, orbital dermoid cysts are predominantly found in the pediatric population and are often located along suture lines. Taking into account localization, superficial and deep dermoid cysts are distinguished [90, 103]. In the case of the superficial type, the tumor is easily noticeable by ophthalmological inspection and is mainly diagnosed before the age of 4, while deep dermoid cysts have a subclinical course and are diagnosed only when a compressive process is initiated in middle-aged patients [147].

Orbital cavernous hemangiomas constitute from 4.5% to 7.4% of primary and secondary orbital tumors. The age of symptom manifestation is the fourth and fifth decades of life. From a pathophysiological perspective, orbital cavernous hemangioma is a slow-growing tumor that does not produce clinical symptoms for an extended period [21, 72]. The preferred anatomical localization is the intraconal space, which causes progressive proptosis, the most common clinical sign of orbital cavernous hemangioma. It is predominantly at this stage that various instrumental diagnostic methods are involved in verifying this disease and planning further treatment [67].

Meningiomas originating from the sheath of the optic nerve belong to slow-growing, benign neoplasms. Their intraocular localization and direct connection to optical structures, considering the possibility of inducing severe deterioration or complete loss of vision and the difficulties of treatment, make the diagnosis of this tumor a crucial part of modern ophthalmoradiology [111].

Another type of meningioma that often manifests with extension into the eye socket is known as sphenoid-orbital meningiomas. Sphenoid-orbital meningiomas constitute only 2-9% of intracranial meningiomas. Like meningiomas in other anatomical regions, their two main morphological components are: intraosseous growth secondarily provoked by hyperostosis and intradural or soft tissue component [91, 93]. Despite their benign morphological nature, sphenoid-orbital meningiomas belong to locally aggressive tumors and over time often cause mass effect and compression of orbital structures. According to the degree of damage to the visual analyzer and orbital structures, a triad of clinical symptoms is distinguished: proptosis, visual impairment, and eye movement defects [139, 146]. Considering the infiltrative-compressive growth, proper radiological assessment represents the most important pre-therapeutic method for determining the boundaries and tactics of targeted surgical resection.

Orbital schwannomas constitute a small portion of tumors of this localization. From a histomorphological perspective, orbital schwannomas are slow-growing tumors that form as a result of hyperplasia of Schwann cells in the perineurium of peripheral nerves. The total percentage of these types of tumors in orbital tumors is 1%. Despite not knowing the exact etiological mechanism, there is speculation about the role of losing the tumor suppression gene 17q11.2 in the process of Schwann cell hyperplasia, as described in type I neurofibromatosis [38]. Given the close connection to the optic nerve, it is important to conduct magnetic resonance imaging differential diagnostics with meningiomas of the same region's optic nerve and sphenoid-orbital localization [28, 29].

Among neurogenic type tumors, optic nerve gliomas and paragangliomas should be noted, which despite a high degree of differentiation, considering the high probability of potential malignancy, will be discussed in the group of malignant tumors of the eye and orbit.

Another group of benign orbital tumors, whose initial cellular etiology is bone and fibrous component, includes fibrous dysplasia, osteoma, non-ossifying fibroma, chondroma, and giant cell granuloma. It should be noted that the total number of tumors in this group constitutes no more than 2% of orbital tumors [153, 77]. Tumors of this group are not characterized by metastatic progression, but considering their locally aggressive nature (fibrous dysplasia), detumor of orbital bone structures, secondary compression on the optic nerve, and other structures of the optical analyzer are common. Instrumental diagnostics, in most cases, is not a problem, and considering the remodeling of bone structure and the bone

matrix of the tumor, computed tomography is the method of choice for diagnosis [38, 82, 99].

Dermolipomas and lipomas constitute 3% of orbital tumors. Dermolipomas are mainly unilateral, and most patients are from the young population [94]. Despite their benign nature, it is important to differentiate these nosologies both from each other and from orbital fat prolapse, since orbital lipomas are resected completely, while surgical treatment of dermolipomas is conservative and subject only to partial surgical resection [147, 143, 3].

Among tumors of lymphoid origin in the group of benign orbital tumors, benign reactive lymphoid hyperplasia is distinguished by frequency. Histologically, benign reactive lymphoid hyperplasia is a borderline condition between inflammatory and neoplastic processes, characterized by slow proliferation of lymphocytes [127]. From a radiological point of view, it is important when interpreting this disease to clearly differentiate it from other aggressive diseases of lymphogenic genesis, such as atypical lymphoid hyperplasia and lymphoma [127].

In modern radiological and ophthalmological practice, the division of malignant orbital tumors is based on their primary or secondary genesis of origin and the method of anatomical arrangement relative to intraorbital structures. Among intraocular malignant tumors, retinoblastoma takes a leading place in the pediatric population [40, 49]. The overall rate of diagnosis of patients with retinoblastoma before the age of 5 reaches 95% [55]. In 40% of cases, retinoblastoma manifests as a bilateral tumor. In case of bilateral manifestation, a genetic mutation factor should be considered [55]. In the case of unilateral retinoblastoma, the percentage of mutation is 15%. In view of this, the nosology should be divided into hereditary and sporadic forms [55].

Despite the aggressive nature of this tumor's growth, the overall recovery rate is very high (>95%). However, the prognostic indicators for metastasized retinoblastoma are unfavorable [52, 69]. Magnetic resonance imaging with intravenous contrast is considered the gold standard of diagnosis for assessing extraconal spread and possible optic nerve infiltration [58, 70].

Unlike the pediatric population, in adult patients, uveal melanoma is the leading malignant intraocular tumor, accounting for 85% of all intraocular melanomas. 5% are conjunctival melanomas and 10% are melanomas originating from other anatomical regions [133, 120]. Unlike skin melanoma, which originates from melanocytes in the basal layer of the epidermis, uveal melanomas grow from melanocytes of the uveal tract and 85-90% of cases

are localized in the choroid. It should be noted that large melanomas cover several parts of the iris [106, 39]. Given the anatomical peculiarity of poor lymphatic drainage in these areas, metastasis of uveal melanoma mainly occurs through local spread or hematogenous routes. The overall metastasis rate is 50%, of which 90% occur in the liver [109, 131].

Malignant lymphoma plays a leading role among extraocular tumors. Primary orbital lymphomas form as a result of metaplasia of mucosa-associated lymphoid tissue. The presence of an orbital component during systemic lymphomas, as a manifestation of systemic lymphoma, occurs in 1.5-5% of cases [33]. Radiological manifestation of lymphoma may include a unilateral orbital well-contrasting mass, as well as bilateral tumors of similar structure (Mantle cell Lymphoma) [138].

Neoplastic diseases of lacrimal glands are quite polymorphic. The degree of metaplasia of primary tumors can range from benign epithelial tumors to squamous cell carcinoma. Among malignant tumors of the lacrimal gland, adenoid cystic carcinomas and squamous cell carcinomas occupy leading positions in frequency. From a radiological point of view, differentiation of lacrimal gland subtypes is difficult and mainly relies on morphological verification of biopsy material. However, timely and detailed multimodal diagnostic assessment of signs characteristic of malignant tumors (invasion into adjacent structures, bone destruction) is crucial for selecting the correct treatment tactics [ 128, 130].

Among neurogenic orbit tumors, in addition to the aforementioned benign processes (optic meningioma, orbital schwannoma, sphenoid-orbital meningioma), optic glioma occupies an intermediate position. This tumor is characterized by a bimodal age distribution. Classic, benign optic glioma is a common pathology in the pediatric population, whereas optic glioma diagnosed in adulthood is characterized by fulminant progression and high mortality [33, 126]. The mention of intraorbital gliomas among malignant tumors is determined not by the degree of differentiation of tumor cells directly, but by their characteristic infiltrative growth tendency, which makes total resection of the tumor practically impossible [32].

A group of intraorbital tumors that do not characteristically affect one specific anatomical area deserves separate mention. The majority of this group is occupied by metastatic processes. Metastatic lesions account for 13% of the total share of orbital tumors [8, 160]. In the presence of a systemic tumor process, the percentage of orbital dissemination ranges from 2 to 5% and is mainly found in advanced cases of systemic disease [138, 158]. Among the frequencies of primary tumor sources that give intraorbital metastases, breast, lung, and prostate tumors lead. It should be noted that of the

mentioned primary tumors, breast cancer occupies a prominently leading position among primary sources of orbital metastases. The main age group for metastatic disease is patients >60 years of age. Clinical symptoms include diplopia (48%), pain (42%), vision loss (30%), and proptosis (63%). In rare cases, strabismus and a palpable mass in the orbit have been described [127, 39].

Rhabdomyosarcomas belong to rare malignant tumors in the pediatric population. 90% of these tumors occur in patients under 16 years of age. The head and neck region, especially the orbital area, are common localization regions for rhabdomyosarcomas (10%). Additionally, involvement of orbital structures is a common phenomenon in nasopharyngeal and paranasal sinus rhabdomyosarcomas, as a result of local dissemination of the process [118, 155].

Despite the diversity in etiology and growth types of primary and secondary orbital tumors, their clinical differentiation is often complicated. Proptosis (exophthalmos) is the most important clinical manifestation that is primarily encountered during orbital tumors, although exophthalmos of the eye socket up to 4mm in size is not clinically diagnosed [150]. Other clinical signs that occur less frequently but raise significant clinical suspicion include: palpable mass, ptosis, erythema, conjunctival edema, limited eye socket movement, diplopia, increased retropulsion, decreased visual acuity, periocular paresthesia and anesthesia (in case of secondary or primary damage to the optic nerve) [135, 114].

Reduction of the differential-diagnostic list is possible through detailed collection of anamnestic data and physical examination. In case of involvement of both orbits, the existence of an inflammatory and systemic neoplastic process is more likely. Diagnostic tests for systemic disease may be negative, as the orbital manifestation may represent the starting sign of the disease. Additionally, serological tests are negative in some cases, as inflammatory markers often mask the main etiological cause. In the case of specific diseases, initial treatment with corticosteroids provides important diagnostic data [108].

Orbital tumors and cysts are characterized by stationary exophthalmos. It can be axial (the line of anterior displacement of the eye is parallel to the visual axis), or with displacement to one side or another. In this case, the direction of eye displacement and the visual axis do not coincide.

Changes in eyelid position (usually ptosis of the upper eyelid) develop as a result of damage to the eye's motor apparatus during orbital tumors.

Inflammatory changes in the skin of the eyelids (hyperemia, swelling) usually accompany the growth of malignant tumors in the orbit and become more pronounced when areas of necrosis appear in the tumors.

Pain occurs in the presence of exophthalmos in the case of rapid growth of a malignant tumor in the orbit. During adenocarcinoma of the lacrimal gland, neuralgic pain in the forehead and orbital area often becomes the reason for a visit to the doctor, which is associated with the involvement of branches of the trigeminal nerve in the process. The symptom of pain may also exist during benign orbital tumors, for example, in the case of optic nerve meningioma. Often, during the above-listed diseases of the orbit, the symptom of pain in patients begins before the appearance of exophthalmos [139, 118].

Diplopia and limited mobility of extraocular muscles are usually mechanical in nature: limited eye movement in the case of orbital tumors is observed only during pronounced exophthalmos. However, malignant tumors can also directly invade nerve fibers and infiltrate and cause dysfunction of one or more extraocular muscles. In such cases, it is difficult to differentiate the neuroparalytic nature of extraocular muscle dysfunction from mechanical. In the case of encapsulated tumors, limitation of movement is always directed toward the direction of tumor location, and it never exceeds half of the full normal range of eye movement. The sudden manifestation of diplopia with limited movement of one or more extraocular muscles is often the first clinical manifestation of metastatic damage in the orbit.

Changes in visual acuity may manifest as pseudo-myopia (during exophthalmos), which is not correctable with glasses. A pathological process at the apex of the orbit always causes persistent unilateral, gradual reduction in vision.

Changes in central and peripheral vision are most characteristic of optic nerve tumors (meningioma, glioma). Based on the nature of defects in the patient's visual field, the level of damage and, consequently, the localization of the tumor causing it can be determined quite accurately. The combination of high visual acuity with peripheral scotoma or loss of peripheral visual field with unilateral exophthalmos is a characteristic sign of optic nerve meningiomas in its orbital segment. The presence of central scotoma in the exophthalmic eye with a sharp decrease in central vision, in both eyes, often indicates an optic chiasm glioma.

Disturbance of corneal sensitivity is more often observed during malignant tumors and orbital schwannomas and is associated with compression of ciliary nerves.

Despite the correlative informativeness of clinical signs for tumors of different origins, the use of additional diagnostic methods, such as radiological diagnostic methods, is justified for differential diagnostics.

According to many authors, radiological diagnostics provide approximately 60-80% of the intumor needed to diagnose a neoplasm of the orbit or eye socket. The most important methods of radiological examination of oncopathology are computed tomography and magnetic resonance imaging.

# CHAPTER 2. ULTRASOUND EXAMINATION OF EYE AND ORBITAL NEOPLASMS

## 2.1. Ultrasound Examination of Tumors

Despite the development of new medical imaging methods, ultrasound examination remains the most practical and frequently used method for assessing eye conditions in practical ophthalmology, as it allows for objective evaluation of intraocular structures. This is particularly relevant when examining the eye socket when the transparency of light-conducting structures is significantly reduced. Ultrasound examination methods are currently considered the most accessible and safe investigations. Such studies must necessarily be conducted with consideration of the biological effects of ultrasound on eye structures. According to many researchers, the use of ultrasonic waves for diagnostic purposes in pulsed mode is completely safe even during prolonged examinations. The ultrasonic impact on eye structures during diagnostic procedures is significantly lower than the therapeutically permissible value (0.3 W/cm²) and constitutes only 2-3 mW/cm².

In ophthalmological practice, high-frequency transducers (7.5-12.5 MHz) are used for ultrasound examinations. After ultrasonic waves pass through the eye structures, part of them is reflected and returns to the emission source as a reflected wave, is converted into an electrical signal, which is then used to form an image. The characteristics of the ultrasound image of eye structures depend on their size, shape, structure, and acoustic resistance. B-scanning devices with digital image processing have high sensitivity and informativeness. They enable reliable assessment of the anterior segment of the eye, determination of the localization, density, and mobility of vitreous opacities, and diagnosis of intraocular hemorrhages, which are extremely difficult to identify using traditional radiation methods. Pathological processes detected by this method are confirmed in 96% of cases according to all anatomical parameters. The use of digital diagnostic technologies has significantly improved the quality of images of objects to be analyzed and eye tissues. It has become possible to visualize small eye structures and simultaneously record static anatomical elements and blood movement. With the help of color and power Doppler mapping for contrasting individual structural elements of the eye socket and orbit, it is possible to differentiate the structure of the choroid and retina, assess the topography of the ophthalmic artery branches, and also identify zones of pathological neovascularization. Two-dimensional echography performed using the B-system (two-dimensional imaging system) allows us to obtain an

acoustic cross-section of the eye in a given scanning plane. Indication is carried out using a CRT, which converts echo signals into video images. During the examination, reflected echo signals are scanned and sequentially recorded, which together form an image of the eye and its structural components in one tomographic plane on the monitor.

G. Baum and I. Greenwald first reported in 1958 about the detection of orbital tumors using the B-scanning method [89]; the diagnosis was confirmed in 80% of patient cases.

Ultrasound examination in B-mode allows for determining the localization of pathological focus, performing morphometry of eye structures and pathological tumors on the orbit, and determining the degree of its spread. Shroeder investigated 155 patients with orbital diseases using two-dimensional echography and obtained data that allowed him to characterize expansive and infiltrative processes in the orbit.

Working in B-mode significantly simplifies the spatial orientation of the tissues under study and provides the possibility of topographical characterization of processes occurring in the orbit. According to many authors, the main sign of a confined volume tumor on the orbit during B-scanning is a contour of various shapes with internal echo signals of different brightness in the corresponding part of the echogram. With rapidly growing solid tumors, pronounced detumor of the eye is observed. Based on the nature of echo signals from the external boundaries of orbital confined volume tumors and from their internal tissue structures, we can distinguish solid, cystic, vascular, and infiltrative types of tumors. An echographically typical example of a cystic tumor is a neuroma, which has a low reflection ability. The tumor is solid and connected to the optic nerve, characterized by slow growth inside the muscular part and causes detumor of the eye socket. In cases of meningioma and optic nerve glioma, an acoustically non-homogeneous sonographic picture is noted, and according to numerous data, the coincidence between sonographic and clinical diagnoses is 68%.

Cavernous hemangioma has a high reflection ability, irregular internal structure, and can cause minor detumor of the eye socket. Orbital sarcoma often does not have clear boundaries, is characterized by very rapid growth, and causes severe detumor of the eye. In addition, small malignant tumors may have a number of signs characteristic of benign neoplasms.

Based on the results of ultrasound examination use in ophthalmology, this method can be highly valued for its diagnostic worth [159]. As K.S. Ossoinig notes, using standardized echography on the orbit makes it possible to detect tumor tissue as small as 3-5mm in size, which indicates the high sensitivity of the method [12].

Many works are devoted to improving ultrasound diagnostic methods for oncological diseases of the eye and orbit. In addition to assessing the size, definition, and area of intraocular neoplasms, echograms can be used to evaluate the structure of the tumor and the condition of the sclera.

Studies conducted in A-mode make it possible to differentiate between various types of orbital tumors and pseudotumors. The diagnosis of vascular tumors of the orbit can be clarified by Doppler studies of blood flow in the orbital arteries; in particular, the literature describes Doppler symptoms of carotid-cavernous anastomosis.

Ultrasound examinations conducted by various authors have shown that pseudotumors of the lacrimal gland occupy an intermediate position between infiltrative and solid tumors in terms of acoustic properties. In more than half of the patients, the “lobular” structure of pseudotumors was revealed in the form of acoustic voids, some of which are characteristic of solid tumors, some of infiltrative ones. This may be caused by varying severity of inflammatory phenomena, the presence of fibrosis and sclerosis of the lacrimal gland tissue.

The choice of ultrasound imaging method depends on the specific objectives of the study. Accordingly, the ultrasound image of the eye received on the screen is edited: the first three-dimensional image of the eye was obtained by summarizing the acoustic sections of the bistable image. Now three-dimensional images are created in the computer's operational memory by direct input of the echo signal.

According to S. Maslak, computer sonography represents an alternative to traditional ultrasound imaging. The first commercial devices of this type appeared in the second half of the 1980s. Currently, rapid scanning devices are used, or, as they are more often called, real-time operating devices. Their advantages are: the ability to directly observe the movement of organs and structures; reduction of study duration; ability to work with small acoustic windows. They provide Doppler blood flow modes: continuous wave, pulse wave, and color Doppler mapping [140].

Computer sonography allows: 1) B-scanning of tissue structures; 2) examination of tissues in color Doppler mapping and power Doppler modes; 3) detailed study of hemodynamics. The advantages of the computer sonography method are: 1) examination speed; 2) no significant pressure on the eye socket; 3) objectivity, high speed and accuracy of simultaneous processing of multiple parameters; 4) complete visual control of all characteristics in real time; 5) high sensitivity with minimal exposure intensity.

Among the tumors of the anterior orbit, conjunctival retention cysts are common, which are not difficult to diagnose. Echographically, cysts are round or oval anechogenic inclusions with a clear, even contour and more thin-walled capsule, which usually do not contain internal echo structures and give distal sound enhancement. In terms of echo semiotics, conjunctival retention cysts do not differ from simple cysts of other localization, including retrobulbar ones.

In addition to retention and dermoid cysts, malignant lymphomas are easily identifiable by echography, which usually originate from conjunctival lymphoid tissue. They represent diffuse or focal accumulations of lymphocytes or lymphocyte-like cells and are part of systemic damage. The cellular composition determines the low echogenicity of the lesion foci, which are sonographically similar, for example, to areas of lymphoid infiltration in the thyroid gland during cellular type autoimmune thyroiditis. However, there is no clear distal sound enhancement characteristic of fluid structures. The content of malignant lymphomas is moderately heterogeneous due to the presence of randomly arranged linear inclusions, which sometimes appear in the mode of maximum enhancement of the reflected ultrasound signal. The contour of the tumor is quite clear, although it may be blurred. Tumor tissue may be located in virtually any area of the orbit. However, in most cases, they occupy the upper quadrants.

Among the true benign tumors located in the thickness of the eyelids, hemangiomas and lipomas are most common. The latter (their variants are fibrolipoma, angiolipoma) are mainly located not in the projection of the eyelids, but in the palpebral area of the orbit, they are formed from fat cells and, accordingly, in terms of echogenicity, they are close to retrobulbar tissue. Their structure is homogeneous. Since the lipoma is surrounded by a capsule, its contour is sharp and even. In some cases, the lipoma is isoechoic with adjacent tissues. Among tumors of the eyelids and conjunctiva originating from blood vessels, capillary hemangiomas are more easily recognizable than others. In most cases, they are detected in early childhood with predominant localization in the upper inner part of the orbit. On the echogram, the hemangioma is homogeneous, its contour is clear, sometimes uneven. Compared to hyperechogenic adjacent tissues (connective, cartilaginous, scleral), the tumor appears as a tumor of medium echogenicity. Despite the fact that hemangiomas of the anterior orbit resemble hemangiomas in the liver and seem to be easily identified, we should not forget that such an aggressive neoplasm as rhabdomyosarcoma is disguised as this benign tumor. Although rhabdomyosarcoma is malignant, it is still quite homogeneous and has a clear and almost even contour.

Rhabdomyosarcoma also occurs in early childhood, and its favorite localization is the same upper inner part of the orbit.

Conjunctival melanoma is accessible for external examination, so the task of ultrasound examination is to determine the presence of its spread in the eye and orbit. The tumor has reduced echogenicity, and the contour in the area of invasion is blurred. The same task arises when scanning areas of eyelid skin cancer. Along with the size, the spread of the tumor into the depth of the orbit is assessed. Most of these neoplasms (up to 85%) are presented in the form of basaliomas, predominantly localized on the lower eyelid, in the inner canthus. It is diagnostically difficult to identify tumors that spread to the orbit from the eye socket. It is even more difficult to predict the spread of a tumor from the paranasal sinuses to the orbit. Some such tumors can be large, almost completely filling the orbit, which makes it difficult to make a correct diagnosis. Some are localized adjacent to one of the walls of the orbit, which makes it possible to notice a bone defect that connects the volumetric tumor with the paranasal sinus.

As we can see, according to the literature data, despite the development of new medical imaging methods, ultrasound diagnostics remains the most informative method in practical ophthalmo-oncology when assessing orbital pathology. Ultrasound diagnostics of the eye and orbit (ophthalmoscanning) - a combination of two-dimensional (B) mode with real-time scanning, color Doppler imaging, as well as Doppler sonography of blood vessels, allows visualization of intraocular tumors, their spread into the orbit, determination of the degree of orbital wall destruction, the degree of vascularization of neoplasms. In addition, the method of ultrasound examination of the eye is simple, accessible, and harmless to the patient's health.

Furthermore, the existing literature does not sufficiently address the issues of ultrasound diagnostics of secondary orbital tumors, including recurrent tumors. Practically no intumor is found about postoperative changes and complications in the orbits. In addition, the combined use of ultrasound, computed tomography, and magnetic resonance imaging is of interest.

However, none of the above-mentioned instrumental diagnostic methods can make a final, morphological diagnosis using only individual modes. It is important to use complex high-resolution modes of magnetic resonance imaging in the diagnosis and differential diagnosis of orbital tumors. In modern medical literature, intumor about the role of contrast perfusion and spectroscopic modes in determining the etiological factor and malignant nature of eye and orbit nosologies is still difficult to find. The correlative accuracy of the radiological diagnosis with histomorphological

results when fully using complex multiparametric modes is of interest. The current challenges in the most important direction of ophthalmoradiology became the reason for conducting this research.

### 2.2. Clinical Material Characteristics

The paper presents the results of a study of 67 patients with orbital pathological processes, whose treatment and examination were carried out at New Hospitals from September 2023 to May 2024. The patients' ages ranged from several months to 81 years. Of these, 23 (34.3%) were male and 44 (65.7%) were female. Among the examined patients, the number of children from 0.5 to 18 years was 12 (17.9%), of which 7 (58.3%) were male and 5 (41.7%) were female. The largest number of patients was in the active working age (41 to 60 years), and women outnumbered men (65.7% and 34.3% respectively). Data on the distribution of patients by gender and age are given in Table 2.1

When analyzing data on the prevalence of orbital diseases in different age groups, it was found that the maximum number of observations in both men and women falls on the fifth and sixth decades of life.

Table 2.1.

Distribution of Patients by Gender and Age

| Age | | 0-10 | 10-50 | 50-70 | >70 |
|---|---|---|---|---|---|
| Number of studies | Male | 2 (2,98 %) | 10 (14,92 %) | 11 (16,42 %) | 2 (2,98) |
| | Female | 3 (4,48 %) | 18 (26,87 %) | 18 (26,86 %) | 3 (4,49%) |
| Total | | 5 (7,46 %) | 28 (41,79%) | 29 (43,28%) | 5 (7,47%) |
| Total | | 67 (100 %) | | | |

Primary orbital tumors were detected in 43 (64.2%) patients, secondary - in 24 (35.8%).

The largest group consisted of patients with primary neoplasms - 43 (64.2%). Secondary orbital tumors were detected in 24 (35.8%) patients. For all patients, morphological confirmation of the diagnosis was obtained

according to the results of cytological examination of the biopsy or histological examination of the removed tumor.

Table 2.2.

Distribution of Patients by Nature of Orbital Damage

| Orbital Damage | Number of cases | |
|---|---|---|
| | Number | % |
| Primary Tumors of the Eye socket and Orbit | 43 | 64.2 |
| Secondary Tumors | 24 | 35.8 |
| Total | 67 | 100 |

The distribution of patients according to the histological type of tumors is shown in Table 2.3.

Table 2.3

The distribution of patients according to the histological structure of tumors

| Nosological entity | | Number of cases | |
|---|---|---|---|
| | | Number | % |
| Primary tumors | Melanoma | 18 | 26,9 |
| | Cavernous hemangioma | 7 | 10,4 |
| | Adenocarcinoma of the lacrimal gland | 5 | 7,5 |
| | B-cell lymphoma of soft tissues | 4 | 6,0 |
| | Retinoblastoma | 6 | 8,9 |
| | Basal cell carcinoma | 3 | 4,5 |
| Secondary tumors | Adenocarcinoma | 13 | 19,3 |
| | Chondrosarcoma | 3 | 4,5 |
| | Basalioma | 4 | 6,0 |
| | Meningioma | 4 | 6,0 |
| Total | | 67 | 100 |

Among primary neoplasms, melanoma was the most frequent - 26.9%, followed by cavernous hemangioma and pleomorphic adenocarcinoma of the lacrimal gland in smaller quantities - 10.4% and 7.5% respectively, retinoblastoma, lymphoma, and basal cell carcinoma - 8.9%, 6.0%, and 4.5% respectively. Secondary tumors were mostly represented by adenocarcinomas - 19.3%, chondrosarcomas (4.5%), basaliomas (6.0%), and meningiomas (6.0%). Primary tumors were more frequently localized in the eyelid - 22.4% or in the outer parts of the orbit: in the upper outer quadrant 10.6%, in the

lower outer quadrant of the orbit 5.9%. Secondary tumors of the orbit were located adjacent to one of the orbital walls in 84% of cases, more frequently localized in the upper-inner and lower-inner quadrants of the orbit - 26.9% and 22.4% respectively (Table 2.4).

Table 2.4

Distribution of patients based on the localization of the tumor process in the orbit

| Localization | | Number of cases | |
|---|---|---|---|
| | | Number | % |
| Primary tumors | Eye socket | 15 | 22,4 |
| | Upper-inner quadrant of the orbit | 7 | 10,6 |
| | Lower-inner quadrant of the orbit | 4 | 5,9 |
| Secondary tumors | Upper-inner quadrant of the orbit | 18 | 26,9 |
| | Lower-inner quadrant of the orbit | 15 | 22,4 |
| | Lower-inner quadrant of the orbit | 6 | 8,9 |
| | Upper-inner quadrant of the orbit | 2 | 2,9 |
| Total | | 67 | 100 |

The diagnosis of orbital neoplasms was based on patient complaints, which included: decreased visual acuity, presence of tumors of various sizes noticeable to the patient, visual field defects, pain and compression sensations, lacrimation, white or gray color changes on the eyelid, eye twitching, photophobia, ptosis, pulsation sensations; as well as anamnestic data, comprehensive clinical, instrumental and laboratory examination, ophthalmological examination, fine-needle aspiration biopsy and trephine biopsy of tumors. Final diagnosis was established based on pathohistological and immunohistochemical studies of biopsy material and surgical specimens.

When evaluating the anamnesis, circumstances such as living in places with unfavorable ecological conditions, presence of occupational hazards, hereditary oncological diseases, "background" pathologies, and the time elapsed from the onset of first complaints until the visit to the doctor were clarified.

General clinical and instrumental examination included patient examination with mandatory palpation of regional lymph nodes (cervical and submandibular), laboratory studies (complete blood count and biochemical analysis, general urine analysis, immunological blood analysis as indicated), chest X-ray, ultrasound scanning of abdominal organs; computed tomography and magnetic resonance imaging of the brain and abdominal organs were performed as indicated.

During statistical processing, we relied on the dimensions of tumors according to orbital CT and MRI as the most accurate data. To simplify further data processing, the dimensions of neoplasms measured in axial and frontal planes were converted to volume units after mathematical calculations using the ellipsoid volume calculation formula: V= 4/3π(DdH⅛). Orbital tumors were conditionally divided into small (Me = 0.7 cm³ [0.5-1.0 cm³]), medium (Me = 3.5 cm³ [2.4-5.3 cm³]) and large (Me = 16 cm³ [11.8-23 cm³]) tumors. Medium-volume neoplasms predominated (68.7%) (Table 2.5).

Table 2.5

Morphometric indicators of neoplasms

| Tumor volume, $cm^3$ | Me $cm^3$/mm) | Number of patients (n=67) |
|---|---|---|
| Small (0,3-1,1 $cm^3$) | 0,7 $cm^3$/13x10x9mm | 8 |
| Medium (1,2-8,8 $cm^3$) | 3,5 $cm^3$/23x18x17mm | 42 |
| Large (9-40 $cm^3$]) | 16 $cm^3$/40x30x27mm | 17 |

### 2.3. Ultrasound examination method

Ultrasound examination of patients was performed using a Toshiba Aplio i800 device with a 10 MHz linear sensor and a 3.5 MHz convex sensor utilizing multi-positional grayscale scanning (B-mode), color Doppler mapping (CDC), as well as real-time power Doppler (ED) and spectral Doppler (SD) imaging. The sensor parameters were determined by the size and location of the pathological tumor. High-frequency linear transducers were used for tumors located in the anterior parts of the orbit and for intraocular tumors, as well as during Doppler measurements. Tumors located in the posterior parts of the orbit, in the retrobulbar space, as well as growing tumors from adjacent anatomical areas, were examined using a convex sensor, including in second harmonic mode.

Scanning was performed transpalpebral through the closed upper and lower eyelids (transcutaneously), with the patient in a standard horizontal position, lying down or in a vertical sitting position, without special equipment. To ensure the ultrasound beam bypassed the lens of the eye, patients were asked to look to the side.

When selecting parameters for ocular ultrasound examination, we were guided by FDA recommendations, "Intumor for Manufacturers Seeking Marketing Clearance of Diagnostic Ultrasound Systems and Transducers" (Appendix E), as well as provisions developed by the American Institute of Ultrasound in Medicine. During ophthalmological examinations, the thermal

bioeffect index (TI) did not exceed 1.0, the cavitation index (MI) was 0.23, and the ultrasound beam intensity was up to 50 mW/cm².

The ultrasound examination proceeded in the following sequence: in the first stage, the eye socket and retrobulbar space were examined in real-time grayscale mode, with visualization of the eye socket and orbital space structures.

Subsequently, for segmental examination of the retrobulbar space, we sequentially changed the position of the sensor. First, it was placed on the closed upper eyelid from the outside, and the scanning direction was oriented toward visualizing the lower inner part of the retrobulbar space. Then the sensor was placed on the inner part of the closed eyelid (ultrasound beam direction - downward outward) to examine the lower outer quadrant of the orbit, and on the inner part of the lower eyelid with open eyes (scanning direction - upward outward) to assess the upper outer quadrant of the orbit. After this, the sensor was placed on the outer part of the lower eyelid with open eyes (direction of gaze and scanning was upward inward) to assess the upper inner quadrant of the orbit.

To obtain images of the rectus muscles on the monitor screen, the sensors were positioned as follows:

• For visualization of the inferior rectus muscle - on the closed upper eyelid (gaze and ultrasound beam direction - downward; transverse scanning);

• For visualization of the superior rectus muscle - on the lower eyelid with open eyes (vision and ultrasound beam direction upward; transverse scanning);

• For visualization of the lateral rectus muscle - in the inner corner of the palpebral fissure with closed eyes (vision and ultrasound beam direction outward; longitudinal scanning);

• For visualization of the medial rectus muscle - in the outer corner of the palpebral fissure with closed eyes (vision and ultrasound beam direction inward; longitudinal scanning).

During the examination, the condition of the eye sockets, their position, posterior parts of the eye, muscles, optic nerve, orbital walls and vascular structures, retro-orbital tissue, and the presence of tumors in the orbital cavity were assessed.

When identifying a tumor, its size, shape, echogenicity, structure, contours, relationship with adjacent tissues and blood vessels, vascularization (nature of blood flow), and blood supply to adjacent tissues were evaluated. Examples of sonograms are shown in Fig. 2.1 and Fig. 2.2.

When planning organ-preserving treatment, the localization and topometry of the pathological focus (dimensions, area, volume) were specified, the distance of the focus from the outer edge of the orbital bone wall was calculated, and its relationship to the soft tissue structures of the orbit was determined, such as the optic nerve, blood vessels, oculomotor muscles, and bone structures.

Ultrasound examination includes the following stages:

a) Multi-positional examination in B-mode in real time. When a volumetric tumor was detected, its localization was determined, and the size, shape, echogenicity, structure, contours, and number of pathological tumors were assessed.

b) Study of qualitative parameters of intratumoral blood flow. During color Doppler coding according to flow velocity (CCV) and/or energy (ED), the detected intratumoral blood flow, the nature of vessel architectonics, and their distribution patterns in the tumor mass were studied. In duplex mode, the color flow window size was set according to the visualized area of the tumor. This was followed by optimization of color mode parameters (Doppler signal amplification coefficient, velocity scale) and multi-planar scanning of the area of interest.

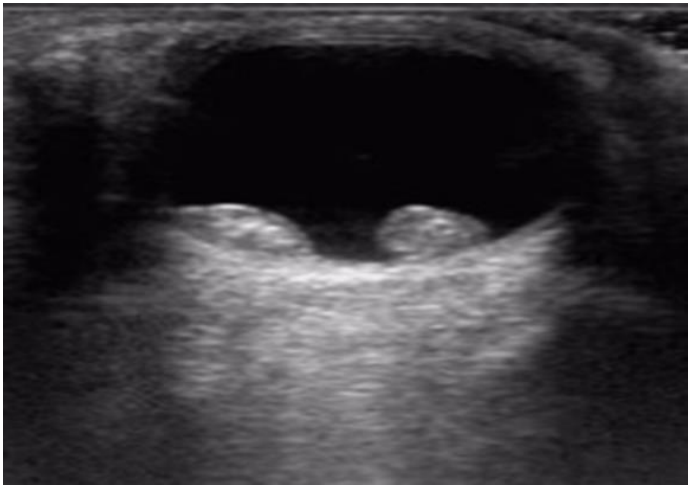

**Fig. 2.1. Fragments of sonogram of a 42-year-old patient**

### 2.4. Ultrasound examination results

Ultrasound examination was conducted on 47 patients with orbital and eye socket neoplasms. Of these, 30 patients had primary tumors, while 17 patients had secondary tumors.

In the group of patients with primary tumors of the eye socket and orbit, 30 patients aged 24 to 75 years were examined (average age 49±0.2 years). Women were significantly more frequently affected - 11 (57.9%), compared to men - 8 (42.1%).

The tumor was located on the right orbit in 58.8% of cases, while tumors were less frequently localized on the left orbit - 41.2%. Bilateral orbital involvement was not observed in our studies. In patients with primary orbital tumors, tumor localization in the eye socket constituted 58.8%. In the remaining cases, the tumors were located in the orbit, with 26.4% of cases involving the upper outer quadrant, and 14.8% - the lower outer quadrant.

Patients with primary orbital tumors exhibited clinical manifestations characteristic of this pathology, and the main complaints were:

- Decreased vision - 47.1%
- Exophthalmos - 29.4%
- Limited eye socket movement - 24.5%
- Eye socket displacement - 32.4%
- Nodular tumor in the periorbital area - 24.5%
- Eyelid edema - 38.2%
- Upper eyelid ptosis - 29.4%
- Pain syndrome of varying severity - 44.1%.

Eye socket displacement was detected in 32.4% of patients. When a tumor was localized in the upper outer quadrant, the eye socket shifted downward and medially. With tumors in the lower outer quadrant, the eye socket moved medially and upward. In isolated cases, upward and lateral displacement was noted. Eye socket detumor was established in 47% of cases. Analysis of echographic signs of primary orbital tumors was based on the following quantitative and qualitative parameters:

- Shape of the pathological focus;
- Localization of the process;
- Structure of the pathological tumor;
- Presence of additional inclusions in the structure of the tumor;
- Nature of growth (solitary or multinodular);
- Prominence into the vitreous body in case of intraocular tumors;
- Choroidal excavation;

- Presence or absence of retinal detachment and its dimensions;
- Surface of the tumor;
- Contours of the pathological focus;
- Echogenicity of adjacent tissues;
- Vascularization of the tumor;
- Destruction of the orbital bone walls.

The frequency of ultrasound signs of primary orbital tumors according to standard ultrasound examination is presented in Table 2.6.

Analysis of the semiotic signs of primary orbital tumors revealed their common features: the structure of tumors in 93.3% of cases was solitary. An oval form of neoplasm predominated - 73.3%, while irregular forms were less common - 26.7%. It should also be noted that during the examination, the shape of the tumor may change due to compression by the transducer. For intraocular tumors, such a sign as tumor prominence into the vitreous body was also considered. This sign was recorded in all patients with intraocular tumors.

The echogenicity of tumor tissue was low in 93.3%. The echostructure in 66.7% of cases was homogeneous; heterogeneous structure of tumor tissue was revealed in 33.3% and was caused by the presence of anechoic inclusions morphologically represented as cystic component and (or) necrotic component. In isolated cases, hyperechoic inclusions were found due to areas of pathological bone tumor or fibrous component.

Table 2.6.

The frequency of ultrasound signs of primary eye socket and orbital tumors according to standard ultrasound examination

| Ultrasound signs | | Primary damage of the orbit, n=30 | |
|---|---|---|---|
| | | Abs. | % |
| Architectonics | Solitary | 28 | 93,3 |
| | Multi-node | 2 | 6,7 |
| Shape | Oval | 22 | 73,3 |
| | Irregular | 8 | 26,7 |
| Echogenicity | Low | 28 | 93,3 |
| | Medium | 2 | 3,7 |
| Echostructure | Heterogeneous | 10 | 33,3 |
| | Homogeneous | 20 | 66,7 |
| Inclusions | Hyperechogeneic | 2 | 6,7 |
| | Anechogenic | 6 | 20,0 |
| | Mixed | - | - |
| | No inclusions found | 16 | 53,3 |
| Surface | Smooth | 24 | 80,0 |
| | Rough | 6 | 20,0 |
| Tumor vascularization | High | 19 | 63,3 |
| | Medium | 6 | 20,0 |
| | Low | 5 | 16,7 |

The surface of the neoplasm was smooth (80.0%), but in 20.0%, surface irregularities were caused by the peculiarities of tumor growth (diffuse nature), as well as compression of adjacent tissues.

In 63.3% of cases of orbital tumor lesions, a high degree of vascularization was recorded due to a chaotically arranged vascular network. Blood flow was not detected in areas of tumor tissue necrosis.

Detailed analysis of ultrasound images of tumors with different morphological structures revealed certain features, which are systematized in Table 2.7.

Melanomas were characterized by solitary structure, had smooth surface in 91.7% of cases, tumor shape was mostly oval (83.3%). Echogenicity was low in all cases. Structure was homogeneous in 83.3% of cases, structural heterogeneity was caused

Table 2.7.

Ultrasound characteristics of primary tumors according to the morphological variant of the tumors

| Ultrasound characteristics | | Melanomas, n=12 | | Cavernous heman gioma, n=4 | | Pleomorphic adenocarcinoma of the lacrimal gland, n=3 | |
|---|---|---|---|---|---|---|---|
| | | Abs. | % | Abs. | % | Abs. | % |
| Tumor architectonics | Solitary | 12 | 100 | 4 | 100 | 2 | 66,7 |
| | Multi-node | - | - | - | - | 1 | 33,3 |
| Shape | Oval | 10 | 83,3 | 1 | 25,0 | 2 | 66,7 |
| | Irregular | 2 | 16,7 | 3 | 75,0 | 1 | 33,3 |
| Surface | Smooth | 11 | 91,7 | 1 | 25,0 | 2 | 66,7 |
| | Rough | 1 | 8,3 | 3 | 75,0 | 1 | 33,3 |
| Echogenicity | Low | 12 | 100 | 4 | 100 | 3 | 100 |
| | Medium | - | - | - | - | 1 | 33,3 |
| | High | - | - | - | - | - | - |
| Internal structure | Evenly heterogeneous | 2 | 16,7 | 3 | 75,0 | 2 | 66,7 |
| | Homogeneous | 10 | 83,3 | 1 | 25,0 | 1 | 33,3 |
| | Unevenly heterogeneous | - | - | - | - | - | - |
| Inclusions | Anechogenic | 1 | 8,3 | 2 | 50 | 1 | 33,3 |
| | Hyperechogenei c | - | - | - | - | 1 | 33,3 |
| | Mixed | - | - | - | - | - | - |
| Blood flow | No found | 1 | 8,3 | 1 | 25,0 | - | - |
| | 1-3 CL | 6 | 50 | 1 | 25,0 | 2 | 66,7 |
| | 3-5 CL | 2 | 16,7 | 2 | 50,0 | 1 | 33,3 |
| | >5 CL | 3 | 25 | | - | - | - |

by necrosis and hemorrhages. Anechoic inclusions in tumors were detected in 8.3% of cases. In most cases, melanoma dimensions did not exceed 15 mm in 81.8% of cases and only in 18.2% tumor dimensions were more than 15 mm. Retinal detachment was detected in 72.7% of cases in patients with melanoma (Fig. 2.2).

In color Doppler mapping (CDm) mode, neovascularization of tumor tissue was detected in all cases. Newly formed blood vessels were of various sizes, had chaotic, tortuous appearance.

Mainly central location of color locus (CL) predominated - 90.9% of cases. In half of the cases, moderate vascularization of the tumor was revealed.

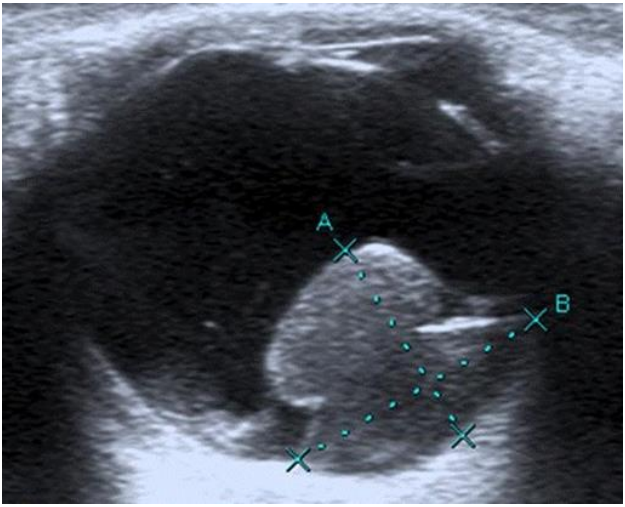


**Fig.2.2. Orbital melanoma**

When analyzing sonographic signs of cavernous hemangioma, the following data were obtained: typical tumor location in 71.4% of cases is the upper outer quadrant of the orbit. In this case, there was displacement and compression of the eye socket medially and downward. In 28.6%, the tumor spread from the upper outer quadrant to the lower outer, in some cases causing compression on the eye socket and its displacement medially and upward.

In all cases, the tumor was of solitary structure, but the shape was mostly irregular - 85.7%. Tumor contours were indistinct in 85.7% of cases, indicating the infiltrative nature of tumor growth. Its surface was uneven in 71.4% of cases.

Echogenicity was low in all cases, while structure was uniformly heterogeneous in 71.4% of cases, structural homogeneity was less common - 28.5%. Anechoic inclusions in tumors were visualized in 42.8% of detected cases and indicated the presence of necrotic areas in tumor tissue.

Intratumoral blood flow was detected in 85.6% of cases. In other cases, signs of tumor blood flow were not detected, possibly due to low velocity and small caliber of blood vessels. When having its own vascular

network, against the background of hypoechoic, predominantly heterogeneous structure, 3-5 CL were visualized in 57.1% of cases. Peripheral CL location was visualized in 28.5% of detected cases, central location in 14.2%; in remaining patients, CL was arranged chaotically and diffusely. Newly formed blood vessels had tortuous appearance. However, during rapidly growing malignant orbital tumors (28.5%), predominance of extensive avascular zones with single CL was noted, indicating that the construction of own vascular network lags behind tumor cell proliferation, causing tumor of necrotic areas in tumor tissue.

When analyzing ultrasonic signs of pleomorphic adenocarcinoma of the lacrimal gland, we identified the following features: predominant location of tumor in the outer orbit. In most examined cases, it spread to the retrobulbar space, displaced the eye socket upward and inward. It was noted that in 20% of pleomorphic adenocarcinoma cases, it had multinodular structure, which was practically not observed in tumors of other morphological groups. Tumor shape was mostly oval (80%).

Tumor contours were clear in 80.0% of cases, indistinct contours were noted only in 20.0%. In most cases, its surface was smooth.

Echogenicity was low; it should be noted that according to echogenicity, the tumor was close to fluid, but distal ultrasonic enhancement behind the tumor was not detected.

Heterogeneous tumor structure was detected in 80.0% of cases, however, in 20.0% of cases, homogeneous structure was also noted. Anechoic and hyperechoic inclusions in tumors were visualized with equal frequency - in 40% of cases. Three patients were found to have thin-walled hyperechoic pseudocapsule 0.5-1.5 mm thick. During examination in power Doppler mapping mode, well-defined vascular network was visualized; CL location was mixed, numbering from 2 to 5.

Since the scale of surgical intervention primarily depends on tumor spread, initial localization and growth direction, great importance is given to assessing tumor spread on orbital structures (muscles, blood vessels, optic nerve) during sonography. We studied the condition of extraocular muscles, optic nerve, retrobulbar tissue, boundaries of malignant neoplasms, tumor spread to various orbital structures and presence of choroidal excavation in intraocular tumors (Table 2.8).

When assessing primary tumor spread, it was established that in 20.0%, the tumor infiltrated extraocular muscles. Muscle contours are indistinct, echogenicity is reduced and the boundary between tumor and muscle is indistinct.

Retrobulbar tissue changed in 26.7% of cases, in all these cases its echogenicity reduction was detected, which was caused by edema or tumor tissue infiltrate.

In 10.5% of cases, there was suspicion of optic nerve infiltration by tumor, since the tumor was located adjacent to the optic nerve and there was no boundary between them.

Echogenicity of adjacent orbital tissue to tumor decreased by 70.0%.

In 23.9% of cases, destruction of orbital bone walls was revealed. Difficulties arose in identifying destruction in posterior parts of the orbit, especially in projection of upper and lateral walls, because orbital wall configuration and ultrasonic transducer surface did not match each other - studied structures were located parallel to ultrasonic wave path. This caused incorrect results in 5.8% of cases.

During intraocular tumors, for assessing tumor growth beyond the eye socket, we consider choroidal excavation symptom as the most significant sign. In our studies, choroidal excavation was revealed in 21.1% of cases.

Table 2.8

Relationship of primary tumors with orbital structures according to ultrasound data

| Ultrasound signs | | Primary damage of the orbit (n=30) | |
|---|---|---|---|
| | | Abs. | % |
| Infiltration of the extraocular muscles | Yes | 6 | 20,0 |
| | No | 24 | 80,0 |
| Sizes of the extraocular muscles | Unchanged | 23 | 76,7 |
| | Reduced | - | - |
| | Increased | 3 | 10,0 |
| Changes in the retrobulbar tissue | Yes | 8 | 26,7 |
| | No | 22 | 73,3 |
| Optic nerve infiltration | Yes | 3 | 10,5 |
| | No | 27 | 89,5 |
| Echogenicity of the adjacent tissues | Increased | 8 | 26,7 |
| | Reduced | 21 | 70,0 |
| | Unchanged | 1 | 3,3 |
| Destruction of orbital bone walls | Medial | - | - |
| | Lateral | 3 | 10,5 |
| | Upper | 2 | 6,7 |
| | Lower | 2 | 6,7 |
| Choroidal excavation | Yes | 6 | 20,0 |
| | No | 11 | 36,7 |

Thus, obtained data testifies to quite high informativeness of ultrasonic method in assessing intraocular tumor spread. By analyzing sonographic signs of primary orbital tumors and comparing them with morphological examination data, it is possible to determine diagnostic effectiveness of ophthalmosonography.

Sonography sensitivity was 93%, while specificity and accuracy were 75% and 88% respectively.

False-positive responses were obtained in cases of long-term pseudotumor processes, as a result of which ultrasonic picture (low echogenicity of tumor, moderate heterogeneity, indistinct contours) was close to sonographic picture of tumor process. False-negative results were obtained in cases of small tumors less than 10 mm, accompanied by endocrine ophthalmopathy, against which tumor process was not identified.

It was confirmed that according to sonography, false-positive results of tumor growth outside the eye socket were detected in 4.5% of cases, which was caused by presence of concomitant pathologies (endocrine ophthalmopathy). False-negative ultrasonic results were noted in 9.0% of cases.

Thus, use of ophthalmosonography at the primary examination stage in patients with orbital tumors can significantly reduce financial costs and time needed for diagnosis. Additionally, it was confirmed that ophthalmosonography is an effective diagnostic method for determining tumor process spread to orbital structures. This, in turn, is an important criterion for further planning of surgical intervention volume and tactics.

17 patients with secondary tumors were examined ultrasonically, of which 8 (47.1%) men and 9 (52.9%) women aged 18 to 81 years.

Tumor was located on right orbit in 47.1% of cases, tumor on left orbit was localized in 52.8%, while bilateral orbital involvement with secondary tumors was detected in 7.5% of cases.

Secondary tumors were mostly represented by adenocarcinomas - 19.3%, chondrosarcomas - 4.5%, basaliomas - 6.0% and meningiomas - 6.0%.

Most frequently, primary focus was breast, prostate and lung cancer. Primary focus was also located in maxillary sinus and ethmoid labyrinth cells. Less commonly, primary tumor was localized in nasal cavity and upper jaw. Data on primary tumor location is presented in Table 2.9.

Table 2.9

Distribution of patients according to the localization of the primary focus

| Initial growth of the tumor | Number of patients | |
|---|---|---|
| | Abs. | % |
| Breast, prostate, and lung cancers | 7 | 41,2 |
| Maxillary sinus | 3 | 17,6 |
| Ethmoidal labyrinth | 3 | 17,6 |
| Nasal cavity | 2 | 11,8 |
| Maxilla | 1 | 5,9 |
| Soft tissue of the facial region | 1 | 5,9 |
| Total | 17 | 100 |

Patients with sinoorbital tumor damage had characteristic clinical manifestations and symptoms were often dependent on primary focus localization. At the same time, general complaints of sinoorbital neoplasms of the orbits were:

– Pain syndrome of various severity - 79.2%
– Exophthalmos - 69.8%
– Eye socket displacement - 56.6%
– Limitation of eye socket movement - 52.8%
– Eyelid swelling - 39.6%
– Upper eyelid ptosis - 35.8%
– Vision impairment - 32.1%
– Nodular tumor in periorbital area - 26.4%
– Lacrimation - 26.4%

Eye socket displacement was revealed in 56.6% of cases. When tumor is localized in upper inner quadrant, eye socket displaces downward and laterally. When tumor exists in lower inner quadrant area, eye socket was positioned laterally and upward. In isolated cases, displacement upward and medially or downward and medially was noted. Eye socket detumor was established in 41.5% of cases, optic nerve displacement - in 18.9%.

When analyzing echographic signs of sinoorbital tumors of the orbit, we considered the following qualitative parameters:

- Tumor localization
- Pathological focus shape
- Structure (nature of tumor growth)
- Tumor surface

- Pathological focus contours
- Neoplasm structure
- Presence of additional inclusions in tumor structure
- Echogenicity of adjacent tissues
- Tumor vascularization
- Destruction of orbital bone walls

Sonography showed that in most cases secondary tumors were located adjacent to one of the orbital walls - 84%.

Tumors were more frequently localized in upper inner and lower inner quadrants of the orbit - 27.6% and 23% respectively, less commonly occupied lower outer quadrant - 8.1% and upper outer quadrant - 2.3%.

The frequency of ultrasonic sign detection of orbital secondary tumors according to standard ultrasonic examination is presented in Table 2.10.

Table 2.10

The frequency of ultrasonic sign detection of orbital secondary tumors

| Ultrasonic signs | | Sinoorbital tumors (n=17) | |
|---|---|---|---|
| | | Abs. | % |
| Architectonics | Solitary | 15 | 88,2 |
| | Multi-node | 2 | 11,8 |
| Shape | Oval | 4 | 23,5 |
| | Irregular | 13 | 76,5 |
| Surface | Smooth | 5 | 29,4 |
| | Rough | 12 | 70,6 |
| Echogenicity | Low | 14 | 82,4 |
| | Medium | 3 | 17,6 |
| Echostructure | Heterogeneous | 13 | 76,5 |
| | Homegeneous | 4 | 23,5 |
| Inclusions | Hyperechogeneic | 2 | 11,8 |
| | Anechogenic | 4 | 23,5 |
| | Mixed | 2 | 11,8 |
| | No inclusions found | 9 | 52,9 |
| Tumor vascularization | High | 13 | 76,5 |
| | Medium | 3 | 17,6 |
| | Low | 1 | 5,9 |

Table data shows that metastatic tumors more frequently had irregular shape (76.5%) and were characterized by solitary structure (Fig. 2.3). In 82.4% of cases, low echogenicity of tumor tissue was established. Tumor echostructure heterogeneity was revealed in 76.5% of cases, in isolated cases heterogeneity was accompanied by presence of anechoic inclusions, which

morphologically was caused by cystic component and/or necrotic substrate, while in some cases hyperechoic inclusions were found due to pathological bone tumor areas or fibrotic component. Tumor size in maximum dimension ranged from 10 to 43 mm and in most cases tumor was located along the wall, repeated its contour and entered orbital cavity by 3-20 mm. In CDm mode, high degree of tumor vascularization was detected in 76.5% of cases, in 25% it was accompanied by presence of feeding vessel, while in 41% during orbital tumor damage, high degree of vascularization was determined due to chaotically arranged vessel network.

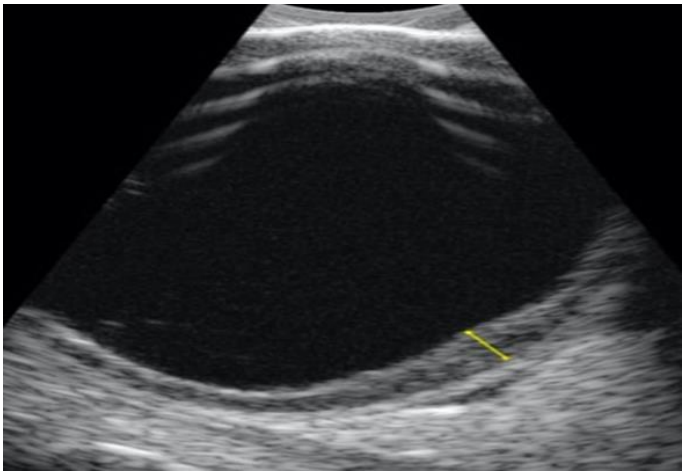

**Fig. 2.3. Orbital lymphoma**

By analyzing ultrasonic semiotics of tumors according to primary focus location and morphological structures, we obtained the following data.

Tumor grown from jaw sinuses and upper jaw into orbit was more frequently localized on lower wall - 47.1%, or medial - 35.3%, less commonly on lateral - 17.6% of cases.

During ethmoid labyrinth cell damage, metastatic tumor was located in 64.2% on medial wall, and in 35.7% of cases on upper wall.

In case of primary tumor overgrowth from nasal cavity, tumor component in orbit was detected in medial wall projection (60%) or in lower wall (30.0%).

According to morphological structure, echosemiotics of sinoorbital tumors is presented in Table 2.11.

During adenocarcinomas, in most cases tumor structure was solitary - 88.9%, only in 11.1% multinodular tumor structure was revealed.

Neoplasm shape was irregular in all cases.

Indistinct contours were detected in 69.2% of cases, while partially indistinct contours were detected in 15.4% of cases.

Adenocarcinomas had mostly rough surface (66.7%). Tumor echogenicity was reduced in 88.9% of cases.

In all cases it was established that internal structure of new tumors was heterogeneous. Inclusions in tumor structure were detected in 44.4% of cases, more frequently of anechoic nature (33.3%), less commonly - mixed. We offer clinical observation.

Table 2.11

Characteristics of ultrasound signs of sinoorbital tumor

| Ultrasound signs | | Adenocarcinoma (n=9) | | Chondrosarcoma (n=2) | | Basalioma (n=3) | | Meningioma (n=3) | |
|---|---|---|---|---|---|---|---|---|---|
| | | Abs. | % | Abs. | % | Abs. | % | Abs. | % |
| Architectonics | Solitary | 8 | 88,9 | 2 | 100 | 2 | 66,7 | 2 | 66,7 |
| | Multi-node | 1 | 11,1 | - | - | 1 | 33,3 | 1 | 33,3 |
| Shape | Oval | - | - | 1 | 50 | 1 | 33,3 | - | - |
| | Irregular | 9 | 100 | 1 | 50 | 2 | 66,7 | 3 | 100 |
| Surface | Smooth | 3 | 33,3 | - | - | 1 | 33,3 | 1 | 33,3 |
| | Rough | 6 | 66,7 | 2 | 100 | 2 | 66,7 | 2 | 66,7 |
| Echogenicity | Low | 8 | 88,9 | 1 | 50 | 2 | 66,7 | 2 | 66,7 |
| | Medium | 1 | 11,1 | 1 | 50 | 1 | 33,3 | - | - |
| | High | - | - | - | - | - | - | 1 | 33,3 |
| Internal structure | Evenly heterogeneous | 9 | 100 | 1 | 50 | 2 | 66,7 | 1 | 33,3 |
| | Homogeneous | - | - | - | - | 1 | 33,3 | - | - |
| | Heterogeneous | - | - | 1 | 50 | - | - | 2 | 67,3 |
| Inclusions | Anechogenic | 3 | 33,3 | - | - | 1 | 25 | - | - |
| | Hyperechogeneic | - | - | 1 | 50 | - | - | 1 | 33,3 |
| | Mixed | 1 | 11,1 | 1 | 50 | - | - | - | - |

Chondrosarcomas had solitary structure in all cases and predominantly irregular shape. Tumor contours were partially indistinct in

50% of cases, less commonly tumors had clear contours (30%). Tumor surface was rough in all cases.

Basalioma sonographic data analysis showed that in most cases solitary tumors were found (66.7%), irregular shape was revealed in 66.7%, tumor indistinct contours predominated (71.4%) and surface roughness (66.7%). Low echogenicity was detected in 66.7% of cases, while uniform heterogeneity of tumor echostructure was noted in 66.7% of cases with predominance of anechoic inclusions.

In 71.4% of cases, tumor neovascularization phenomenon was revealed, represented by 1-3 color loci. In other cases, due to small tumor size, blood flow determination did not occur.

Meningioma semiotic picture practically did not differ from basalioma picture, i.e., it was characterized by solitary tumor structure - 66.6%, irregular shape, tumor indistinct contours - 66.6% of cases and rough tumor surface, low echogenicity in 66.6%, but unlike squamous cell carcinoma, tumor heterogeneity was caused by hyperechoic inclusions (33.3%).

Considering completed studies, analysis of diagnostic effectiveness of ophthalmosonography for identification of secondary orbital tumors was conducted.

The following data were obtained: ultrasonic method sensitivity in detecting orbital secondary tumors was 90.4%, while specificity and accuracy were 81.8% and 88.6% respectively.

False-positive result was obtained in 2 patients' cases during acute inflammatory processes in retrobulbar space against endocrine ophthalmopathy background. False-negative results were revealed in 1 case during chronic inflammatory process against severe post-traumatic orbital detumor background, while in 3 cases tumor intraorbital component size did not exceed 5-7 mm, and tumor component itself was located in posterior parts of orbit.

Using sonography to determine further treatment tactics and scale, great importance was given to assessing degree of tumor spread to various orbital structures (muscles, blood vessels, optic nerve). Condition of extraocular muscles, optic nerve, tumor spread to orbital structures and retrobulbar tissue condition were evaluated.

Correct assessment of adjacent tissue condition is of great importance, since in cases of preserving integrity of tumor-adjacent orbital structures, organ-preserving treatment can be performed, which in turn affects patient's quality of life.

When analyzing data on condition of tumor-adjacent structures (Table 2.12), it was shown that extraocular muscle infiltration was revealed in almost half of cases.

Extraocular muscle size did not change in most cases - 70.6% of cases, but changes in retrobulbar tissue were established in 76.5% of cases, which was presumably caused by tumor tissue infiltration. Optic nerve infiltration was revealed in 22.6%.

Increased echogenicity of tumor-adjacent orbital tissues was detected in 17.6% of cases, occurred in cases of long-growing tumors and was caused by development of fibrotic component in adjacent tissues.

Orbital bone wall destruction was revealed in 74.9% of cases, while destruction of medial and lower orbital bone walls was more frequent (35.3% and 23.5%, respectively) than lateral and upper walls - in 11.8% and 5.9% of cases respectively

Table 2.12

The relationship between secondary tumors and orbital structures according to ophthalmosonographic data

| Ultrasonic signs of orbital structure inclusion | | Secondary tumors (n=17) | |
|---|---|---|---|
| | | Abs. | % |
| Extraocular muscle infiltration | Yes | 8 | 47,1 |
| | No | 9 | 52,9 |
| Extraocular muscle sizes | Unchanged | 12 | 70,6 |
| | Reduced | - | - |
| | Increased | 5 | 29,4 |
| Retrobulbar tissue changes | Yes | 13 | 76,5 |
| | No | 4 | 23,5 |
| Echogenicity of adjacent tissues | Increased | 3 | 17,6 |
| | Reduced | 13 | 76,5 |
| | Unchanged | 1 | 5,9 |
| Destruction of orbital bone wall | Medial | 6 | 35,3 |
| | Lateral | 2 | 11,8 |
| | Upper | 1 | 5,9 |
| | Lower | 4 | 23,5 |

Discrepancy between data obtained by ultrasonic examination method and surgical intervention results was in all cases caused by tumor process localization in upper parts and apex of orbit, as well as small size of tumor orbital component and proximity of tumor echogenicity to echogenicity of extraocular muscles or retrobulbar space.

# CHAPTER 3. COMPUTED TOMOGRAPHIC EXAMINATION OF ORBITAL NEOPLASMS

## 3.1. Computed Tomographic Examination of Tumors

The tumor and development of computed tomography (CT) is associated with fundamental research on the mathematical reconstruction of objects from multiple projections. In 1963, A. Cormack developed a mathematical method for brain reconstruction using X-ray radiation sources. Similar research was independently conducted by G.N. Hounsfield (1967-1971). Based on these studies, the first X-ray computed tomograph for brain examination was designed in 1970. Clinical studies of computed tomography showed not only the possibility of obtaining brain images, but also the detection of tumor foci and determining their relationship with adjacent areas. The convincing results obtained from using computed tomography in diagnosing brain pathologies served as an impulse for developing computed tomography for examining the entire body.

CT diagnostics is based on the registration of attenuated X-ray radiation after passing through the zone of diagnostic interest. The method allows obtaining high-quality axial tissue images through the exposure of thin sections to X-ray radiation. Data for imaging is obtained in hundreds of projections during the rotation of the X-ray tube around the patient - during scanning. Based on this data, converted by detectors into electrical signals proportional to the intensity of radiation that has passed through the patient's body, the computed tomograph, using special programs, performs reconstruction of a specific layer image, which is created in the form of numbers reflecting the distribution of densities in the section, and then converted into a brightness distribution on the monitor screen.

CT provides the possibility of obtaining images in the axial plane, which are not accessible in traditional X-ray diagnostics. Obtaining images in this plane does not require additional image reconstruction and special positioning, unlike coronal and sagittal planes. The X-ray density of tissues, i.e., their ability to attenuate radiation, is evaluated in non-systemic Hounsfield units (H or HU units). In this scale, X-ray absorption by water is taken as 0 HU units, air as -1000 HU units, dense bone as +1000 HU units.

The main advantage of computed tomography is the possibility of visualizing bone and soft tissues in real scale. At the same time, the obtained image has the appearance of a real anatomical section. An undeniable advantage of CT is the possibility of qualitatively and quantitatively assessing the obtained data (distances, areas, volumes, X-ray density measurements)

with high precision. Mathematical processing of images increases the informativeness of the study and, accordingly, the diagnostic significance of the method.

CT provides good visualization of bone, fatty, and muscle tissues, which is irreplaceable when examining the orbit; it allows determining the volumetric characteristics of orbital soft tissue tumors. Modern computed tomographs provide the possibility of three-dimensional image reconstruction [23].

The use of intravenous contrast technique makes possible significant improvement in the differentiation of soft tissue components in various pathological processes, determination of the nature of vascularization and avascular areas of the mentioned tumors, which cannot be visually determined by ordinary CT examination in some cases. Intravenous administration of radiocontrast agents increases CT's resolution ability by increasing the contrast of normal or pathological tissues, helps clarify the nature of various pathological processes and the boundaries of tumor spread. For these purposes, mainly non-ionic monomeric contrast agents (Ultravist, Omnipaque, and others) are used.

The capabilities of modern computed tomographs are widely used for visualizing vascular structures (so-called CT angiography or CTA). Direct administration of contrast agent during tomography and reconstruction of these images makes possible clear visualization of target vascular components [116].

Typically, when examining the orbits, the X-ray tube and receiving detectors rotate 360° around the patient's head. For orbital studies, sections of 0.5-3 mm thickness are mainly used in axial, sagittal, and coronal projections. When examining healthy orbits, the following structures are clearly visualized: eye socket, optic nerve, extraocular muscles, lacrimal gland, retrobulbar fatty tissue, superior ophthalmic vein, orbital bony walls, superior and inferior orbital fissures, optic canal. The optic nerve is often represented by a hypodense central zone, which is the result of its density and physiological fluid content [122, 163]. The normal diameter of the optic nerve on tomograms is 3-4 mm, with density of 35-45 Hounsfield units. The rectus oculi muscles have a fusiform shape with sharp and straight contours. When examining orbits with sections of 5 mm or greater thickness, the degree of differentiation of the lateral rectus muscle is low due to its insignificant thickness and close proximity to the outer wall of the orbit [145, 170, 36, 111]. Normal muscle density ranges from 30 to 50 Hounsfield units. The lacrimal gland is located in the upper outer part of the orbit and is well defined only by its orbital portion located adjacent to the eye socket. Normal fatty

tissue has a homogeneous structure. Normal asymmetry of linear dimensions of orbital structures does not exceed 2-2.5 mm in 95% of cases. In cases of pathological processes in the orbit, CT allows determination of the presence of pathology, size, spatial localization, relationship with muscles, optic nerve, and in some cases (presence of invasion and destruction of bone structure) to differentiate malignant tumors from benign tumors, true tumors from pseudotumorous orbital diseases, and also determines the locally disseminated part of the tumor to paranasal sinuses and skull structures. According to computed tomography data, tumor diagnosis can be made in 95.1% of cases, the nature of neoplasm (benign, malignant) - in 72.3% of cases, while the histological type of tumor (hemangioma, meningioma, dermoid cyst, optic nerve tumors) can be determined in 53.2% of cases [126].

### 3.2. Computed tomographic examination method

The studies were conducted on a SIEMENS Somatom Perspective 128 type computed tomograph, which represents an ultra-modern, 128-slice model. The Somatom Perspective 128 improves visualization and provides high-quality imaging. Its main advantage is image accuracy and reconstruction quality, which is particularly important for examining small-sized structures. The use of Somatom Perspective is safe for patients and staff, as it is equipped with SAFIRE technology and reduces patient radiation exposure by 60%. The technical characteristics of orbital examination are presented in Table 3.1.

Table 3.1.

Technical characteristics of the orbit examination

| Examination parameters | Method | |
|---|---|---|
| | MSCT - computed tomography | fMSCT - Functional multispiral computed tomography |
| Examination mode | Spiral | Dynamic |
| Number of slices | 320 | 320 |
| Slice thickness | 0,5 | 0,5 |
| Detector width | 16 cm | 16 cm |
| Voltage | 120 kV | 120 kV |
| Amperage | 125 mA | 125 mA |
| Examination area | About 9 cm | About 6 cm |
| Examination time | 8 sec | 4-8 sec |
| Reconstruction algorithm | Soft-tissue, bony | Soft-tissue |
| Effective area | 3-3,5 mSv | 1,5-2 mSv |

***Note**: cm – centimeter; kV - kilovolt, mA – milliampere; mSv - millisievert.*

Orbital CT was performed in automatic mode scanning using a special program embedded in the tomograph's computer program. The program allows us to obtain images in different planes, specifically in sagittal, frontal, and axial sections, at desired angles. Initially, the examination was conducted in axial projection (patient in supine position) with the X-ray tube tilted at an angle corresponding to the orbital roof line. The examination zone was marked from the upper edge of the maxillary sinus to the upper edge of the frontal sinuses; in this area, 1 mm thick sections were made through which the tumor's location, size, shape, structure, density (fatty (-120 to -30 Hounsfield units), liquid (-29 to +29 Hounsfield units), soft tissue (+30 to +70 Hounsfield units)), tissue (more than +70 Hounsfield units), spread to adjacent structures, destruction of orbital bone walls, infiltration of extraocular muscles, orbital tissue, and optic nerve were assessed.

Contrast enhancement was performed by intravenous injection of contrast agent Omnipaque - 300 mg/ml or Ultravist - 300 mg/ml, followed by scanning with tomograph step of 1.0 mm and slice thickness of 0.5 mm. Contrast enhancement made possible clearer visualization of tumor boundaries with adjacent tissues, its connection, internal structure, and the degree of blood supply to the tumor and the speed and intensity of contrast accumulation. Insignificant contrast accumulation by neoplasm is considered contrast accumulation of 1-13 Hounsfield units, moderate accumulation 14-27 Hounsfield units, and intensive 28-40 Hounsfield units.

Special preparation of patients was not required for conducting MSCT examination of orbits. The patient lies on their back, their head is placed in a standard headrest and fixed to prevent position changes. The first series of sections was performed in spiral mode, in axial plane without gantry tilt, from the alveolar level of the maxilla without head tilt or turn. The study began with a topogram, which was used to plan the tomography plane. Scanning proceeds toward the skull base. After obtaining images in the axial plane, where slice thickness was 0.5 mm in all cases, multiplanar reconstruction (MPR) and 3-D reconstruction were performed.

Despite the effectiveness of computed tomography in diagnosing orbital tumors, it was not always possible to identify tumors existing parallel to the slice plane in axial projection. In connection with this, in some cases, it became necessary to conduct examination in the coronal plane to determine the condition of the orbital floor. Currently, using multiplanar reconstructions, it became possible to obtain images from the axial plane in the coronal plane, which was performed in all conducted studies. The plane during multiplanar reconstruction was always parallel to the orbital plane. For

more accurate assessment of orbital structures, the multiplanar reconstruction plane can be changed until the desired result is achieved (Fig. 3.1, Fig. 3.2).

Construction of the coronal plane is not dependent on the patient's "correct" position. Multiplanar reconstructions make possible obtaining the coronal plane according to the location of orbits and their walls. It also becomes possible to construct any plane that is necessary for more accurate assessment of orbital structures without additional radiation load.

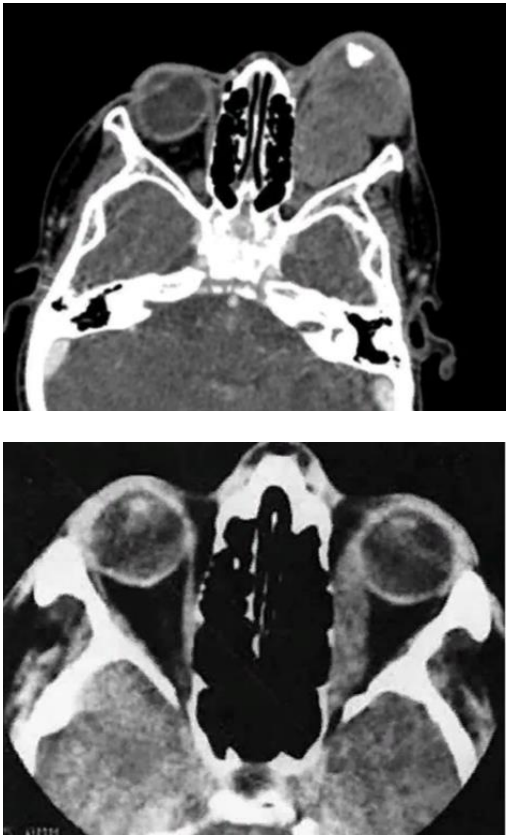

a) Retinoblastoma of the left eye in a 49-year-old patient
b) Enlargement of the left medial rectus muscle in a 69-year-old patient with endocrine ophthalmopathy

Fig. 3.1. CT scan results of the orbit

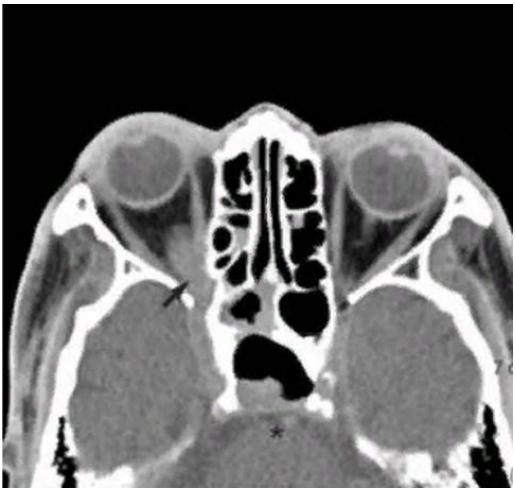

**Fig. 3.2. CT of the orbital cavities with contrast administration**

Using multi-slice computed tomography with subsequent multiplanar reconstruction and 3D reconstruction, in all cases it became possible to assess all anatomical structures of the orbit, such as: integrity of orbital bone; retrobulbar orbital tissue; ophthalmic artery; eye socket, optic nerve and extraocular muscles in static state and parameters of tumors existing in these structures.

In cases of malignant neoplasm visualization, all patients underwent chest computed tomography to find tumor spread and detect possible metastasization. On computed tomography, 1 mm sections were taken in pulmonary, mediastinal and bone modes, with multiplanar reconstruction (MPR). Figures 3.3 and 3.4 present the results of patients' chest CT examinations.

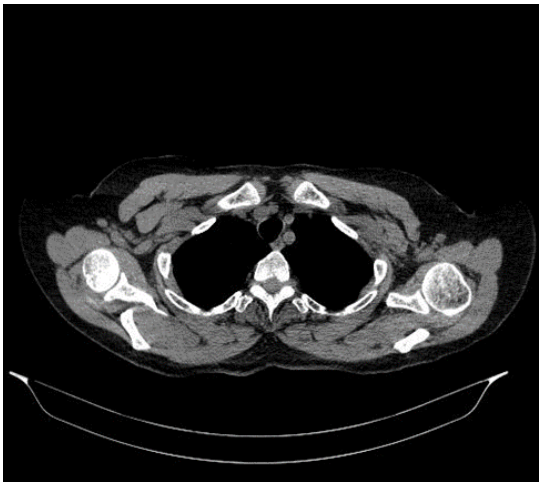

a)

b)

c)

**Fig. 3.3. Chest CT scan results of patients**

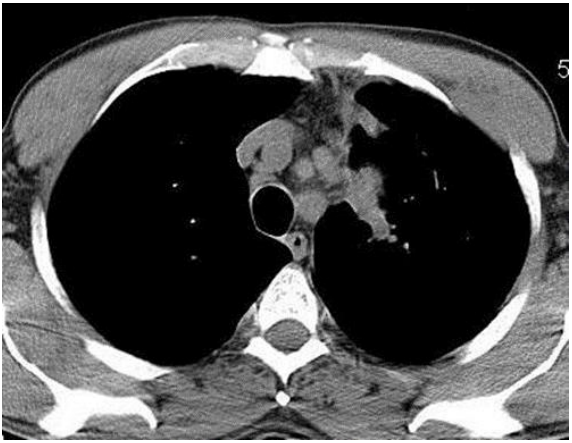

**Fig. 3.4. Non-contrast chest CT of patients**

### 3.3. Computed Tomography Examination Results

Computed tomographic examination was performed on 59 patients with primary and secondary orbital neoplasms. Of these, 38 patients had primary neoplasms, while 21 patients had secondary neoplasms.

Computed tomographic examination was the next stage of differential diagnosis following preliminary clinical and ultrasonographic studies. The objectives of the CT examination were to establish differential diagnostic signs of primary and secondary orbital neoplasms of different histogenesis, as well as to identify the spread of the tumor process to adjacent anatomical zones of the orbit.

During the study, we evaluated the following parameters:

- Localization of the neoplasm
- Dimensions of the pathological focus
- Tumor shape
- Structure of the neoplasm
- Relationship between the tumor and orbital structures

Analysis of CT semiotics of primary tumors of the orbit and eye socket (Table 3.2) revealed their common features: predominance of oval-shaped neoplasms - 68.4%, irregular shape was found in only 31.6%. The tumor surface was smooth in 78.9% of cases, nodular surface was noted in only 21.1%.

The structure of pathological neoplasms was homogeneous in 71.1% of cases. Heterogeneity of tumor structure was revealed in 28.9% of cases, with no additional inclusions detected in half of the patients, while in the remainder, low densitometric density inclusions (5-16 HU) were determined, and in isolated cases, high densitometric density inclusions (200-400 HU) were recorded due to bone tumor and/or calcified areas.

Table 3.2

Computed tomographic signs of primary formations of the orbit and eyelid

| Computed tomographic signs | | Primaqry tumors (n – 38) | |
|---|---|---|---|
| | | Abs. | % |
| Architectonics | Solitary | 36 | 94,7 |
| | Multi-node | 2 | 5,3 |
| Shape | Oval | 26 | 68,4 |
| | Irregular | 12 | 31,6 |
| Structure | Heterogeneous | 11 | 28,9 |
| | Homogeneous | 27 | 71,1 |
| Inclusions | High-density | 2 | 5,3 |
| | Low-density | 7 | 18,4 |
| | Combination | - | - |
| | No inclusions found | 20 | 52,6 |
| Surface | Smooth | 30 | 78,9 |
| | Rough | 8 | 21,1 |
| Contrast accumulation | High | 23 | 60,5 |
| | Medium | 8 | 21,1 |
| | Low | 7 | 18,4 |

During studies under conditions of intravenous bolus contrast enhancement with Omnipaque, active high accumulation of contrast was revealed in 60.5%, indicating a developed vascular network in the tumor neoplasm. In 21.1% of cases, moderate accumulation of contrast agent was noted, while in 18.4%, contrast agent was minimally accumulated or not accumulated in tumor tissue.

When analyzing the computed tomographic picture of primary neoplasms of the orbit and eye socket, depending on the morphological variant of the tumor, the following features were revealed.

All melanomas were localized in the eye socket, had a smooth surface (90.9%) and homogeneous structure. In some studies, small-sized retinal detachment was visualized. No changes were recorded in the extraocular muscles or orbital tissue.

**Clinical Study Example:** Patient A., 71 years old, presented with complaints of ptosis of the right lower eyelid, pain, and decreased visual acuity of the right eye.

During computed tomography (Fig. 3.5), a soft tissue density, slightly hyperdense (30-34 HU), homogeneous structure neoplasm was visualized in the right eye socket along the medial contour, located adjacent to the inner wall of the eye socket.

The dimensions of the pathological focus were 11x3 mm. The neoplasm had smooth, partially indistinct contours. Tumor spread beyond the eye socket was not detected, and the contours of the extraocular muscles were clear. The patient was diagnosed with choroidal melanoma of the right eye socket.

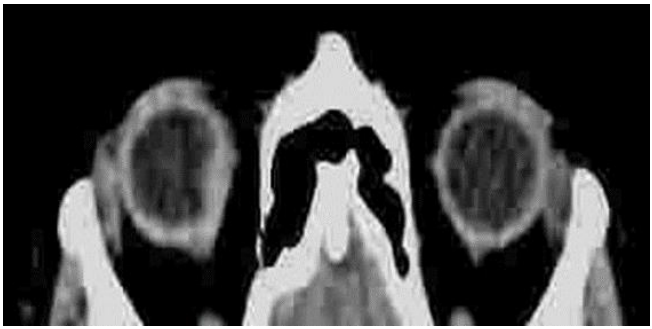

**Fig. 3.5. Patient A., 71 years old. Computed tomography fragment. A heterogeneous structure formation measuring 11x3 mm is visualized medially to the right eyelid**

Cavernous hemangioma was solitary in most cases - 92.3% of cases. The shape of cavernous hemangioma was irregular in all cases, with indistinct contours in 53.8%. The internal structure of cavernous hemangioma was mostly uniformly heterogeneous - 84.6%, inclusions were determined in 30.8% of neoplasms, while mixed-character inclusions were visualized in 15.4%.

**Clinical Study Example:** Patient M, 65 years old, presented with the main complaint of left eye proptosis.

During spiral computed tomography (Fig. 3.6), an irregularly shaped, well-defined contour tissue neoplasm was visible in the left orbit, between the left optic nerve and lateral rectus muscle, which was isodense with adjacent muscles and showed pronounced uptake of contrast agent on post-contrast sections. The neoplasm caused a mass effect on the optic nerve, causing its medial deviation and grade II proptosis. Bone invasion or hyperostosis was not evident.

**Fig. 3.6. Patient M., 65 years old. Computed tomography fragment. A tissue tumor with clear contours is visualized in the left orbit**

The patient was diagnosed with cavernous hemangioma of the left orbit.

For carcinoma arising from pleomorphic adenoma of the lacrimal gland, characteristic tumor localization is noted - in the upper outer parts of the orbit, which corresponds to the localization of the lacrimal gland.

The tumor shape was irregular with indistinct contours in 85.7% of cases. Structural heterogeneity was revealed in 71.4% of cases due to a large number of cystic structures.

**Clinical Study Example:** Patient B., 51 years old, presented with complaints of diplopia, left-sided proptosis, and decreased vision in the left eye.

Ophthalmological examination revealed conjunctival chemosis, limited movement of the eye socket laterally and upward, and narrowing of the left palpebral fissure. Visual acuity on the affected side was 0.6, on the healthy side - 1.0. Fundus showed signs of optic disc swelling. Visual field boundaries were unchanged.

During computed tomography (Fig. 3.7), a left orbital neoplasm was revealed with both cystic and solid components. The epicenter of the neoplasm was located in the projection of the left lacrimal gland. Left-sided proptosis was noted with medial dislocation of the optic nerve and extraocular muscles. Remodeling of adjacent bone was also evident, without osteolytic damage, without CT signs of intracranial spread.

**Fig. 3.7. Patient B., 51 years old. Computed tomography fragment. A heterogeneous structure tumor is visually observed in the lateral parts of the left eyelid**

The neoplasm had an irregular, indistinct contour, markedly heterogeneous structure with the presence of cystic and solid (contrast-enhancing) elements. Adenocarcinoma of the left lacrimal gland was morphologically confirmed.

In B-cell lymphoma of orbital soft tissues, oval-shaped neoplasms predominated, with clear contours in 80% of cases. The tumor was most often localized in the posterolateral parts of the orbit.

Structural heterogeneity is characteristic (80%). Low and high density densitometric inclusions were found in equal percentage ratios.

Accumulation of contrast agent by tumor tissue was high in 60% of cases, in the remaining 40% moderate, minimal accumulation of contrast or the presence of avascular component was recorded. Changes in adjacent tissues were revealed in 40% of cases - their densitometric density decrease and structural changes were noted.

**Clinical Study Example:** Patient K, 74 years old, presented to the clinic with complaints of left eye proptosis and restricted movement on the corresponding side.

During ophthalmological examination, limited movement of the left eye socket laterally and downward was noted, difficulty in eye reposition, left-sided exophthalmos within 2.1 mm, visual acuity 1.0, visual field boundaries unchanged.

As a result of computed tomography (Fig. 3.8), the obtained tomograms show a homogeneous, soft tissue left orbital neoplasm with irregular, indistinct contours, which is isodense relative to extraocular

muscles and causes left-sided proptosis and medial deviation of the eye socket and optic nerve.

**Fig. 3.8. Patient K, 74 years old, post-contrast computed tomography fragment**

The patient was diagnosed with B-cell non-Hodgkin's lymphoma, specifically MALT-associated lymphoma.

In retinoblastoma cases, irregular tumor tumor predominated, with unclear contours in 70% of cases. The tumor was most frequently localized in the eye socket and lower quadrant. Retinoblastoma is characterized by structural heterogeneity (85%).

**Clinical Case Example:** Patient L, 33-month-old boy, changes were noted during fundoscopic examination.

Computed tomography was performed (Fig. 3.9). On the unenhanced tomogram, an irregular, partially calcified soft tissue tumor with unclear contours is visible in the left eye socket. Given the patient's age and the presence of hyperdense inclusions in the tumor, retinoblastoma is practically the uncompetitive diagnosis.

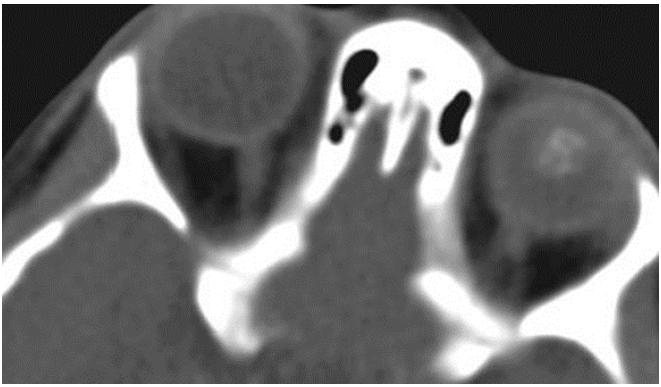

**Fig. 3.9. Patient L, 33 months old, non-contrast computed tomography fragment**

In basal cell carcinoma cases, the tumor mostly had irregular shape, with unclear contours in 80% of cases. The tumor was most frequently localized in the eye socket and parts of the lower quadrant. Structural heterogeneity is characteristic (80%).

**Clinical Case Example:** Patient E., 88 years old, presented with complaints of right eye lower eyelid pain and decreased visual acuity in the right eye.

During spiral computed tomography (Fig. 3.10), a soft tissue density tumor (25-35 HU) of heterogeneous structure was visualized along the medial contour in the right orbit, in close connection with the lower eyelid, with spread to the inner angle and eye socket.

**Fig.3.10. Patient E., 88 years old. Computed tomography fragment (with IV contrast). In the right orbit, in close contact with the inferior orbital rim, a heterogeneous, irregularly contoured, well-enhancing tumor is visualized**

The pathological focus measured 15x12 mm. The tumor had irregular, partially unclear contours. Deep intraorbital tumor spread was not detected, and the contours of the ocular muscles were clear. The patient was diagnosed with basal cell carcinoma of the lower eyelid.

Based on analysis of the obtained data, CT sensitivity for diagnosing primary tumors of the orbit and eye socket was 95%, while specificity was relatively lower at 91.4%.

When analyzing semiotic signs of tumor spread to various orbital structures, the following parameters were evaluated:

- Tumor contour characteristics
- Infiltration of extraocular muscles
- Muscle size
- Optic nerve infiltration
- Presence of changes in retrobulbar tissue
- Destruction of orbital bone walls

From the data in Table 3.3, it follows that according to computed tomography data, suspicion of extraocular muscle infiltration was present in 13.1% of cases, because no clear boundary was determined between the tumor and any muscle group, while there was corresponding muscle size increase.

In 5.3% of cases, optic nerve infiltration was suspected based on close proximity to the tumor and inability to clearly visualize it.

In 26.3% of cases, changes in retrobulbar tissue and its infiltration were revealed, accompanied by changes in its densitometric density.

In 20.5% of cases, orbital bone wall destruction was noted. Medial orbital wall destruction was recorded in 2.9% of cases, lateral wall in 7.9%, and superior wall in 7.9%. When evaluating orbital bone wall condition, it was noted that destructive changes were more frequently manifested in the lateral and superior orbital walls.

Table 3.3

Frequency of spread of primary tumors of the eyelid and orbit to various orbital structures according to spiral CT data

| CT signs | | Primary tumors (n – 38) | |
|---|---|---|---|
| | | Abs. | % |
| Infiltration of the extraocular muscles | Yes | 5 | 13,2 |
| | No | 33 | 86,8 |
| Sizes of the extraocular muscles | Unchanged | 31 | 81,6 |
| | Reduced | - | - |
| | Increased | 7 | 18,4 |
| Changes in the retrobulbar tissue | Yes | 10 | 26,3 |
| | No | 28 | 73,7 |
| Optic nerve infiltration | Yes | 2 | 5,3 |
| | No | 36 | 94,7 |
| Destruction of orbital bone wall | Medial | 1 | 2.9 |
| | Lateral | 3 | 7,9 |
| | Upper | 3 | 7.9 |
| | Lower | - | - |

Computed tomography was performed on 21 patients with secondary orbital tumors. During the study, we evaluated the following CT parameters:

- Process localization
- Tumor shape
- Structure (growth character of the tumor)
- Tumor surface
- Pathological focus contours
- Pathological tumor structure
- Presence of additional inclusions in the tumor structure
- Adjacent tissue condition
- Orbital bone wall destruction

The frequency of CT signs of secondary orbital tumors is presented in Table 3.4.

Table 3.4

Frequency of CT signs of metastatic tumors

| CT signs | | Secondary tumors (n – 21) | |
|---|---|---|---|
| | | Abs. | % |
| Architectonics | Solitary | 19 | 90,5 |
| | Multi-node | 2 | 9,5 |
| Shape | Oval | 4 | 19,1 |
| | Irregular | 17 | 80,9 |
| Structure | Heterogeneous | 15 | 71,4 |
| | Homogeneous | 6 | 28,6 |
| Inclusions | 150-350 HU | 3 | 14.3 |
| | 5-15 HU | 5 | 23.8 |
| | Combination | 2 | 9.5 |
| | No inclusions found | 11 | 52.4 |
| Surface | Smooth | 7 | 33.3 |
| | Rough | 14 | 66.7 |

Secondary tumors were more frequently localized in the inner orbital quadrants - upper-inner (27.6%) and lower-inner quadrants (23%), less frequently in the lower-outer quadrant (8.1%) and upper-outer quadrant (2.3%).

Tumor structure was mostly solitary in 90.5% of cases; multi-nodular tumors were found in 9.5% of cases.

Irregular tumor shape predominated (80.9%). Tumor structure was mostly heterogeneous (71.4%) due to the presence of low-density (5-15 HU) inclusions, and in 14.3% of cases high-density (150-350 HU) inclusions caused by calcification and pathological bone tumor. Combination of

different types of inclusions was visualized in 9.5% of cases. Neoplasm surface was mostly nodular in 66.7% of cases.

When analyzing the frequency of characteristic CT signs for secondary orbital tumors, we noted the following common criteria: solitary structure, unclear contours, and internal structure heterogeneity.

Despite common CT signs, certain differences were revealed in semiotic characteristics of different morphological forms of secondary tumors, presented in Table 3.5.

Adenocarcinomas constitute 80-90% of secondary tumors and mainly manifest as metastases from breast, prostate, and lung cancer.

In our studies, adenocarcinomas were mostly of solitary structure in 93.7% of cases. Adenocarcinoma shape was irregular in all cases, with unclear contours in 53.8%.

Table 3.5

Characteristics of computed tomography symptoms of sino-orbital tumors depending on the morphological variant of the primary tumor

| Computed tomography signs | | Adenocarcinoma (n – 16) | | Chondrosarcoma (n – 2) | | Meningioma (n – 3) | |
|---|---|---|---|---|---|---|---|
| | | Abs. | % | Abs. | % | Abs. | % |
| Tumor architectonics | Solitary | 15 | 93,7 | 2 | 100 | 3 | 100 |
| | Multi-node | 1 | 6,3 | - | - | - | - |
| Shape | Oval | - | - | 1 | 50 | 1 | 33,3 |
| | Irregular | 16 | 100 | 1 | 50 | 2 | 66,7 |
| Surface | Smooth | 7 | 43,0 | 1 | 50 | 1 | 33,3 |
| | Rough | 9 | 57,0 | 1 | 50 | 2 | 66,7 |
| Internal structure | Evenly heterogeneous | 13 | 81,3 | 1 | 50 | 2 | 66,7 |
| | Homogeneous | 3 | 18,7 | - | - | - | - |
| | Unevenly heterogeneous | - | - | 1 | 50 | 1 | 33,3 |
| Inclusions | Liquid | 5 | 31,3 | - | - | 2 | 66,7 |
| | High-density | - | - | 1 | 50 | - | - |
| | Mixed | 2 | 12,5 | 1 | 50 | 1 | 33,3 |

The internal structure of adenocarcinomas was mostly uniformly heterogeneous in 81.3% of cases, with liquid inclusions determined in 31.3% of tumor tumors, while mixed-character inclusions were visualized in 12.5%.

**Clinical Case Example:** Patient T, 45-year-old woman, presented to the clinic with complaints of left eye pain, movement restriction, and decreased vision.

During ophthalmological examination, left eye reposition was difficult, 7mm exophthalmos was noted, and limited mobility of the left eye socket medially and downward. Visual acuity was 1.0 on the healthy side and 0.7 on the affected side. Eye fundus showed signs of optic disc swelling. Visual field boundaries were unchanged.

During CT examination (Fig. 3.11), tomograms showed a soft tissue tumor with unclear contours in the left orbit, with invasion of the optic nerve and extraocular muscles. Invasion of the lacrimal gland is also suspected. The patient was diagnosed with orbital metastasis, primary source - breast cancer.

**Fig. 3.11. Patient T, 45-year-old female, computed tomography scan fragment**

When analyzing CT signs of chondrosarcoma, we obtained the following data: tumor structure was solitary in all cases, tumor shape was close to irregular in 50% of cases. Chondrosarcoma contours were unclear in 50% of cases. Internal structure was visualized as unevenly heterogeneous. In some cases, high-density inclusions (150-250 HU) were revealed in tumors, presumably caused by pathological bone tumor or calcified areas. Mixed inclusions were present in 50% of cases.

**Clinical Case Example:** Patient S., 62 years old, presented to the clinic complaining of pain in the right facial area, right facial soft tissue swelling, right-sided exophthalmos, lateral and anterior displacement of the eye socket.

During ophthalmological examination, right eye reposition was complicated, 8mm exophthalmos was noted, and limited medial mobility of

the right eye socket. Visual acuity was 0.8 on the healthy side and 0.5 on the affected side. Eye fundus showed signs of optic nerve disc swelling. Visual field boundaries were narrowed on the right.

During CT examination (Fig. 3.12), a volumetric tumor was visualized in the right ethmoid labyrinth cells, with partially unclear contours and irregular surface. The tumor spread to the medial parts of the right orbit with medial wall destruction, occupying 2/3 of the orbital volume (dimensions 39x45 mm) and displacing the eye socket laterally and anteriorly. Tumor structure is heterogeneous with multiple high-density inclusions (185-230 HU). The patient was diagnosed with: right ethmoid labyrinth cell tumor with spread to the right orbit, presumably chondrosarcoma.

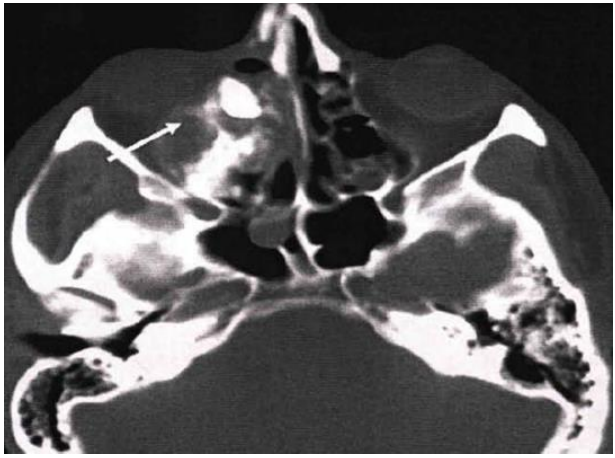

**Fig. 3.12. Patient S., 62-year-old, computed tomography scan fragment**

Basalioma was characterized by solitary tumor structure in 66.8% of cases. In all cases, the tumor had irregular shape. Neoplasm contours were clear in half the cases. Tumor surface was mostly nodular in 83.3% of cases. Internal tumor structure was either homogeneous or unevenly heterogeneous. High-density and liquid inclusions in neoplasm structure were found in 16.7%.

In meningioma cases, it was determined that tumors had both irregular shapes (56.7%) and in 33.3% of cases had correct, oval geometric shape. Contours were mostly clear (57.1%), unclear contours were recorded in 28.6%. In most cases, tumor surface was nodular (66.7%), while only 33.3% had smooth tumor surface. Internal structure was uniformly heterogeneous in

66.7% of cases. Liquid inclusions were revealed in 66.7% of cases, while mixed type was found in 14.3%.

**Clinical Case Example:** Patient F., 45 years old, presented to the clinic with complaints of left-sided proptosis.

During ophthalmological examination, left eye reposition was unchanged; no limitation of left eye socket movement was noted. Visual acuity was 1.0. Eye fundus was without pathological changes. Visual field boundaries were unchanged.

During CT examination (Fig. 3.13), tomograms show a left orbital tumor that is isodense to adjacent extraocular muscles and enhances homogeneously on post-contrast images, measuring 3.3x2.2 cm, causing left-sided proptosis and closely related to retrobulbar fat and left optic nerve. Patient diagnosis: meningioma arising from the left optic nerve sheath.

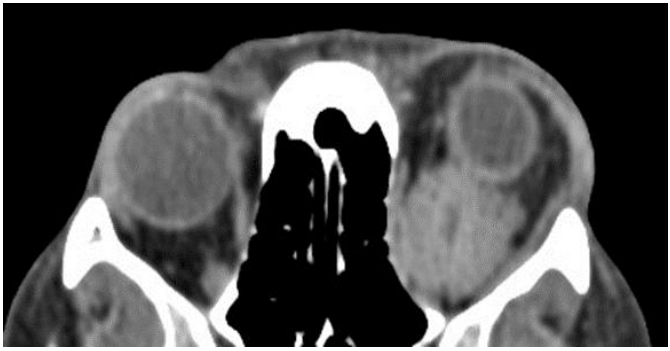

**Fig. 3.13. Patient S., 45-year-old, computed tomography scan fragment**

When analyzing secondary tumor spread to various orbital structures, the following parameters were evaluated:

- Presence of extraocular muscle infiltration
- Muscle size
- Presence of optic nerve infiltration
- Presence of changes in retrobulbar tissue
- Orbital bone wall destruction.

Data on the frequency of secondary tumor spread to various orbital structures according to CT results are presented in Table 3.6.

When evaluating secondary tumor spread to various orbital structures using CT method, the following data were obtained: In 38.1% of cases,

extraocular muscle infiltration was noted with increase in extraocular muscle size in 28.3% of cases; decrease in extraocular muscle size was not recorded.

In 19% of cases, optic nerve infiltration was revealed. In 71.4% of secondary neoplasm cases, changes in retrobulbar tissue were noted.

Table 3.6

Characteristics of metastatic tumor spread to orbital structures

| CT signs | | Sinoorbital tumors (n – 21) | |
|---|---|---|---|
| | | Abs. | % |
| Infiltration of extraocular muscles | Yes | 8 | 38,1 |
| | No | 13 | 61,9 |
| Sizes of extraocular muscles | Unchanged | 15 | 71,4 |
| | Reduced | - | - |
| | Increased | 6 | 28,6 |
| Changes in the retrobulbar tissue | Yes | 15 | 71,4 |
| | No | 6 | 28,6 |
| Optic nerve infiltration | Yes | 4 | 19,0 |
| | No | 17 | 81,0 |
| Destruction of orbital bone wall | Medial | 8 | 38,1 |
| | Lateral | 3 | 14,3 |
| | Upper | 4 | 19,0 |
| | Lower | 5 | 23,8 |

# CHAPTER 4. MAGNETIC RESONANCE IMAGING OF ORBITAL NEOPLASMS

## 4.1. Magnetic resonance imaging of tumors

In 1946, research groups from Stanford and Harvard universities independently discovered a phenomenon called Nuclear Magnetic Resonance (NMR). Its essence lies in the fact that certain atomic nuclei in a magnetic field, under the influence of external electromagnetic fields, can absorb energy and then release it in the form of radio signals. For this discovery, F. Bloch and E. Purcell were awarded the Nobel Prize in 1952. The first NMR tomograms of living human internal organs were presented in 1982 at the International Congress of Radiologists in Paris. Lauterbur was the first to demonstrate the possibility of obtaining two-dimensional images using nuclear magnetic resonance signals (NMR signals). Currently, the term "Magnetic Resonance Imaging" (MRI) is used.

Magnetic Resonance Imaging (MRI) is one variant of magnetic resonance introscopy. MRI, like computed tomography, allows us to obtain images of any layer of the human body. In the late 1970s, magnetic resonance imaging and computed tomography were proposed to improve medical visualization. Tissue imaging, as with CT, can be obtained in three planes: axial, coronal, and sagittal. Currently, MRI has significant advantages compared to CT. The slice thickness ranges from 2-5 mm, which is significantly greater than in the case of CT (0.5-3 mm).

MRI allows assessment of all parts of the visual analyzer, provides high visual resolution in soft tissue differentiation and their multiplanar examination, which, in turn, allows us to reject other methods of radiation diagnostics [7, 135]. MRI contraindications include the presence of foreign bodies with metal density incompatible with magnetic fields, both of traumatic origin (intraocular, intraorbital) and iatrogenic (cochlear implants, intracranial vascular clips, pacemakers, etc.), which can move under the influence of magnetic fields. In the contemporary world, MRI usage limitations due to operational complexity and high equipment costs are practically irrelevant, as the number of diagnostic devices has sharply increased. MRI is limited in cases of cortical bone layer, calcifications, and the presence of non-magnetic foreign bodies in the eye, orbit, and maxillofacial region.

The main components of magnetic resonance tomographs are a powerful magnet, radio transmitter, radiofrequency receiver coil, and computer. The inner part of the magnet is tunnel-shaped, large enough to

accommodate an adult human inside. Most magnets have a magnetic field oriented parallel to the longitudinal axis of the patient's body. Magnetic field strength is measured in Tesla (T) or Gauss. For clinical MRI, fields from 0.02 to 3 Tesla are used. When a patient is placed in a strong magnet, all protons (hydrogen nuclei) in the patient's body rotate oriented in the direction of the magnetic field like a compass needle. Additionally, each proton's magnetic axis begins to rotate around its own magnetic field direction. This specific rotational movement is called precession, and its frequency is called resonance frequency, or Larmor frequency (named after the French physicist).

Magnetic resonance tomogram construction occurs according to the re-emission of radio waves by hydrogen nuclei (protons) contained in body tissues, after they receive energy from radio wave signals that the magnetic resonance tomograph directs at the patient. In magnetic resonance images, contrast is determined by differences in the magnetic properties of tissues. Anatomical areas with low proton quantities, such as air-containing organs (lungs), always induce very weak magnetic resonance signals and, accordingly, are represented in black in the image. Water and other fluids that have very high proton density are represented with high intensity. However, this is not always the case. The reason for this phenomenon lies in the fact that image contrast is determined not only by proton density. Other parameters also play a role; the two most important are relaxation times T1 and T2. T1 is the longitudinal magnetization recovery time, T2 is the transverse time.

In practice, they try to obtain images that depend only on one of the relaxation times. They are called T1- (T1WI) or T2- (T2WI) weighted images. Using one or another weighted image allows changing tissue contrast. For example, vitreous body or cerebrospinal fluid is dark on T1 images but bright on T2 images. Obtaining weighted images using specific pulse sequences differs in both relaxation (TR) and echo delay times (TE). T1WI image use provides good anatomical detail, while T2WI images are good for assessing pathological processes (exceptionally, we can consider uveal pigmented melanoma, which has a specific high-intensity signal on T1WI images).

During MRI, it is possible to use intravenous enhancement methodology by introducing gadolinium-based preparations, which is particularly important for tumor process diagnostics. Tissue imaging can be obtained in three planes: axial, coronal, and sagittal, although unlike computed diagnostics, where multiplanar reconstruction is used, in

magnetic resonance tomography, each planar image is obtained independently [50, 161].

Non-contrast magnetic resonance angiography (MRA) is used to obtain images of vascular structures, and visualization principles are similar to MRI. MRA has a significant advantage - no contrast material is used during its performance and the methodology is non-invasive, its execution is possible during the MRI process. The basis for image acquisition is signal registration from stationary structures (tissues) and structures moving at different speeds.

***MRI advanatages are as follows***:

1.Particularly high tissue contrast ability based not on density but on several parameters dependent on tissues' physical and chemical properties and visualization through these changes, which are not differentiated during ultrasound and CT examination.

2.During intravenous contrasting, visualization not only of vascularization degree but also of tissues' physical-chemical properties (using perfusion, spectroscopic, and other modes).

3.Absence of bone artifacts that often cause differentiation difficulties (particularly notable are posterior fossa structures) on CT.

4.MRI shows blood flow without artificial contrasting due to sensitivity of simple modes to movement.

5.MRI has caused further reduction in invasive diagnostic examination areas.

6.MRI diagnostic capabilities expand with the use of paramagnetic contrast agents as a result of intravenous contrasting.

***MRI negative aspects***:

1.Unlike CT, difficulty in differentiating calcified foci.

2.Magnetic resonance tomography is highly sensitive to dynamic and respiratory artifacts.

3.Long image acquisition time, which is often additional discomfort for the patient and the main cause of respiratory or movement artifacts.

MRI contraindications include the presence of pacemakers in patients, foreign bodies in the orbit and skull cavity, limb prostheses incompatible with magnetic resonance tomography, since the main risk of the examination is the influence of magnetic fields on metal foreign bodies present in the organism, as well as the influence of radiofrequency fields on implanted electronic devices.

Vision plays a leading role among sensory organs. 80% of sensory perception falls on the human optical analyzer [162, 133, 145]. Traumatic and tumor damage to the orbit are the leading reasons for instrumental

visualization of this area [202, 10, 105, 248]. During patient presentation, in some cases, identification of clinical-anamnestic data is complicated, and radiological examination methodology becomes the initial and simultaneously key stage of overall picture development.

Despite the fact that practically 2/3 of orbital neoplasms are of benign nature, they can cause significant damage to the patient's sensory visualization, which leads to sharp deterioration in human quality of life [155, 86, 102, 163]. Early and correct diagnosis of orbital pathology, which is carried out through adequate, high-tech, instrumental examinations, plays the most significant role in determining treatment tactics (surgical or conservative) and avoids possible complication development (progressive infiltrative growth and destruction of adjacent bone structures) [33, 165].

For the practicing radiologist working in the contemporary diagnostic rooms, detailed knowledge of histological and imaging classical patterns of intraorbital volumetric tumors is essential. In ophthalmoradiology, main attention is devoted to using magnetic resonance tomography in diagnosing pathologies of this area, which provides not only the possibility of pathological process visualization but also histomorphological tissue characterization using various high-tech modes. The role of computed tomography should also be considered as an unalternative method for imaging microcalcifications and involvement of adjacent bone structures in pathological processes.

Knowledge of detailed orbital anatomy is important both at the diagnostic stage and at the surgical intervention planning and implementation stage. The orbit can be divided into three components: extraocular muscles that control eye socket movement; intraconal component, which includes the eye socket, optic nerve-perineurium complex, orbital blood vessels, nerves; and extraconal component - orbital bone walls, fat, and lacrimal glands [157, 164, 19].

The general computed tomographic picture of benign orbital tumors is presented in many authors' publications: According to CT results, orbital benign tumors are defined as tumors of both homogeneous and heterogeneous structure, more often of hypodense density (compared to adjacent normal anatomical structures), with clear contours. During the disease's multi-year course, remodeling of adjacent bone structure may be revealed, which has a long-term, compressive genesis of volumetric tumor. This process may also involve extraocular muscles (changes developed as a result of pressure). However, only a small number of publications characterize individual nosological forms in detail, such as vascular maltumors (orbital cavernous hemangioma), neurogenic tumors (glioma, meningioma, neuroblastoma, and

neurofibroma), orbital fibroma, orbital cystic-type neoplasms (dermoid cyst), etc.

Orbital cavernous hemangioma on computed tomogram represents a tumor of homogeneous or heterogeneous structure with clear contours, the tumor shape is oval or round, and density ranges from 37 to 47 HU. After contrasting, tumor density increases directly proportional to tumor vascularization.

Optic nerve meningioma on tomogram at its initial growth stage may have three types of growth: isolated eccentric, finger-like, and cylindrical. The first two growth types are found almost equally; cylindrical type is much less common. Sometimes mixed forms of tumor growth are described, which is presumably a manifestation of the tumor's natural growth. The density of optic nerve meningiomas averages 40 HU, contours are smooth, sharply demarcated from adjacent tissues. Tumor structure is often homogeneous, sometimes fine granulation is visually apparent [168, 137, 160].

Optic nerve meningioma with infiltrative growth has a different tomographic picture: characterized by irregular shape, neoplasm contours appear blurred. After contrasting, the degree of meningioma density increase is 39-40% [136, 35].

Fibroma has clear contours on computed tomography. The tumor structure is homogeneous, with density (30-50 HU) increasing after contrast. It is typically located in the posterior parts of the orbit. On tomography, dermoid cysts have a round shape with smooth contours and are located in the upper outer part of the orbit. Linear or convoluted dense structures are identified within the cyst thickness, cystic areas with mixed density, sometimes with fatty inclusions, and do not absorb contrast material [115, 126].

Since primary malignant orbital tumors do not exceed 0.1% of all human malignant tumors, publications regarding their computed tomographic semiotics are scarce, which should also be attributed to the active introduction of magnetic resonance imaging as a leading diagnostic tool in oncoophthalmology [120, 131, 132].

Among modern imaging methods, the high diagnostic role of magnetic resonance and positron emission tomography should be noted in the diagnosis and differential diagnosis of volumetric tumors of the eye and orbit. The use of such magnetic resonance imaging regimes as T1WI, T2WI, FLAIR/STIR, post-contrast T1-weighted imaging with fat suppression, post-contrast perfusion study, DWI and ADC map use in some cases provides not only the possibility of identifying the tumor, but also studying its functional and morphological characteristics [97, 56,167].

Retinoblastoma is the most common malignant orbital tumor in the pediatric population. Magnetic resonance imaging is the gold standard method for both identifying retinoblastoma dimensions and determining the possible degree and boundaries of extracurricular spread of the tumor and optic nerve infiltration. On T2-weighted images, retinoblastoma is somewhat hypointense compared to the vitreous body and cerebrospinal fluid. Calcified areas existing within the neoplasm thickness are hypointense in T1WI and T2WI regimes. It should be noted that for visualization of the calcified part of the neoplasia, computed tomography exceeds magnetic resonance tomography, considering the physical properties of calcinates and fundamental mechanisms of X-ray exposure [ 32, 98,]. In T1WI regime, retinoblastoma is iso/hypointense compared to adjacent structures, easily/moderately absorbs contrast material on post-contrast sections and markedly restricts diffusion in DWI regime with low ADC indicators, indicating its hypercellular nature. Radiologically, both types of tumor growth should be assessed and noted - endophytic (in the vitreous body) and exophytic[ 24, 11, 100].

Accurate assessment of optic nerve infiltration on magnetic resonance imaging is complicated. Contrast enhancement of the optic nerve does not directly correlate with the involvement of the latter in the process. However, recent studies have shown that contrast enhancement of the anterior chamber may secondarily indicate tumor infiltrative invasion in the mentioned structure [52, 133, 137].

Optic nerve involvement in the process is associated with poor prognosis. According to nerve invasion, the mortality rate ranges from 13% to 89%. The lethality rate largely depends on the boundaries of surgical resection [54, 141]. In clinical ophthalmology, there are several classifications of retinoblastomas: International Classification of Intraocular Retinoblastomas (IIRC) and Classification of Intraocular Retinoblastomas (ICRB). This differentiation is based on their dimensions, growth type, and invasion indicators in adjacent structures [101, 102].

In adult patients, the most common malignant volumetric tumor - uveal melanoma - is characterized by different magnetic resonance and computed tomographic signs. Recently, ultrasound diagnostics of this neoplasia is practically no longer used in daily ophthalmo-oncology, considering the limited area of the obtained image and the inability of morphofunctional characterization [33, 25, 78, 41, 150]. In all countries of the world, MRI study methods are considered the gold standard for diagnosing pigmented and apigmented uveal melanoma. The classic MRI sign of intraocular melanoma is a hyperintense signal with clear contours

(relative to the vitreous body) on pre-contrast T1WI images. The existence of this signal in neoplasia is based on the presence of melanin pigment, which is sensitive to T1WI relaxation time. The tumor moderately absorbs contrast material, although determining the volume of contrasting is complicated due to melanin's naturally hyperintense signal. To reliably determine tumor contrasting in modern radiological departments, the so-called subtraction method is often used, which is obtained by mutual subtraction of post- and pre-contrast regimes.

The polymorphism of uveal melanoma determines its growth type and, accordingly, the diversity of radiological imaging. Small melanomas may remain unchanged with unchanged visualization indicators for a certain period along with high potential for scleral infiltration [151, 88, 47, 62]. Rapidly growing tumors may spread in the extracellular space existing between the retinal pigmented epithelium and choroid and disseminate in the subretinal space, acquiring typical mushroom-like configuration [71, 27, 16, 142]. Unlike melanomas with mushroom-like configuration, dome-shaped melanomas are mainly characterized by compressive growth on adjacent orbital structures [75, 74, 34, 147].

On T2WI images, uveal melanoma is slightly hypointense relative to the vitreous body. Retinal detachment and combination with subretinal fluid collection is frequent. When describing the tumor, it is important to assess melanoma in axial, sagittal, and coronal sections for adequate assessment of exact localization and degree of invasion in adjacent structures. The main difficulty in diagnosing melanoma is its pigment-poor or apigmented type. This subgroup of neoplasia does not show the hyperintense signal characteristic of pigmented melanoma in T1WI regime, making clinical-ophthalmological studies the decisive diagnostic method [112, 59, 31, 160].

Orbital lymphomas are characterized by special tomographic signs and anatomical localization types. According to research conducted by Priego and his colleagues, among lymphoma intraorbital localizations, the leading place is occupied by the lateral-superior quadrant (59%), the superior-medial quadrant was secondarily involved in the process (26%), while involvement of the orbital caudal parts in the process was observed only in 19% [174, 140, 6, 92]. Unilateral spread was found in 95% of patients, bilateral only in 1 patient - 5%. According to the classic anatomical division of the orbit, extra- and intraconal types of tumor spread are distinguished. Extra-intraconal spread was noted in 47% of patients; isolated extraconal in 42% and intraconal in 11%. The percentage of orbital structure involvement in the process was represented as follows: superior rectus muscle - 59%, eyelid -

57%, and lacrimal gland - 47% [114, 237, 128, 108]. Intracranial, dural spread of orbital lymphomas is also described in literature [5, 15, 74, 104].

On magnetic resonance and computed tomographic images, lymphoma is visualized as a well-demarcated, homogeneous tumor of lobulated structure, which is tightly wrapped around adjacent anatomical structures. As a rule, erosion of orbital walls is not manifested. On CT study, lymphoma is isodense with adjacent muscles and markedly, homogeneously absorbs contrast material. Similar are the visualization data of T1WI, T2WI, and post-contrast regimes. The iso/hypointense signal of lymphoma in T1WI regime is caused by its hypercellular matrix. Rich cellular content causes high signal in DWI regime and marked restriction of diffusion coefficient on ADC maps [133, 109, 83, 4].

The radiological signs of neurogenic etiology intraorbital tumors are somewhat different. Optic gliomas, which belong to slowly growing pediatric population tumors, on computed tomography, in bone regime, show the phenomenon of optic canal widening. On magnetic resonance tomography, the optic nerve is fusiformly dilated and deformed. Contralateral (with healthy side) comparison is a significant auxiliary nuance in identifying anatomical changes of the optic nerve. In T1 regime, the tumor is iso or slightly hyperintense compared to the healthy side and hyperintense relative to the brain cortex in T2WI regime during study. On post-contrast sections, visible contrast enhancement is not manifested. T1WI regime without fat signal suppression is the best means for describing and measuring optic nerve changes, at the expense of the latter's high anatomical informativeness. Normally, in the pediatric population, the maximum transverse diameter of the optic nerve does not exceed 5mm. Calcification and hemorrhages are extremely rare [44, 42, 129].

In practical radiology, great importance is given to which segment of the optic nerve is involved in the tumor process and how much other associated changes of orbital gliomas as possible systemic manifestations are manifested in the visualized part of the study [44, 164, 81].

Meningiomas arising from the optic nerve sheath are characterized by homogeneous, isointense signals in T1WI, T2WI regimes. On post-contrast anatomical regimes, intraorbital meningiomas show homogeneous contrast enhancement. Computed tomography is useful for identifying intratumoral calcinates. The directly preserved optic nerve may be located in the center of the tumor or eccentrically relative to it. Post-contrast T1WI with fat signal suppression is considered the gold standard for diagnosing optic nerve meningiomas [141, 53, 158, 134]. Meningiomas are characterized by segmental or diffuse, circular thickening of the optic nerve sheath, which

represents the specific sign of "tram track" [117, 146, 66, 102]. In differential diagnosis with optic nerve gliomas and intraorbital lymphomas, calcified foci and marked, homogeneous contrasting type play a significant role.

Optic schwannomas represent a small part of neurogenic tumors. Despite the scarcity of clinical cases, considering potentially locally aggressive growth, detailed knowledge of radiological signs characteristic of this group of tumors is important. On magnetic resonance tomography, schwannoma is represented by iso/hypointense signals in T1WI, markedly high-intensity signals in T2WI, as a non-homogeneously contrasting, lobulated tissue tumor. Special importance is given to conducting radiological differential diagnosis with cavernous hemangiomas, which in some cases is complicated [118, 130, 43, 1]. Computed tomography has the role of assessing adjacent bone structures and planning surgical procedures in schwannoma diagnostics. The density of the neoplasm itself is isodense with the density of orbital muscles [2, 113, 142].

Among lacrimal gland tumors, adenocarcinomas of this region should be noted that are tomographically represented as tissue masses with clear contours, homogeneously contrasting, in rare cases partially calcified. Destruction of adjacent bone structures is typical for this group of tumors. On magnetic resonance tomography, these neoplasias are imaged with hypointense signal in anatomical and hyperintense signal in T2WI regime. Computed tomography helps us accurately assess damage to adjacent bone structures [149, 96, 65].

The first case of orbital metastases was considered by Horner in 1864 as a result of hematogenous dissemination of lung tumor [14, 85, 156]. Orbital metastasization in frequency does not lag behind pathologies of similar etiology in the uveal region, although in recent years the number of secondary tumor damage to the orbit described in literature is increasing, which should be associated with the availability of high-tech diagnostics. It is believed that cases of orbital metastasization somewhat exceed the statistical data existing in literary reports. Such a phenomenon is directly proportional to the subclinical course of small intraorbital and intraocular tumors and difficulties in interpreting ophthalmoradiological studies.

Shields, together with his colleagues, conducted a study that included 100 patients with secondary tumor disease of the orbit. The leading position was occupied by breast gland tumor confirmed by biopsy. Prostate gland tumor appeared in second position, followed by lung and melanoma malignant tumors [167,111]. In Henderson's study, bronchogenic carcinoma occupied the second position by frequency of metastasization primary source, while Goldberg named skin melanoma, after lung tumors, as the most

common cause [87, 101, 42]. Completely different data were obtained by a study conducted in China, where nasopharyngeal region tumors took the leading position [121, 168]. Such variation in the obtained data may be based on the different geographical location of the studied patients [63, 137].

Instrumental diagnostics of orbital metastasis is one of the most complex challenges in contemporary radiology. Correct interpretation of obtained tomograms becomes even more complicated in cases where there is no primary tumor in the medical history. It has been established that the number of such patients ranges from 19 to 25% [87, 116]. In such patient populations, initial ophthalmological and laboratory studies are of great importance. In the group of non-diagnostic primary neoplasms, the histological type discovered after morphological verification is hepatocellular carcinoma in one-third of cases [87, 115].

Magnetic resonance imaging is the method of choice for morpho-functional characterization of metastatic tissue. Using contemporary regimens (DWI, ADC, post-contrast T1WI, perfusion studies), it is possible to determine the mitotic and necrotic activity of the tumor, as well as identify its vascularization and the degree of infiltration/invasion into adjacent soft tissues. Metastasis is not characterized by pronounced selective anatomical localization and may be located in any segment of the eye and orbit. In cases of infiltration of extraocular muscles and/or destruction of orbital walls, the probability of secondary genesis of the tumor is high. Metastatic tumors of renal cell carcinomas and melanomas are often represented by well-circumscribed tissue tumors, which distinguishes them from neoplasms of other etiologies. All tumors of secondary genesis show signal intensity enhancement in post-contrast T1WI regimen, with homogeneous or heterogeneous type of contrast uptake (in cases of intratumoral necrosis). In prostate tumors, computed tomography is useful for assessing osteoblastic metastasis. Osteoclastic activity is frequent in hepatocellular carcinomas with orbital wall thinning, erosion, and destruction [64]. The final diagnosis is based on histo-morphological results of fine-needle aspiration biopsy. Individual cases of tumor dissemination during biopsy sampling have been described [123, 151]. In cases of widespread systemic neoplastic process, biopsy material collection loses its relevance and the diagnosis is based on instrumental imaging results.

Puncture biopsy is considered the gold standard method for diagnosing and classifying rhabdomyosarcomas. However, computed and magnetic resonance imaging studies are significant methods for early assessment of tumor detection, its anatomical and growth characteristics. On non-contrast computed tomography, rhabdomyosarcomas are slightly

hypodense compared to adjacent extraocular muscles, with pronounced increase in Hounsfield values on post-contrast images. In T1WI regimen, rhabdomyosarcoma is isointense relative to extraocular muscles and hypointense compared to orbital fat, with pronounced hyperintense signal in T2WI regimen. In cases of nasal-maxillary and paranasal sinus wall destruction, computed tomography is the diagnostic method of choice. For assessing existing intratumoral microhemorrhages in alveolar and pleomorphic subtypes, magnetic resonance imaging (SWI) and computed tomography are distinguished by high sensitivity.

Among intraconal benign tumors, the diagnostic characteristics of venous varices should be distinguished. Dilated venous vessels may manifest primarily or secondarily during intracranial pathologies. The expanded venous network is mainly of unilateral distribution, though literature describes cases of bilateral orbital involvement [168]. Primary venous varices are of congenital genesis and mainly involve one specific vessel. Secondarily developed changes mainly develop during diseases with increased blood flow velocity, such as arterio-venous maltumors and carotid-cavernous fistulas with orbital vein involvement [136, 106]. From medical history data, episodes of transient diplopia and position-dependent exophthalmos should be considered. Acute complications include intraorbital thrombosis and hemorrhage. During such disease course, clinical symptomatology is presented as disorientation in time and space, visual disturbances, and suddenly onset retro-orbital pain. It should be noted that under venous hypertension conditions, varices increase in size, while normotensive periods cause their collapse. This explains the temporal changes in imaging signs of venous varices. Under normal pressure conditions in the venous system, detection of pathological changes on computed and magnetic resonance tomography may be complicated. In such situations, provocative tests, Valsalva maneuver, and internal jugular vein compression are useful [133]. Negative data from tomograms obtained in supine position do not exclude the existence of orbital varices, and in cases of high clinical suspicion, provocative tests should be performed directly during imaging acquisition. On pre-contrast computed tomography, dilated veins are visualized as hypodense tumors, whose contrast enhancement type is similar to adjacent veins. On magnetic resonance imaging, varices are hypointense in T1WI, T2WI regimens, with pronounced hyperintense signal on FLAIR/STIR images. In cases of phleboliths and dynamic changes in tumor size, the degree of correct diagnosis is very high [133, 152].

Among other vascular genesis diseases, orbital cavernous hemangiomas (maltumors) should be mentioned. Cavernous hemangiomas

constitute 5-8% of orbital tumors. Most cases occur in middle-aged patients. Due to slow growth rate, patient complaints are related to gradually increasing proptosis over years, partial visual field defects, and diplopia. Cavernous maltumor may be encountered in any part of the orbit, however, as we will highlight in the anatomical classification of pathologies, the priority localization of hemangiomas is the intraconal segment of the orbit. In typical cases, they are encapsulated. On computed tomography, they are slightly hyperdense compared to adjacent muscles. Bone remodeling phenomenon and microcalcifications may be revealed [153]. It is represented by heterogeneous signal on pre-contrast T1, T2 regimens of magnetic resonance imaging, with moderate, gradual signal enhancement on post-contrast T1WI regimen. Correct radiological interpretation of the disease is also important because the size of the tumor, degree of pressure on adjacent structures, and bone remodeling determine the choice of treatment type [123].

Unlike cavernomas, the main localization of capillary hemangiomas is the extraconal part of the orbit [20, 9]. Capillary hemangiomas are usually located ventral to the eyelid and are easily noticeable on inspection. Only when hemangioma is represented as a large tissue tumor involving an extraorbital component do visualization tools actively participate in diagnostics and treatment planning. Clinically, superficial, deep, and mixed forms of capillary hemangiomas are distinguished. Superficial tumors (up to dermis) acquire characteristic blue coloration by external observation. Deeply located maltumors are invisible to the eye and are diagnosed by clinical-instrumental visualization methods [76].

On MRI T-regimens, capillary hemangioma is represented as extraconally located, well-defined, lobulated tissue hyperintense tumor. The presence of septa is typical. One of the characteristic signs is pronounced, homogeneous contrast uptake in the neoplasm due to the presence of vascular flows. Adjacent bone structures are intact. Calcifications are very rare [133].

Among extraconal tumors, the most common congenital neoplastic tumor is dermoid cysts. They form as a result of epithelial sequestration and are mainly located between the eyelid and lateral orbital wall. They mainly grow slowly. Rupture of the tumor is possible, which often mimics acute inflammatory process. Small dermoids do not require specific intervention and are subject to surgical resection up to 3 years of age. It is important to resect the tumor without violating its integrity to avoid local inflammatory reaction and disease recurrence. Macroscopically, dermoid cysts are fat-containing round or oval encapsulated new tumors. Along with clinical signs, radiological analysis of the neoplasm is important. In cases of superficial dermoid, ultrasound examination may be performed. Magnetic resonance and

computed tomography are mainly used in cases of large tumor size and compression of adjacent structures. On tomographic examination, dermoid cyst has fat density and clear borders. In T1WI, T2WI regimens, dermoid cyst is hyperintense, with signal suppression in FLAIR/STIR regimens, which completely replicates subcutaneous fat MRI data [44, 107]. Despite individual cases described in literature, pathological diffusion restriction is mainly not manifested.

Despite the smallness of the eye and orbit as an anatomical region, its complex structural-functional construction and the multi-etiological nature of developed diseases remain a great challenge for contemporary diagnostic radiology. Clinical and, in many cases, imaging signs of many neoplastic diseases are similar. Considering this reason, it is important to determine not only the location, size, and shape of the tumor, but also to identify its functional and some histological characteristics for correct differential diagnosis.

Regarding magnetic resonance imaging, in an article published by Xian, the leading role in differential diagnosis of orbital tumors was based on post-contrast regimen results [144]. The study included 102 patients with orbital tumors. All underwent intravenous contrast administration. The final diagnosis was based on histo-morphological results in correlation with MRI data. The study was conducted with 1.5 Tesla GE (General Electric) Signa with 8-channel head coil. All patients underwent pre-contrast T1WI and T2WI with 3mm slice thickness and 0 interval between slices. Matrix resolution was 288x256. Field of view was 16cm [144]. As a result of combined analysis of obtained data, an assumption was expressed about high correlational accuracy of correct interpretation of post-contrast slices, with sensitivity of 83% and specificity of 88% compared to biopsy data [144]. Despite Simon's assumption about the ineffectiveness of instrumental studies in final diagnosis verification [23], considering the relationship of tumors with adjacent structures and contrast enhancement type, it is possible to determine the general nature of neoplasm with high specificity [162]. For malignant tumors, such radiological signs include preseptal space location, unclear borders, close connection with adjacent structures, isointense T2 signal, homogeneous contrast enhancement, and presence of wash-out phenomenon. Special importance is given to comparing tumor signal with extraocular muscles on T2 images. For example, primary orbital lymphoma presents with various presentation variations. However, this study established isointense signal of tumor relative to extraocular muscles in all patients with lymphoma, which contradicts previously existing views [153].

In differential diagnosis of lacrimal gland tumors, importance is given to tumor size. Mainly small-sized tumors with clear borders reveal benign nature, contrary to malignant tumors characterized by large size, unclear borders, and destruction of adjacent bone structures [105]. From obtained data, we can conclude the significant role of intravenous contrast administration in determining the degree of tumor malignancy and high correlational data of post-contrast anatomical images with final histological results. However, in some cases, small malignant tumors do not show wash-out type contrast enhancement and do not cause bone structure destruction. In such cases, combined inclusion of other contemporary regimens in the diagnostic algorithm is necessary.

In a study conducted by Ro Sa-Ra and colleagues, emphasis was made not only on differentiation by tumor contrast enhancement type, but also on the role of magnetic resonance imaging as a multiparametric diagnostic method in differential diagnosis of orbital tumors [134]. The final study cohort included 65 patients, whose scanning was performed on a 3 Tesla Siemens apparatus [124]. An inverse proportional relationship of malignant tumors with ADC map data was established. Diffusion map parameters of benign tumors significantly exceeded corresponding data of malignant tumors [184]. Data obtained through DWI regimen is an indicator of tissue cellularity (cellular matrix) degree. In highly cellular tumors, restriction of free diffusion of water molecules causes increased signal in DWI regimen and hypointense signal on ADC maps. However, diffusion regimen data, from a physical standpoint, largely depends on T2 regimen, which often causes the so-called influence phenomenon of the latter. To avoid such effect, b-factor is used in magnetic resonance tomograms. Increasing b-factor is directly proportional to reducing T2 regimen influence. Considering all described phenomena, in contemporary radiology, ADC maps are given decisive importance for determining tissue cellularity. Study results confirm the high diagnostic significance of diffusion restriction degree in determining the nature of orbital tumors, increasing the degree of confidence of practicing radiologists in study interpretation and creating a clear understanding of tumor cellular matrix [164].

In the diagnostic algorithm, special attention is paid to fat suppression regimens - FLAIR/STIR. Such technique involves signal suppression from fat in regimens where fat is represented by hyperintense signal. STIR/FLAIR regimens are a significant part of standard orbital protocol, through which easy identification of fat-containing tumors (dermoid cyst) is possible compared to pre-suppression images. In optic nerve complex assessment, with fat signal suppression, easy identification of small contrast-enhancing

areas is possible. STIR/FLAIR regimens are the gold standard method in diagnosing optic neuritis and neoplasms in this area. Accurate assessment of signal from perioptic cerebrospinal space is crucial in diagnosing idiopathic intracranial hypertension [119].

CISS/FIESTA are high-resolution magnetic resonance imaging regimens that enable detailed, three-dimensional imaging. Considering the sharp hyperintense signal of cerebrospinal fluid, easy detection of associated tumors is possible. Seitz J and others clearly demonstrated optic disc protrusion in the eye socket, with sharp differentiation from orbital fat, optic nerve sheath, adjacent cerebrospinal fluid, and optic chiasm in patients with clinically diagnosed papilledema [166]. Additional advantages include short acquisition time and suppression of artifacts from cerebrospinal pulsation. In clinical radiology, high-resolution images are used in diagnosing cranial and optic nerve schwannomas, meningiomas, and optic gliomas [119].

In work published by Purohit BS on the role of multiparametric visualization in diagnosis and differential diagnosis of orbital tumors and tumor-like diseases, attention is paid to distinguishing signs based on anatomical compartment [135]. Among malignant eye socket tumors, retinoblastoma is distinguished by characteristic CT and MRI signs. Classic radiological signs providing reliable differential diagnostic signs are related to pathophysiological characteristics of the tumor. Rapid growth of retinoblastoma, disproportionate to vascularization degree, causes appearance of intratumoral necrosis and calcifications (90% of cases). Described intratumoral changes cause presence of hypodense and sharply hyperdense (calcifications) areas in the tumor on computed tomography. DWI regimen examination reveals pathological diffusion restriction with hypointense ADC parameters from the contrasted part. No other disease causing leukocoria is characterized by such imaging signs [155]. Differential diagnosis of pigmented, malignant uveal melanomas usually does not present difficulties due to hyperintense signal of melanin protein sensitive to T1 relaxation time. Melanoma diagnostic difficulties arise in its pigment-poor or apigmented forms. In such cases, ophthalmoscopic examinations are rational differential diagnostic tools [155].

Fibrous dysplasia (FD) is an osteogenesis disorder where normal bone marrow is replaced by fibro-osseous tissue with medullary canal expansion. Cranio-facial fibrous dysplasia usually involves frontal, ethmoidal, or sphenoidal bones. It mainly manifests in children and adolescents. 70-80% of FD cases are monoostotic, while the rest are polyostotic. Orbital wall involvement causes hypertelorism, exophthalmos, vision impairment, and

blindness. Surgical intervention is necessary in cases of facial deformity or severe optic nerve compression.

FD shows replacement of lamellar bone with pathological metaplastic immature bone, which during histological examination creates irregular non-linear trabeculae; this histological picture is described as “Chinese hieroglyphs”. The fibrous part contains spindle-shaped cells without significant mitotic activity. Possible complications of fibrous dysplasia include bleeding and cystic degeneration.

Radiography and CT show medullary canal expansion with specific densitometric ground-glass effect. Optic nerve compression may occur with canal stenosis and optic nerve damage. Fibrous stroma and osteoid material usually appear hypointense on T1W images. On T2W images, signal intensity may be low (18-38% of cases), intermediate (18%), or high (62-64%). Similar to benign head and neck tumors, FD shows significantly high ADC values compared to malignant bone tumors [135].

Inflammatory orbital pseudotumor (IOP) is the most common cause of painful orbital tumor in adults and the third most common orbital disease after thyroid ophthalmopathy and lymphoproliferative disorders. IOP represents a benign, non-infectious inflammatory disease without identifiable local or systemic causes and usually manifests in the 4th-6th decades of life. The disease may manifest as scleritis, uveitis, lacrimal gland adenitis, myositis, perineuritis, or diffuse orbital inflammation. The classic clinical triad consists of unilateral orbital pain, proptosis, and eye movement disorders. Associated fibrous mediastinitis or retroperitoneal fibrosis may develop. IOP diagnosis is made after excluding other pathologies such as thyroid ophthalmopathy, lymphoma, Wegener's granulomatosis, and sarcoidosis.

IOP is histologically characterized by mixed inflammatory infiltrate consisting of lymphocytes, plasma cells, macrophages, and eosinophils. Fibrosis may also manifest. Imaging results may be non-specific. On CT and MRI, orbital pseudotumor may be visualized as contrast-enhancing orbital mass with adjacent fat infiltration and contrast enhancement of the lacrimal gland and optic nerve sheath. Extraocular muscles are usually enlarged and show contrast uptake. The inflammatory contrast-enhancing component is typically hypointense relative to fat on T1W images and iso/hypointense on T2W images. Extension of the process to the nasopharynx and cavernous sinus is possible.

IOP is an excellent imitator of several other pathologies [146]. The differential diagnostic list includes myositis caused by other etiological factors (thyroid ophthalmopathy, infectious cellulitis) and other T2-

hypointense infiltrative lesions (lymphoma, IgG4-RD and granulomatous diseases). Thyroid ophthalmopathy causes bilateral inflammation of extraorbital muscles, most commonly the inferior and medial rectus muscles, with preservation of muscle-tendon junctions and is associated with elevated thyroid hormone levels. IgG4-RD (immunoglobulin G4-related disease) can manifest signs similar to thyroid ophthalmopathy with normal thyroid-stimulating hormone levels. Infectious cellulitis is usually accompanied by fever, leukocytosis and, in some cases, abscess tumor. Clinical signs such as pain, conjunctival and eyelid swelling allow differentiation of IOP from lymphoma, which usually presents as a painless palpable mass. As already noted, ADC values help us accurately distinguish between IOP and lymphoma.

Despite the development of new medical imaging methods, ultrasound examination remains the most practical and frequently used method for assessing eye condition in practical ophthalmology, as it enables objective assessment of intraocular structures. This is particularly relevant when assessing the eye socket, when the transparency of light-transmitting structures is significantly reduced. Ultrasound examination methods are currently considered the most accessible and safe investigation. Such studies must necessarily be conducted taking into account the biological effects of ultrasound on eye structures. According to many researchers, the use of ultrasonic waves for diagnostic purposes in pulsed mode is completely safe even during prolonged examinations. Ultrasound effects on eye structures during diagnostic procedures are significantly less than therapeutically acceptable values (0.3 W/cm²) and constitute only 2-3 mW/cm².

High-frequency transducers (7.5-12.5 MHz) are used for ultrasound examinations in ophthalmological practice. After ultrasonic waves pass through eye structures, part of them is reflected and returns to the emission source as a reflected wave, is converted into an electrical signal, which is then used for image tumor. The characteristics of ultrasound images of eye structures depend on their size, shape, structure, and acoustic impedance. B-scan devices with digital image processing have high sensitivity and informativeness. They enable reliable assessment of the anterior eye segment, determination of vitreous body opacity localization, density and mobility, diagnosis of intraocular hemorrhages, which are extremely difficult to recognize using traditional radiological methods. Pathological processes identified by this method are confirmed in 96% of cases according to all anatomical parameters. The use of digital diagnostic technologies has significantly improved the quality of images of objects to be analyzed and eye tissues. Visualization of small eye structures, simultaneous fixation of

static anatomical elements and blood movement became possible. With the help of color and power Doppler mapping, as a result of contrasting individual structural elements of the eye socket and orbit, it is possible to differentiate choroidal and retinal structures, assess the topography of ophthalmic artery branches, and also identify zones of pathological neovascularization. Two-dimensional echography performed using the B-system (two-dimensional imaging system) allows us to obtain an acoustic cross-section of the eye in a given scanning plane. Indication is performed using CRT, which converts echo signals into video images. During the examination, reflected echo signals are scanned and sequentially recorded, which together create an image of the eye and its structural components in one tomographic plane on the monitor.

G. Baum and I. Greenwald first reported the detection of orbital tumors by B-scan method in 1958 [89]; diagnosis was confirmed in 80% of patient cases.

B-mode ultrasound examination allows determination of pathological focus localization, morphometry of eye structures and pathological tumors in the orbit, and determination of the degree of its spread. Schroeder examined 155 patients with orbital diseases using two-dimensional echography and obtained data that allowed him to characterize expansive and infiltrative processes in the orbit.

Working in B-mode significantly simplifies spatial orientation of tissues under study and provides the possibility of topographic characterization of processes occurring in the orbit. According to many authors, the main sign of a space-occupying tumor in the orbit during B-scanning is a contour echogram of various shapes with internal echo signals of different brightness in the corresponding part. Rapid-growing dense tumors show pronounced eye detumor. Based on the nature of echo signals from the external boundaries of orbital space-occupying tumors and from their internal tissue structures, we can distinguish solid, cystic, vascular, and infiltrative types of tumors. Echographically, a typical example of a cystic tumor is neuroma, which has low reflectivity. The tumor is dense and connected to the optic nerve, characterized by slow growth within the muscle part and causes eye socket detumor. In cases of meningioma and optic nerve glioma, an acoustically inhomogeneous sonographic picture is noted, and according to multiple data, the match between sonographic and clinical diagnoses is 68%.

Cavernous hemangioma has high reflectivity, irregular internal structure, and can cause insignificant eye socket detumor. Orbital sarcoma often lacks clear boundaries, is characterized by very rapid growth, and

causes severe eye detumor. Additionally, small malignant tumors may have a whole range of characteristics of benign neoplasms.

Based on the results of using ultrasound examination in ophthalmology, this method can be highly evaluated for its diagnostic value [159]. As K.S. Ossoinig notes, using standardized echography, it is possible to detect tumor tissue of 3-5mm size in the orbit, which indicates the high sensitivity of the method [12].

Many works are devoted to improving ultrasound diagnostic methods for oncological diseases of the eye and orbit. In addition to assessing the size, delineation, and area of intraocular neoplasms, echograms can be used to assess tumor structure and scleral condition.

A-mode studies make it possible to differentiate between different types of orbital tumors and pseudotumors. The diagnosis of orbital vascular tumors can be clarified by Doppler studies of blood flow in orbital arteries; specifically, Doppler symptoms of carotid-cavernous anastomosis are described in the literature.

Ultrasound examinations conducted by various authors have shown that lacrimal gland pseudotumor occupies an intermediate position between infiltrative and solid tumors in terms of acoustic properties. In more than half of the patients, a “lobular” structure of pseudotumors was revealed in the form of acoustic voids, some of which are characteristic of solid tumors, others - of infiltrative ones. This may be caused by different severity of inflammatory events, the presence of fibrosis and sclerosis of lacrimal gland tissue.

The choice of one or another ultrasound visualization method depends on the specific objectives of the study. Accordingly, editing of ultrasound images of the eye received on the screen takes place: initially, three-dimensional images of the eye were obtained by combining acoustic sections of bistable images. Now three-dimensional images are created by direct input of echo signals into the computer's operational memory.

According to S. Maslak, computer sonography represents an alternative to traditional ultrasound imaging. The first commercial devices of this type appeared in the second half of the 1980s. Currently, rapid scanning devices are used, or, as they are more often called, real-time operating devices. Their advantages are: the ability to directly observe the movement of organs and structures; reduction of examination duration; the ability to work with small acoustic windows. They provide blood flow Doppler regimes: continuous wave, pulsed wave, and color Doppler mapping [166, 153].

Computer sonography allows: 1) B-scanning of tissue structures; 2) examining tissues in color Doppler mapping and power Doppler regimes; 3) detailed study of hemodynamics. The advantages of the computer sonography method are: 1) examination speed; 2) no significant pressure on the eye socket; 3) objectivity, high speed and accuracy of simultaneous processing of multiple parameters; 4) complete visual control of all characteristics in real time; 5) high sensitivity with minimal exposure intensity.

Among tumors of the anterior part of the orbit, conjunctival retention cysts are often encountered, whose diagnosis is not difficult. Echographically, cysts are round or oval anechoic inclusions with clear, uniform contours and mostly thin-walled capsules, which usually do not contain internal echostructures and provide distal acoustic enhancement. From an echosemiotic standpoint, conjunctival retention cysts do not differ from simple cysts of other localizations, including retrobulbar ones.

In addition to retention and dermoid cysts, malignant lymphomas are easily recognizable echographically, which usually arise from conjunctival lymphoid tissue. They represent diffuse or focal accumulation of lymphocytes or lymphocyte-like cells and are part of systemic damage. Cellular composition determines the low echogenicity of lesion foci, which are sonographically similar to, for example, areas of lymphoid infiltration in the thyroid gland during cellular-type autoimmune thyroiditis. However, clear distal acoustic enhancement characteristic of liquid structures is not observed. The contents of malignant lymphomas are moderately heterogeneous due to the presence of randomly located linear inclusions, which sometimes appear in the mode of maximum enhancement of reflected ultrasound signal. The tumor contour is quite clear, although it may be indistinct. Tumor tissue may be located in practically any area of the orbit. However, in most cases, they occupy the upper quadrants.

Among true benign tumors located in the thickness of the eyelids, hemangiomas and lipomas are most commonly encountered. The latter (their variants are fibrolipoma, angiolipoma) are mainly located not in the projection of the eyelids, but in the palpebral area of the orbit; they arise from fat cells and accordingly, in terms of echogenicity, they are close to retrobulbar tissue. Their structure is homogeneous. Since the lipoma is surrounded by a capsule, its contour is sharp and uniform. In some cases, the lipoma is isoechoic with adjacent tissues. Among tumors of the eyelids and conjunctiva arising from blood vessels, capillary hemangiomas are relatively easier to recognize compared to others. In most cases, their detection occurs in early childhood with preferential localization in the upper inner part of the

orbit. On the echogram, hemangioma is homogeneous, its contour is clear, sometimes irregular. Compared to hyperechoic adjacent tissues (connective, cartilaginous, scleral), the tumor appears as a tumor of medium echogenicity. Despite the fact that hemangiomas of the anterior part of the orbit resemble hemangiomas in the liver and seem easily identifiable, we should not forget that such an aggressive neoplasm as rhabdomyosarcoma can masquerade as this benign tumor. Despite being malignant, rhabdomyosarcoma is still quite homogeneous and has a clear and almost uniform contour. Rhabdomyosarcoma also occurs in early childhood and its favorite localization is the same upper inner part of the orbit.

Conjunctival melanoma is accessible for external examination, so the task of ultrasound examination is to determine the presence of its spread into the eye and orbit. The tumor has reduced echogenicity, and the contour is indistinct in the invasion area. The same task arises when scanning foci of eyelid skin cancer. Along with size, the tumor's spread into the orbit depth is assessed. Most of these neoplasms (up to 85%) are represented as basal cell carcinomas, preferentially localized on the lower eyelid, in the inner canthus. Diagnostically difficult is the identification of tumors that spread to the orbit from the eye socket. Even more difficult is predicting tumor spread from paranasal sinuses to the orbit. Some such tumors may be large, almost completely filling the orbit, which complicates correct diagnosis. Some are localized adjacent to one of the orbital walls, which makes it possible to notice a bone defect that connects the space-occupying tumor with the paranasal sinus.

As we can see, according to literature data, despite the development of new medical imaging methods, ultrasound diagnostics remains the most informative method in practical ophthalmo-oncology for assessing orbital pathology. Ultrasound diagnostics of the eye and orbit (ophthalmoscanning) - a combination of two-dimensional (B) mode with real-time scanning, color Doppler, and vascular Doppler - allows visualization of intraocular tumors, their spread in the orbit, determination of the degree of orbital wall destruction, and the degree of vascularization of new tumors. Additionally, the ultrasound examination method of the eye is simple, accessible, and harmless to patient health.

Furthermore, the literature does not sufficiently address issues of ultrasound diagnostics of secondary orbital tumors, including recurrent tumors. There are practically no reports about postoperative changes and complications in orbits. Additionally, the combined use of ultrasound, computed tomography, and magnetic resonance tomography is of interest.

However, none of the above-mentioned instrumental diagnostic methods can make a final, morphological diagnosis using only individual modes. Important is the complex use of high-resolution magnetic resonance tomography modes in the diagnosis and differential diagnosis of orbital tumors. In contemporary medical literature, intumor about the role of contrast perfusion and spectroscopic modes in determining the etiological factor and nature of malignancy in eye and orbital nosologies is still difficult to find. Of interest is the correlative accuracy of radiological diagnosis with histo-morphological results when fully using complex multiparametric modes. Contemporary challenges existing in the most important direction of ophthalmoradiology became the reason for conducting this research.

### 4.2. Magnetic resonance imaging method

The method is based on measuring the electromagnetic response of hydrogen atomic nuclei during their excitation by a specific combination of electromagnetic waves in a constant high-intensity magnetic field. The method provides high differentiation capabilities for the orbit, paranasal sinuses, and brain tissue.

Magnetic resonance imaging was performed on a Siemens MAGNETOM Vida 3T apparatus in three projections. The tomograph's technical specifications are presented in Table 4.1.

The main studies were conducted in the axial plane, parallel to the optic nerve. The scanning zone covered all orbital structures and the intracranial portion of the optic nerves. Additionally, for more detailed assessment of retrobulbar space contents, we examined the orbital area in sagittal and frontal planes. Slice thickness ranged from 2-4mm.

Table 4.1

Technical data of the magnetic resonance imaging scanner

| | |
|---|---|
| Magnetic system | |
| Field strength | 3 tesla |
| Hole size | 70 cm open hole design |
| Helium consumption | Helium zero-volatilization technology |
| Regulation | Passive and active |
| Gradient strength | XQ gradients 45/200 simultaneously<br>XT gradients 60/200 simultaneously |

For the purpose of differentiating orbital neoplasms, studies were conducted with sagittal and axial slices using T1tse, T2tse, TIRM, GRE, DWI sequences. Additionally, specifically for assessing intraorbital structures, studies were performed with T1tse 2mm slices in axial, coronal, and sagittal planes, T2tse in coronal and axial slices with fat suppression (fs), and T1tse slices with fat suppression for each eye separately. For more detailed study of orbital tumors, determining their exact location and dimensions, contrast material was administered intravenously during the study, followed by post-contrast T1 imaging in axial, coronal, and sagittal slices with 2mm slice thickness. Cyclolux and Gadovist preparations were used as contrast agents. Additionally, within the research framework, magnetic resonance perfusion of orbital volumetric tumors was performed.

During the study, the patient lies supine with the head positioned centrally relative to the gantry. A head and neck coil is placed on the patient's head and neck area. In rare cases, a specialized loop coil is used, which is attached to the orbit (Figures 4.1 and 4.2).

Using the obtained MRI tomograms, the location of orbital structures (optic nerve, extraocular muscles, retrobulbar fat) and the eye socket was determined. Simultaneously, the condition of adjacent paranasal sinuses and brain tissue was assessed on all tomograms, including the spread of tumor tumors in these spaces. Examples of MRI tomograms are shown in Figures 4.3 and 4.4.

Modern study methods such as magnetic resonance diffusion and perfusion allow for more reliable differentiation between tumor and non-tumor processes, including abscesses, primary lymphomas, and metastases.

The diffusion MRI method enables determination of hydrogen proton mobility in tissues and can be used for differential diagnosis of various pathological processes. Areas with high cell density in tumor structure have lower diffusion coefficient values than in unchanged tissue. Diffusion-

weighted MRI (DW-MRI) can provide more detailed intumor about the degree of tumor malignancy in the orbit even at the initial examination stage.

Perfusion map analysis is important in diagnosing malignant orbital tumors. By quantitatively determining blood flow parameters, we assess tumor condition at the primary examination stage.


**Fig. 4.1. Specialized eye socket coil**

**Fig. 4.2. Head-neck coil**

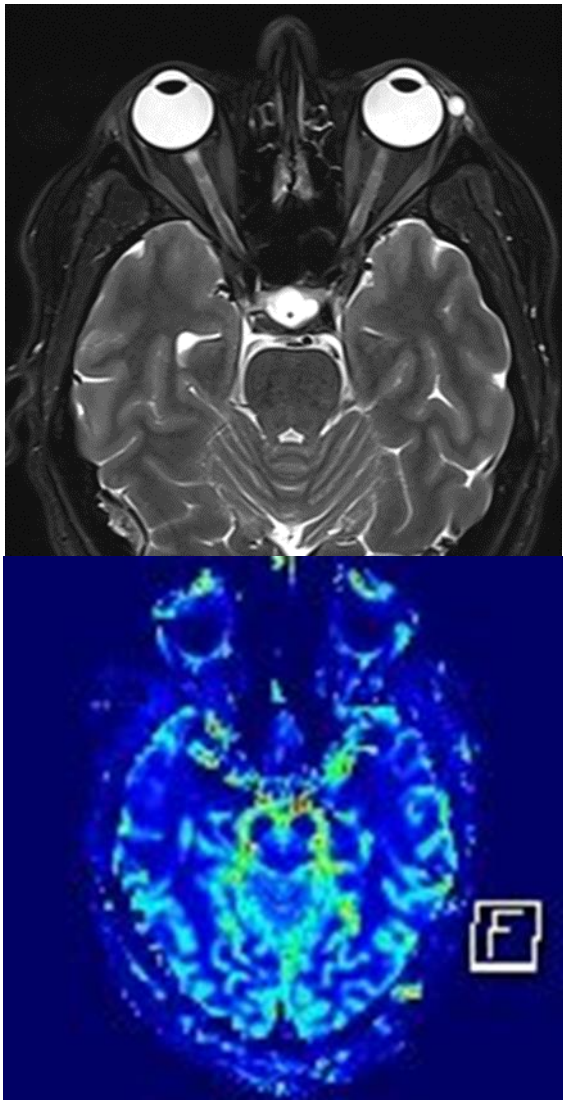

**Fig. 4.3. Left lacrimal gland cyst on MRI tomogram**

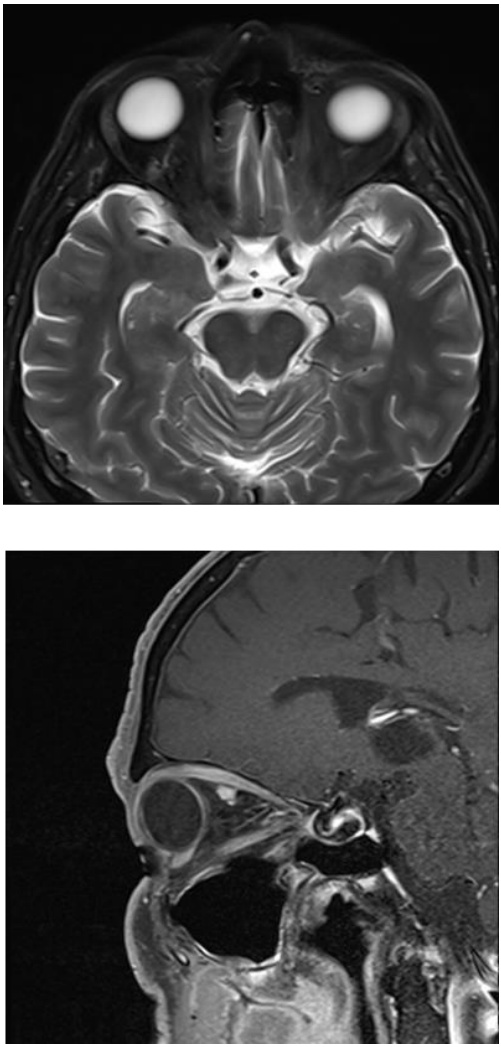

**Fig. 4.4 Cavernous angioma of the right eye socket on MRI tomogram**

MR perfusion study technologies are divided into contrast-dependent and non-contrast methods. Among contrast-dependent perfusion methods currently known are: 1) MR perfusion visualization by dynamic susceptibility contrast-weighted imaging (DSC-MRI); 2) MR perfusion technology with

dynamic contrast enhancement, also known as “permeability” MRI - Dynamic Contrast Enhancement (DCE).

Non-invasive study method - diffusion-weighted MRI (DWI MRI) is a magnetic resonance imaging method that allows obtaining images of biological tissues at the in vivo level. DW MRI can be used as an independent screening method for detecting pathologically altered signal areas, for example, in oncological patients for assessing bone marrow condition of the axial skeleton, for identifying metastatic lesions of lymph nodes in patients with established oncological diagnosis, for determining process staging, and also as a rapid and inexpensive screening method for at-risk populations. When suspicious areas are detected, such studies should be supplemented with other methods that provide anatomical imaging of the area of interest, such as standard MRI. Additionally, DW-MRI excellently complements standard studies when differential diagnosis of detected changes is necessary.

The advantages of using DW-MRI in clinical practice are: 1) it is a relatively simple method; 2) contrast enhancement is not required; 3) DW MRI availability is greater than SPECT/CT, PET/CT due to wider distribution of MR scanners; 4) relatively low cost of the study; 5) possibility of performing the study under free breathing conditions (using DWIBS); 6) possibility of obtaining anatomical and functional intumor in one study.

Orbital DW-MRI allows detection of primary oncological processes and metastatic lesions of organs and tissues of various localizations. Orbital DW-MRI can be used as an addition to conventional MRI, as it is possible to detect small pathological foci in organs. Such foci sharply differ from adjacent unchanged tissues. Tumor foci have high cellular density; on DWI such foci have high signal and, correspondingly, low diffusion coefficient values. However, DW-MR images should always be accompanied by so-called reference anatomical images, as the specificity and accuracy of DW-MRI together with conventional MRI is significantly higher.

In studies that we conducted, along with standard MRI, we used diffusion and perfusion magnetic resonance methods, both with and without contrast enhancement, which allows for more reliable differentiation between tumor and non-tumor processes and enables differential diagnosis of orbital neoplasms at early stages.

Study results were processed using parametric and non-parametric statistical methods, using standard statistical processing packages for mean mathematical values and standard deviations from mean values. The reliability of differences in mean values between examined groups was assessed using Student's parametric t-criterion. The confidence criterion generally accepted in medical research ($p<0.05$) was used.

### 4.3. Diagnosis of neoplasms using magnetic resonance imaging method

The paper presents study results of 67 patients with orbital pathological processes. Of these, primary orbital tumors were detected in 43 (64.2%) patients, secondary tumors in 24 (35.8%).

Magnetic resonance tomography was the final stage of diagnosis differentiation following preliminary clinical, ultrasonographic, and computed tomographic studies. The aim of the study was to establish differential diagnostic features of orbital neoplasms of various origins and to detect the spread of tumors to adjacent tissues.

Magnetic resonance imaging was performed on 43 patients with primary orbital and eye socket tumors. During the study, we evaluated the following parameters:

- Neoplasm location
- Tumor size
- Tumor shape
- Neoplasm structure
- Relationship between tumor and orbital structures

As a result of analyzing the MRI semiotics of primary orbital and eye socket tumors (Table 4.2), their common features were revealed: predominance of oval-shaped tumors - 72.1%, irregular-shaped tumors made up only 27.9%.

Most tumors also had smooth surfaces in 81.4% of cases, while irregular surfaces were found in only 18.6% of cases.

The structure of pathological tumors was homogeneous in 74.4% of cases. Structural heterogeneity of tumors was detected in 25.6% of cases. In more than half of these patients, no additional inclusions were detected, while in the remainder, high-intensity signals were determined, and in isolated cases, low-intensity inclusions were found when bone tumor or calcifications were present.

During studies with intravenous bolus contrast using Cyclolux and Gadovist, 62.8% showed active high contrast accumulation in the tumor, indicating a developed vascular network in the tumor tumor. In 20.9% of cases, moderate contrast material accumulation was noted, while in 16.3%, contrast material accumulated insignificantly or not at all in tumor tissue.

Table 4.2

MRI signs of primary tumors of the orbit and eye socket

| MRI | | Primary tumors (n – 43) | |
|---|---|---|---|
| | | აბს. | % |
| Architectonics | Solitary | 41 | 95.3 |
| | Multi-node | 2 | 4.7 |
| Shape | Oval | 31 | 72.1 |
| | Irregular | 12 | 27.9 |
| Structure | Heterogeneous | 11 | 25.6 |
| | Homogeneous | 32 | 74.4 |
| Inclusions | Hypo-intensive | 3 | 7.0 |
| | Hyper-intensive | 7 | 16.3 |
| | Combination | - | - |
| | No inclusions found | 22 | 51.2 |
| Surface | Smooth | 35 | 81.4 |
| | Rough | 8 | 18.6 |
| Contrast accumulation | High | 27 | 62.8 |
| | Medium | 9 | 20.9 |
| | Lowo/no accumulated | 7 | 16.3 |

When analyzing the magnetic resonance tomographic images of primary orbital and eye socket tumors, the following features were revealed depending on the morphological variant of the tumor.


**Fig. 4.5. A fragment of a magnetic resonance tomography scan of patient C., 64 years old. An irregularly shaped, heterogeneous structure is seen in the right eye socket, adjacent to the posterior membranes.**

Melanomas were mainly found in the eye socket, had smooth surfaces (92.3%) and homogeneous structure. In some magnetic resonance tomography scans (Fig. 4.5), in the right eye socket, adjacent to the posterior layers, in the vitreous body, at the 8:00-10:00 o'clock meridian, an irregular-shaped, heterogeneous structure, hyperintensive (T1tse - MR data corresponds to melanin presence), intensely contrast-enhancing volumetric tumor is visible, which shows restricted diffusion, with dimensions: max. transverse diameter - 0.7cm, max. transverse diameter on short axis - 0.6cm, cranio-caudal size - 0.8cm. The tumor extends to the optic disc, does not extend to retrobulbar space. Retinal detachment is visible adjacent to the tumor.

Particular attention should be paid to the hyperintensive signal of the tumor in the right eye socket in pre-contrast T1tse mode, which indicates the presence of melanin or hemoglobin breakdown products. Post-contrast subtraction studies have decisive importance for differentiation. The patient was diagnosed with right eye socket melanoma.

Most cavernous hemangiomas were of solitary structure - 94.5% of cases. The shape of cavernous hemangiomas was irregular in all cases, with indistinct contours in 57.4%. The internal structure of cavernous hemangiomas was mostly uniformly heterogeneous - 88.6%, inclusions were determined in 30.8% of tumors, while mixed-character inclusions were visualized in 12.7%.

**Clinical Case Example:** Patient D., 65 years old, consulted an ophthalmologist with complaints of right-sided proptosis and diplopia.

The patient underwent magnetic resonance tomography (Fig. 4.6).

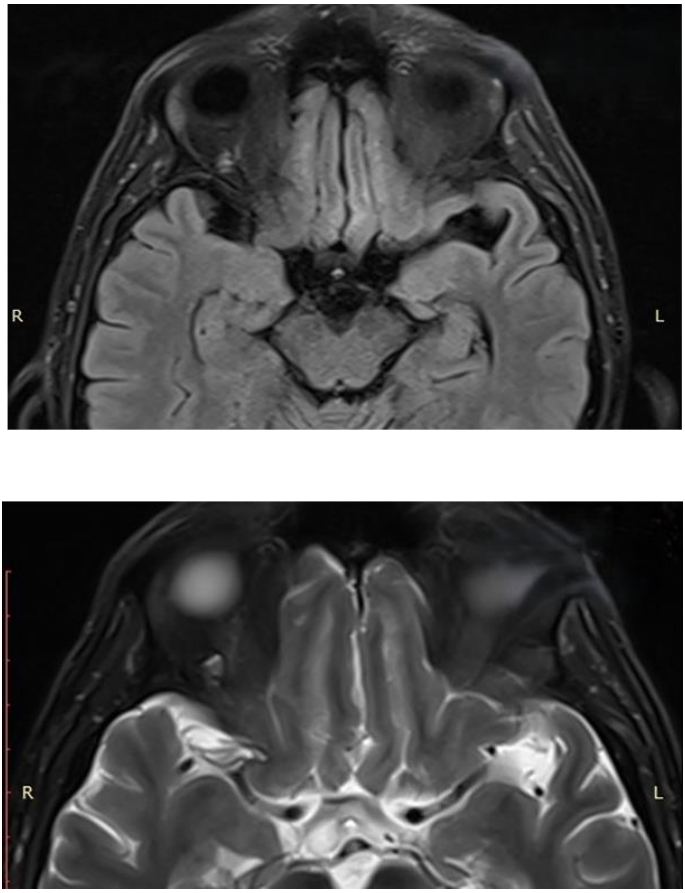


**Fig. 4.6. Fragment of magnetic resonance imaging of patient D., 65 years old.**

The presented images in T2 tse and FLAIR modes show a small hyperintensive, somewhat inhomogeneous tumor located in the right orbit.

On the obtained tomograms, in the right orbit, cranially and laterally, a regular, well-defined contour, inhomogeneous structure, intensely contrast-enhancing volumetric tumor is visible, measuring 0.5X0.9X0.5cm, which does not cause pressure on adjacent anatomical structures.

For final decision-making in radiological diagnostics, decisive importance is given to obtaining and interpreting post-contrast images (Fig. 4.7).

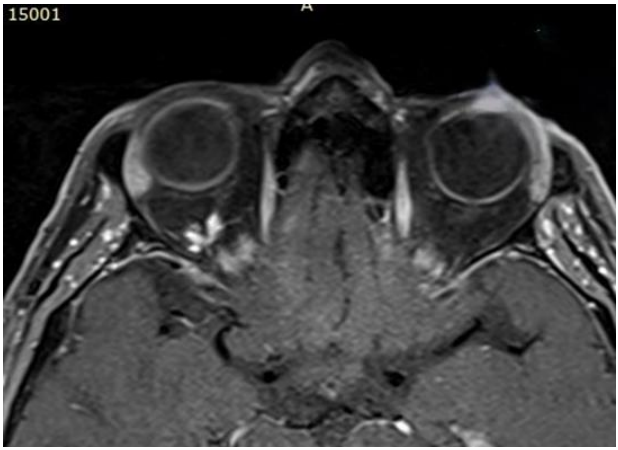


a)

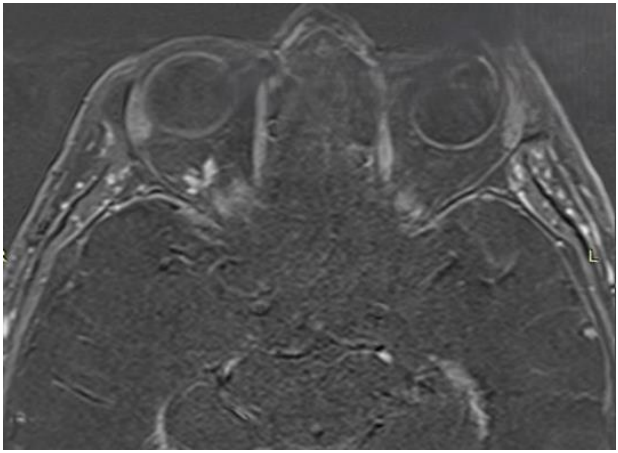


b)

**Fig. 4.7. Fragment of a post-contrast magnetic resonance imaging scan of patient D., 65 years old.**

The aforementioned tumor shows homogeneous and intense contrast uptake - MR semiotics corresponds to cavernous hemangioma. The patient's final diagnosis is cavernous hemangioma.

Lacrimal gland adenomas are characterized by typical tumor localization - in the upper outer parts of the orbit, corresponding to lacrimal gland localization.

Tumor shape was irregular with indistinct contours in 88.5% of cases. Structural heterogeneity was revealed in 75.4% of cases, due to excess cystic component.

**Clinical Case Example:** Patient V., 60-year-old male, consulted the clinic with complaints of vision deterioration, pressure sensation, and compressive character in the right eye.

Ophthalmological examination revealed limitation of eye socket movement laterally and upward, and narrowing of the right palpebral fissure. Visual acuity on the affected side is 0.6, on the healthy side - 1.0. Fundus shows signs of optic disc swelling. Visual field boundaries are unchanged.

On the obtained tomograms, in the right lacrimal gland projection area, a homogeneously and well-contrasting volumetric tumor is visible, which is inhomogeneous in T2 mode examination, does not cause true diffusion restriction, does not invade adjacent structures. MRT signs of perineural tumor growth (through the ophthalmic division of the trigeminal nerve - V1) were not detected, which has decisive importance in treatment planning and determining future prognosis. Morphologically verified as lacrimal gland adenoid cystic carcinoma.

The patient underwent magnetic resonance study (Fig. 4.8). predominated, with clear contours in 83% of cases. The tumor was most frequently localized in the posterolateral parts of the orbit.

Contrast material accumulation by tumor tissue was high in 60% of cases, while in the remaining 40%, moderate contrast accumulation was recorded. Adjacent tissue changes were revealed in 38% of cases - decreased densitometric density and structural changes were noted.

**Clinical Case Example:** Patient O., female, 56 years old, consulted the clinic with complaints of left-sided exophthalmos and sharp vision deterioration.

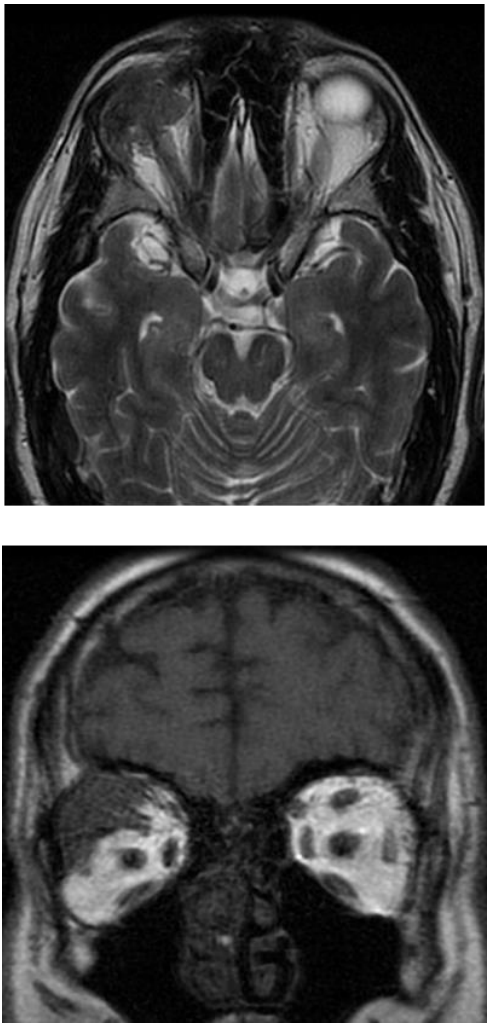

**Fig. 4.8. Magnetic resonance imaging (MRI) fragment of patient V., a 60-year-old man.In orbital lymphomas, oval-shaped tumors**

On tomograms obtained after magnetic resonance tomography (Fig. 4.9), in the left orbital apex, around the optic nerve, cranially, laterally and caudally, an irregular-shaped mass with indistinct contours, intensely contrast-enhancing, is visible, measuring: anterior-posterior 1.2cm,

transverse 0.9cm, cranio-caudal 0.8cm, which shows restricted diffusion (indicating cellular proliferation).

MR perfusion shows increased perfusion. A small defect of the lateral wall is visible in the apex area, the mentioned mass slightly extends into the middle fossa. Distally to this mass, the optic nerve is not differentiated. The eye muscles in the orbital apex are thickened and infiltrated, especially the superior rectus muscle. The left eye socket is deformed, the vitreous body has inhomogeneous structure, MR picture of retinal detachment is visible, centrally with fibrotic adhesion - MR semiotics suggests the presence of intraorbital lymphoma. The patient was finally confirmed to have lymphoma diagnosis.

Most retinoblastomas were characterized by irregular tumor shape, with indistinct contours in 75% of cases. The tumor was most frequently localized in the eye socket and lower quadrant. In retinoblastoma cases, structural heterogeneity predominated (87%).

**Clinical Case Example:** Patient R., 1 year old, with left-sided proptosis. No trauma of any type is mentioned in the anamnesis.

The patient underwent Magnetic resonance tomography (Fig. 4.10).

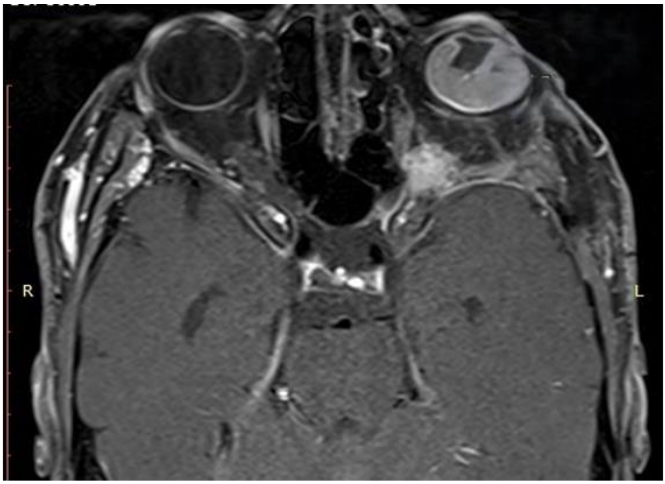


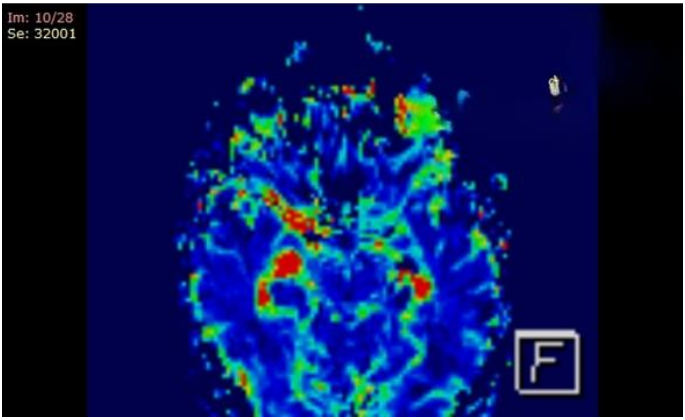


**Fig. 4.9. A fragment of a magnetic resonance imaging scan of patient O., 56 years old.**

On the obtained tomograms in T2-weighted modes, a sharply inhomogeneous structure, partially calcified (hypointensive in T2 mode), intraorbital volumetric tumor is visualized, which extends dorsally along the optic nerve. Intracranial spread of the tumor is also noted near the optic chiasm. The tumor shows increased perfusion and pathological diffusion

restriction. Considering the patient's age and magnetic resonance data, retinoblastoma is an unalternative diagnosis, which was confirmed by morphological verification of the preparation.

**Fig. 4.10. Patient R., 1 year old, magnetic resonance imaging fragment.**

In meningiomas, irregular tumor shape predominated, with clear contours in 87% of cases. Structural heterogeneity is characteristic of meningiomas (89%).

**Clinical Case Example:** Patient U., 25-year-old woman, consulted the clinic with complaints of vision deterioration in the right eye.

On the obtained tomograms (Fig. 4.11), in the right orbit dorsally and in the area of the orbital apex, adjacent to the optic nerve - laterally and cranio-caudally to it, an irregular, well-defined contoured, non-homogeneous structure is visible, intensely contrast-enhancing volumetric tumor, measuring: anterior-posterior: 2.1cm, transverse: 1.1cm, length: 1.3cm, which does not extend intracranially. The right optic nerve is dorsally to the eye socket, approximately 1cm in length, sharply narrowed and intact.

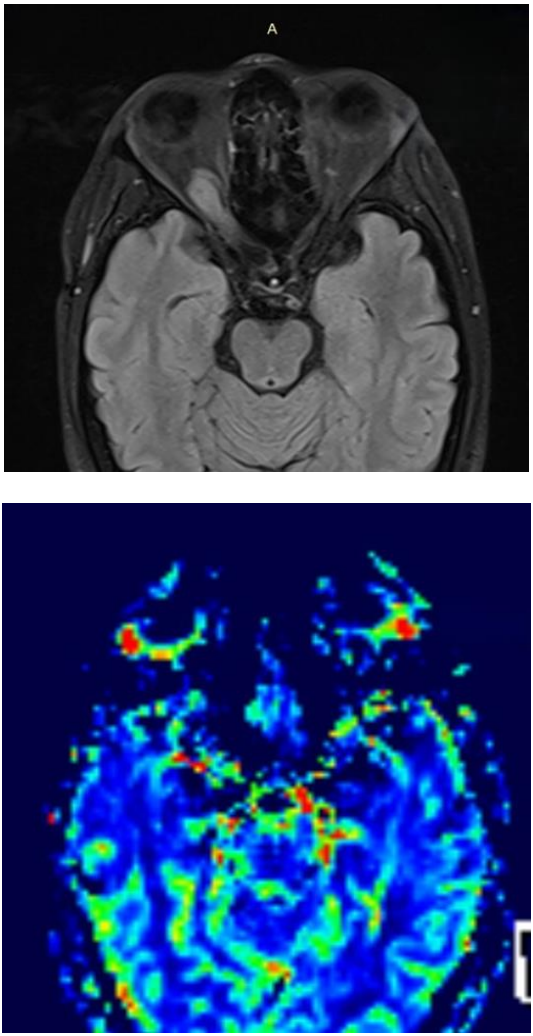


**Fig. 4.11. Patient U., 25 years old, magnetic resonance imaging fragment.**

In the post-contrast perfusion regime, the tumor did not show significant increase in perfusion parameters, nor pathological diffusion restriction - which indicates a highly differentiated cellular matrix of the tumor.

Considering the homogeneity of contrast enhancement and close connection with the optic nerve, MR semiotics suggests the presence of an optic nerve neoplasm - morphologically verified as right optic nerve sheath meningioma.

Based on the analysis of the obtained data, MRI sensitivity for diagnosing primary tumors of the orbit and eye socket was 99%, specificity - 96.4%.

From the data in Table 4.3, it follows that according to magnetic resonance tomography data, suspicion of extraocular muscle infiltration was present in 11.6% of cases, due to the lack of clear boundaries between the tumor and any muscle group, while there was corresponding muscle size increase.

In 4.66% of cases, optic nerve infiltration was suspected based on close proximity to the tumor and inability to clearly visualize it.

In 23.3% of cases, changes in retrobulbar tissue and its infiltration were revealed, accompanied by the appearance of hyperintensive signals.

In 18.61% of cases, destruction of the orbital bone wall was noted; medial orbital wall destruction was recorded in 2.33% of cases, lateral wall in 9.3%, and superior wall in 6.98%. When assessing the condition of orbital bone walls, it was noted that destructive changes were more frequently manifested in the lateral and superior orbital bone walls.

Table 4.3

Frequency of spread of primary tumors of the eye socket and orbit to various orbital structures according to magnetic resonance imaging data

| MRI signs | | Primary tumors (n – 43) | |
|---|---|---|---|
| | | Abs. | % |
| Infiltration of extraocular muscles | Yes | 5 | 11,6 |
| | No | 38 | 88,4 |
| Sizes of extraocular muscles | Unchanged | 35 | 81,4 |
| | Reduced | - | - |
| | Increased | 8 | 18,6 |
| Changes in the retrobulbar tissue | Yes | 10 | 23,3 |
| | No | 33 | 76,7 |
| Optic nerve infiltration | Yes | 2 | 4,66 |
| | No | 41 | 95.34 |
| Destruction of orbital bone wall | Medial | 1 | 2,33 |
| | Lateral | 4 | 9,30 |
| | Upper | 3 | 6,98 |
| | Lower | - | - |

Magnetic resonance imaging was performed on 24 patients with secondary tumors. The magnetic resonance frequency of secondary neoplasms is presented in Table 4.4.

Table 4.4

Frequency of MRI signs of secondary tumors

| MRI signs | | Secondary tumors (n – 24) | |
|---|---|---|---|
| | | Abs. | % |
| Architectonics | Solitary | 22 | 91,7 |
| | Multi-node | 2 | 8,3 |
| Shape | Oval | 4 | 16,7 |
| | Irregular | 20 | 83,3 |
| Structure | Heterogeneous | 18 | 75,0 |
| | Homogeneous | 6 | 25,0 |
| Inclusions | Hypo-intensive | 3 | 12,5 |
| | Hyper-intensive | 6 | 25,0 |
| | Combination | 2 | 8,3 |
| | No iclusions found | 13 | 54,2 |
| Surface | Smooth | 8 | 33.3 |
| | Rough | 16 | 66.7 |

Metastatic tumors were more frequently localized in the inner quadrants of the orbit - superior-inner (27.6%) and inferior-inner quadrants (23%), less frequently in the inferior-outer quadrant - 8.1% and superior-outer quadrant - 2.3%.

The structure of tumors was solitary in most cases - 91.7%; tumors consisting of several nodes were found in 8.3% of cases.

When analyzing the frequency of detection of magnetic resonance imaging signs characteristic of secondary orbital tumors, we noted the following common criteria for them: solitary structure, irregular surface, indistinct contours, heterogeneity of internal structure.

In our studies, adenocarcinomas comprised 80-90% of metastatic tumors and were mainly manifested as metastases from breast, prostate, and lung cancer.

According to the obtained results, adenocarcinomas were of solitary structure in most cases - 95.2% of cases. The form of adenocarcinoma was irregular in all cases, with indistinct contours.

The internal structure of adenocarcinomas was mainly uniformly heterogeneous - 83.6%, while liquid inclusions were determined in 32.5% of tumor tumors, and mixed-character inclusions were visualized in 11.7%.

**Clinical Study Example:** Patient W., 64-year-old woman, diagnosed with breast adenocarcinoma, contacted the radiology service for screening brain magnetic resonance tomography to exclude secondary lesions. No ophthalmological complaints were noted.

On the obtained tomograms (Fig. 4.12), the posterior sheaths of the right eye socket, dorsally and cranially, at the 18-hour meridian are thickened; during i/v contrast administration, a contrast uptake area up to 2mm in size is visible, which slightly protrudes into the vitreous body - secondary lesion cannot be excluded.

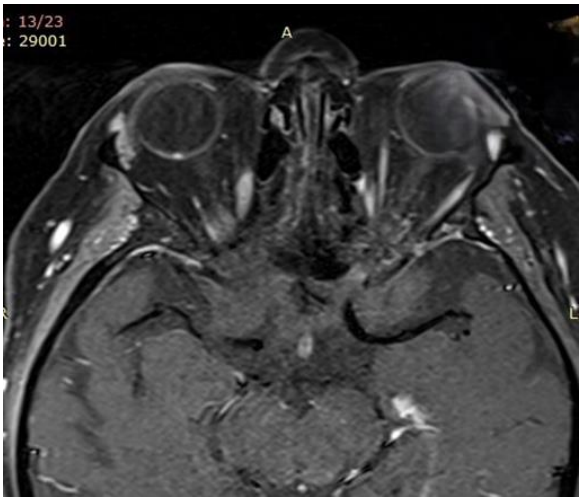


**Fig. 4.12. Patient W., 64-year-old woman, magnetic resonance imaging fragment.**

It should be noted that the tumor visible on pre-contrast sections is not differentiated, does not cause diffusion restriction, and does not show signal increase on FLAIR images, which indicates the necessity of using contrast material to exclude possible secondary lesions in a patient with primary oncological disease. Subsequently, secondary lesion of the right eye socket posterior sheaths was confirmed in the patient.

In TIRM, DWI regimes, the small pathological area is not visualized.

Basalioma was characterized by solitary tumor structure in 66.8% of cases. In almost all cases, the tumor had an irregular form. Neoplasm contours were clear in 50% of cases. The tumor surface was mostly uneven - 83.3% of cases, while the internal structure of the tumor was either homogeneous or

unevenly heterogeneous. High-density and liquid inclusions in the neoplasm structure were found in 14.4% of cases.

**Clinical Study Example:** Patient X, 72 years old, contacted the clinic after histological diagnosis of basal cell carcinoma. The main purpose of visualization was possible orbital spread and the degree of involvement of extraocular muscles in the process. Periocular basal cell carcinoma is one of the most common malignant tumors of the eyelids in elderly age. Intraorbital spread is rare, although in such cases vision problems are frequent, secondary to involvement of extraocular muscles.

The patient underwent magnetic resonance tomography (Fig. 4.13).

On the obtained MR tomograms, a soft tissue tumor is visible in the right periorbital soft tissues, extending intraorbitally to the inferior-lateral edge, in the projection of the inferior and lateral rectus muscles, hyperintensive on T2 regime examination, hypointensive (relative to adjacent muscles) on T1 regime examination, and markedly absorbing contrast material. The tumor causes mass effect on the eye socket and intraorbital structures, without MR data of infiltrative growth, indicating the locally aggressive nature of the neoplasm.

During the study of meningiomas, it was established that tumors were both irregular in form and in one-third of cases had regular, oval geometric form. Contours in most cases (59.3%) were sharp, while mainly tumor surfaces were nodular - 69.2%, only 33.3% had smooth tumor surfaces. Internal structure in 66.7% of cases was uniformly heterogeneous. In 66.7% of cases, liquid inclusions were found in the neoplasm, while 14.3% had mixed-type inclusions.

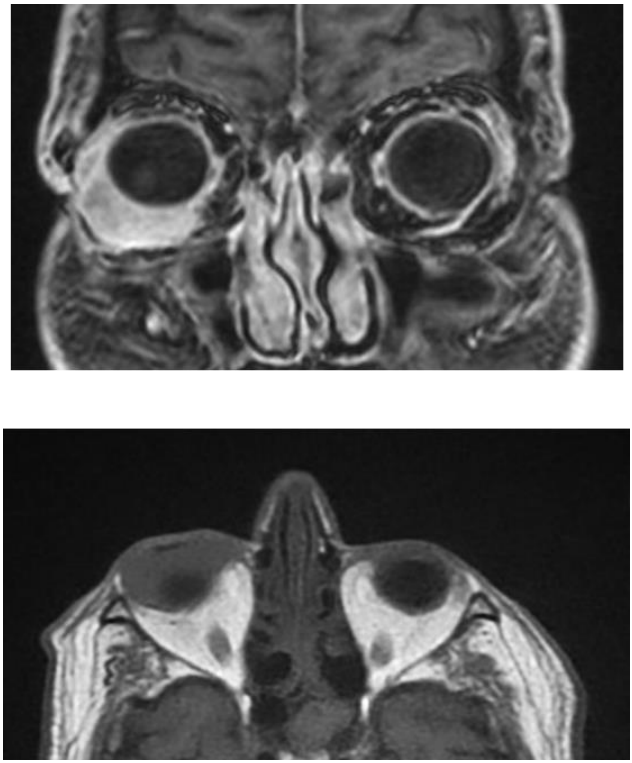

**Fig. 4.13. Patient X., 72 years old, magnetic resonance imaging fragment.**

**Clinical Study Example:** Patient Y., 55-year-old woman, contacted the clinic with complaints of visual acuity impairment and diplopia.

On the obtained tomograms (Fig. 4.14), marked hyperostosis of the right sphenoid bone's greater and lesser wings, as well as the frontal bone, is evident; the bone is thickened up to 3cm, causing curvature of its internal and external contours, pressure on the frontal and temporal lobes, as well as on the lateral rectus muscle. In the orbit in the form of a narrow strip and in periorbital soft tissues, more caudally and laterally, intensely contrast-enhancing soft tissue components are evident, with maximum transverse diameter in periorbital soft tissues on short axis - 1.2cm and long axis - 2.1cm.

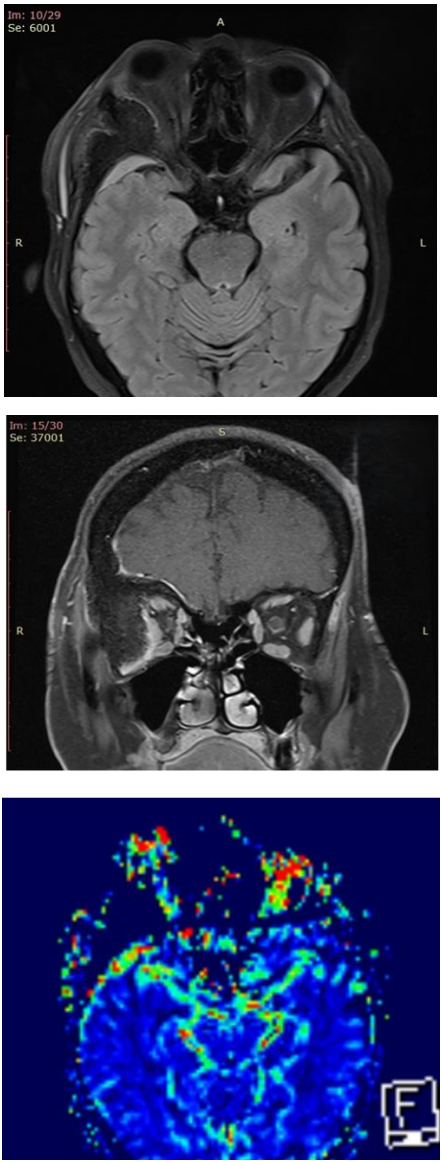


**Fig. 4.14. Patient Y., 55 years old, female, magnetic resonance imaging fragment.**

The soft tissue component is also visualized intracranially in the middle fossa, with thickness - 0.5cm, with evident pressure on the temporal pole. Adjacent, in the frontal and temporal lobes, the dura mater contrasts unevenly - MR data best corresponds to flat meningioma of sphenoid and frontal bones with orbital and intra/extracranial spread. Right-sided proptosis is evident.

On perfusion tomogram in axial section, enhanced perfusion of the soft tissue component of the tumor (adjacent to the temporal lobe pole) is evident.

**Radiological Conclusion:** The existing MRI study reveals sphenoid and frontal bone meningioma with orbital and intra/extracranial spread.

Data on the frequency of metastatic tumor spread to various orbital structures according to MRI results are presented in Table 4.5.

Table 4.5

Characteristics of spread of metastatic tumors to orbital structures

| MRI signs | | Sino-orbital formations (n – 24) | |
|---|---|---|---|
| | | Abs. | % |
| Infiltration of extraocular muscles | Yes | 10 | 41.7 |
| | No | 14 | 58.3 |
| Sizes of extraocular muscles | Unchanged | 17 | 70,8 |
| | Reduced | - | - |
| | Increased | 7 | 29,2 |
| Changes in the retrobulbar tissue | Yes | 18 | 75.0 |
| | No | 6 | 25.0 |
| Optic nerve infiltration | Yes | 5 | 20.8 |
| | No | 19 | 79.2 |
| Destruction of orbital bone wall | Medial | 8 | 33.3 |
| | Lateral | 4 | 16.7 |
| | Upper | 5 | 20.8 |
| | Lower | 6 | 25.0 |

Using the MRI method to assess the spread of secondary tumors to various orbital structures, the following data were obtained. In 41.7% of cases, infiltration of extraocular muscles was noted with enlargement of extraocular muscle dimensions in 29.2% of cases; reduction in extraocular muscle dimensions was not recorded.

In 20.8% of cases, optic nerve infiltration was revealed. In 75.0% of cases with secondary neoplasms, changes in retrobulbar tissue were noted.

## CHAPTER 5. COMPARATIVE ANALYSIS OF THE RESULTS OF MAGNETIC RESONANCE IMAGING, COMPUTED TOMOGRAPHY AND OPHTHALMOSONOGRAPHY IN THE DIFFERENTIAL DIAGNOSIS OF ORBITAL TUMORS

Since one of the objectives of our study was to evaluate the capabilities of contemporary radiological methods in visualizing tumor tumors of the eye socket and orbital space and assessing the degree of their spread, we conducted a comparative analysis of the results obtained from these studies. The results of comparative assessment of magnetic resonance imaging, ophthalmosonography, and computed tomography data for primary tumors of the eye socket and orbit are presented in Table 5.1.

Table 5.1

Comparative characteristics of ultrasound, computed tomography, and magnetic resonance imaging in the diagnosis of primary tumors of the eye socket and orbit

| Signs | | Ultrasound examination (n=30) | | CT (n – 38) | | MRI (n – 43) | |
|---|---|---|---|---|---|---|---|
| | | Abs. | % | Abs. | % | Abs. | % |
| Infiltration of extraocular muscles | Yes | 6 | 20,0 | 5 | 13,2 | 5 | 11,6 |
| | No | 24 | 80,0 | 33 | 86,8 | 38 | 88,4 |
| Sizes of extraocular muscles | Unchanged | 23 | 76,7 | 31 | 81,6 | 35 | 81,4 |
| | Reduced | - | - | - | - | - | - |
| | Increased | 8 | 18,6 | 7 | 18,4 | 8 | 18,6 |
| Changes in the retrobulbar tissue | Yes | 8 | 26,7 | 10 | 26,3 | 10 | 23,3 |
| | No | 22 | 73,3 | 28 | 73,7 | 33 | 76,7 |
| Optic nerve infiltration | Yes | 3 | 10,5 | 2 | 5,3 | 2 | 4,66 |
| | No | 27 | 89,5 | 36 | 94,7 | 41 | 95.34 |
| Destruction of orbital bone wall | Medial | - | - | 1 | 2.9 | 1 | 2,33 |
| | Lateral | 3 | 10,5 | 3 | 7,9 | 4 | 9,30 |
| | Upper | 2 | 6,7 | 3 | 7.9 | 3 | 6,98 |
| | Lower | 2 | 6,7 | - | - | - | - |

Thus, according to ultrasound examination, 6 (20.0%) patients showed infiltration of the extraocular muscles, according to CT data - 5 (13.2%) patients, while magnetic resonance imaging confirmed this sign in 5 (11.6%) patients.

Enlargement of extraocular muscles was determined by ultrasound examination in 18.6% of cases, confirmed by magnetic resonance imaging in 18.6% of cases, while computed tomography revealed enlargement of extraocular muscles in 18.4% of cases.

Data regarding changes in retrobulbar tissue during ultrasound examination and computed tomography almost matched each other at 26.3%, while magnetic resonance imaging confirmed this in 23.3% of cases.

During computed tomography, destruction of orbital bone walls was recorded in 23.9% of cases. In this case, destruction of the lateral and superior orbital walls was 7.9% each, while destruction of the inferior orbital wall was not noted.

During magnetic resonance imaging, destruction of orbital bone walls was visualized in 18.6% of cases. Specifically, destruction of the lateral and superior orbital walls was 9.30% and 6.98% respectively, while destruction of the inferior orbital wall was not recorded. During surgery, destructive changes in the superior orbital wall were confirmed in 6.98% of cases. In this case, ultrasound examination did not reveal destructive changes, which can be explained by the peculiarities of tumor location.

To determine the significance of semiotic signs for assessing the spread of primary tumors during ophthalmosonography, computed tomography, and magnetic resonance imaging studies, Spearman's correlation analysis was conducted. According to the results, a direct relationship should be established between sonographic indicators and surgical data regarding tumor spread in the soft tissue structures of the orbit. A direct relationship was also established between CT and MRI data in identifying destruction of orbital bone walls.

Magnetic resonance imaging data regarding tumor spread to orbital walls and the size of destructive areas were fully confirmed at the surgical stage of treatment.

When analyzing the effectiveness of radiological examination methods in assessing the spread of primary neoplasms of the eye socket and orbit, we evaluated parameters such as sensitivity, specificity, and accuracy (Table 5.2).

The ultrasound examination method gives good results in assessing tumor spread to soft tissue structures of the orbit. However, ophthalmosonography falls behind computed tomography in assessing tumor component spread to orbital bone structures. Additionally, it was determined that the accuracy of ultrasound examination in assessing tumor spread to orbital bone structures depends on tumor location - the accuracy of

ophthalmosonography decreases when the tumor is located in the superior parts and at the orbital apex.

Table 5.2

The effectiveness of radiological research methods in assessing the spread of primary neoplasms of the eye socket and orbit

| Signs | Methods | | | | | | | | |
|---|---|---|---|---|---|---|---|---|---|
| | Ultrasonography | | | CT | | | MRI | | |
| | Sensitivity, % | Specificity,% | Accuracy, % | Sensitivity, % | Specificity,% | Accuracy, % | Sensitivity, % | Specificity,% | Accuracy, % |
| Muscle infiltration | 85,0 | 75,0 | 88,0 | 85,0 | 90,0 | 90,0 | 96,2 | 95,7 | 97,3 |
| Optic nerve infiltration | 83,0 | 71,0 | 84,0 | 78,0 | 83,0 | 83,0 | 95,4 | 96,1 | 97,2 |
| Retrobulbar tissue infiltration | 85,0 | 72,0 | 87,0 | 88,0 | 89,0 | 90,0 | 96,8 | 95,3 | 98,0 |
| Destruction of orbital bone wall | 75,0 | 67,0 | 72,0 | 95,0 | 97,4 | 94,1 | 99,0 | 96,4 | 98,1 |

Considering that surgical treatment tactics depend on data regarding tumor spread to orbital structural elements, magnetic resonance imaging is an irreplaceable preoperative diagnostic modality that provides high-accuracy, reliable data both in assessing tumor spread to soft tissue structures of the orbit and in evaluating tumor component spread to orbital bone structures and the existence and scale of possible orbital wall destruction.

When assessing primary tumor spread to soft tissue structures of the orbit, CT results were lower than MRI data. This is explained by CT's relatively low sensitivity in assessing soft tissue structures of the orbit, which does not contradict literature data.

Thus, according to our data, all used radiological methods (ultrasound examination, computed tomography, and magnetic resonance imaging) are significant both in diagnosing primary tumors of the eye socket and orbit and in the surgical treatment planning stage. However, magnetic resonance imaging leads in sensitivity, specificity, and accuracy.

The results of comparative assessment of ophthalmosonography, computed tomography, and magnetic resonance imaging data for secondary orbital tumors are presented in Table 5.3. Correlation of semiotic signs to determine the scale of the tumor process was performed using the non-parametric rank correlation criterion proposed by Spearman.

When analyzing symptoms of tumor spread to various orbital structures, differences were revealed between ophthalmosonography, computed tomography, and magnetic resonance imaging data.

According to ultrasound examination, extraocular muscle infiltration was revealed in 40.1% of cases, according to CT - extraocular muscle infiltrate was determined in only 38.1%, while according to MRI data, extraocular muscle infiltration was confirmed in 45.8%.

Enlargement of extraocular muscles was determined during ultrasound examination in 25.4% of cases and confirmed according to MRI data in 29.9% of cases, while according to CT, enlargement of extraocular muscles was recorded in only 27.6%.

Table 5.3

Comparative characteristics of ultrasound, computed tomography, and magnetic resonance imaging in the diagnosis of primary tumors of the eye socket and orbit

| Signs | | Ultrasound examination (n – 17) | | CT (n – 21) | | MRI (n – 24) | |
|---|---|---|---|---|---|---|---|
| | | Abs. | % | Abs. | % | Abs. | % |
| Infiltration of extraocular muscles | Yes | 8 | 40,1 | 8 | 38,1 | 11 | 45,8 |
| | No | 9 | 59,9 | 9 | 42,9 | 13 | 54,2 |
| Sizes of extraocular muscles | Unchanged | 12 | 70,6 | 15 | 71,4 | 17 | 69,8 |
| | Reduced | - | - | - | - | | |
| | Increased | 5 | 29,4 | 6 | 27,6 | 7 | 29,9 |
| Changes in the retrobulbar tissue | Yes | 4 | 23,5 | 4 | 19,0 | 6 | 24,0 |
| | No | 13 | 76,5 | 17 | 81,0 | 18 | 75,0 |
| Optic nerve infiltration | Yes | 13 | 70,5 | 15 | 71,4 | 18 | 75,0 |
| | No | 4 | 29,5 | 6 | 28,6 | 6 | 25,0 |
| Destruction of orbital bone wall | Medial | 5 | 29,4 | 8 | 38,1 | 9 | 37,5 |
| | Lateral | 2 | 11,7 | 2 | 10,5 | 3 | 12,5 |
| | Upper | 1 | 5,9 | 3 | 14,2 | 3 | 12,5 |
| | Lower | 3 | 17,6 | 5 | 23,8 | 6 | 25,0 |

Optic nerve infiltration was determined by sonography and MRI data in 23.5%, which was confirmed by surgical results, while CT revealed it in only 19.0%.

During ophthalmosonography, destruction of the medial orbital bone wall was recorded in 29.4%, inferior wall destruction was noted in 17.6%, lateral bone wall destruction was visualized in 11.7%, while superior wall destruction occurred in 5.9%.

In computed tomographic examination, destruction of the medial orbital wall was noted in 38.1% of cases, inferior orbital wall destruction in 23.8%. Superior wall destruction was recorded in 14.2% of cases, while lateral orbital wall destruction occurred in 10.5%.

According to MRI, destructive changes in the inferior orbital wall were revealed in 25.0% of cases. In some cases, CT scanning did not reveal destructive changes due to tumor localization and minor destructive changes.

When the primary tumor was localized in ethmoid labyrinth cells, the intraorbital tumor component was located near the superomedial orbital wall, making tumor visualization difficult.

**Clinical Case Example:** Patient N., 62 years old, complained of pain in the facial area on the right side, upper eyelid ptosis, lacrimation, and difficulty breathing through the nose when presenting to the clinic.

During ophthalmological examination, eye repositioning was unchanged, exophthalmos and limitation of eye socket movement were not detected. Visual acuity was 0.9. Eye fundus showed signs of optic disc swelling. Visual field boundaries were unchanged.

During computed tomography examination (Fig. 5.1.), ethmoid labyrinth cells on the right were occupied by an irregularly shaped tumor tumor with indistinct contours.

The tumor had spread to the right orbit, causing destruction of the superomedial orbital wall. The intraorbital component measured 10x20 mm, with moderately heterogeneous structure and high-density inclusions.

**Conclusion:** Ethmoid labyrinth tumor on the right, with spread to the right orbit, showing signs of infiltrative growth. Muscles, optic nerve, and retrobulbar tissue showed no pathological changes.

**Fig. 5.1. Patient N., 62 years old, fragment of a computed tomography scan. The cells of the ethmoid labyrinth on the right are visualized, a formation extending into the right orbital cavity is visualized, the orbital wall is destroyed.**

When analyzing the effectiveness of radiological examination methods in assessing metastatic tumor spread, we evaluated parameters such as sensitivity, specificity, and accuracy.

During our study, it was determined that ultrasound examination of secondary tumors is highly informative for identifying tumor spread to muscles, optic nerve, and retrobulbar tissue. However, in assessing tumor component spread to orbital bone structures, computed tomography exceeds sonography capabilities. Magnetic resonance imaging provides a complete picture of the structural features of these tumors and their spread to adjacent anatomical regions.

Visual function loss, as a poor vital prognosis in orbital malignant tumors, determines the medical, social, and psychological significance of timely treatment measures, especially in organ-preserving treatment, which can only be implemented in cases of early tumor detection.

The clinical picture of diseases causing increased orbital content volume is characterized by a series of similar symptoms. Existing characteristic signs appear, as a rule, in the late stages of process development.

The capabilities of traditional instrumental examination methods (ultrasound examination, computed tomography) are limited by their resolution. Diagnostic errors are also frequent. Therefore, the interest in

developing and implementing new additional examination methods for timely diagnosis of orbital diseases is understandable.

The advantage of ultrasound examination is its accessibility, simplicity of examination, and absence of radiation exposure, which allows us to use it both for primary diagnosis of orbital tumors and for dynamic monitoring. Conducting Doppler studies makes it possible to assess tumor vascularization and determine the nature of its blood flow. The use of digital diagnostic technologies significantly improved the quality of images of analyzed objects and eye tissues. Visualization of small eye structures, assessment of static anatomical elements and degree of vascularization became possible. Using color and power Doppler mapping, as a result of contrasting individual structural elements of the eye socket and orbit, it is possible to differentiate choroidal and retinal structure and identify pathological neovascularization zones. However, when assessing tumor component spread to orbital bone structures and in cases of complex tumor location, ultrasound examination sometimes provides incorrect and incomplete intumor. A disadvantage of ophthalmosonography is also operator dependence, subjective interpretation specificity, and associated diagnostic errors.

The undoubted advantage of computed tomography is the high speed of examination and the possibility of studying densitometric parameters, which, together with high spatial resolution and contrast enhancement, significantly contributes to diagnosing orbital tumor processes. However, some authors believe that CT signs are still non-specific, since there is no correlation between CT data and morphological examination data. Determining the histological nature of tumors using CT is possible only with a certain probability, and making a final diagnosis based on CT is impossible. Research capabilities are limited by many factors (anatomical, physical, etc.). A disadvantage of computed tomography is the relatively low specificity of soft tissue component differentiation, which significantly complicates differential diagnosis. CT's broad capabilities in assessing the bone system should be noted, with early manifestations of its remodeling, destruction, or hyperostosis.

Magnetic resonance imaging has significant advantages compared to ultrasound and CT examinations. It allows assessment of all parts of the visual analyzer and provides high visual resolution in soft tissue differentiation. However, the high cost of examination, examination time, and high sensitivity to artifacts in some cases complicate the active clinical use of this modality.

Of all tissue visualization methods, magnetic resonance imaging provides the closest picture to pathoanatomical findings.

MRI is more sensitive than CT and ultrasound examination in terms of detecting small-sized tumors of both soft tissues and bone structures of the orbit and eye socket. Therefore, MRI examination is an unconditional leader in differential diagnosis of orbital neoplasms.

## Conclusions

1. Comparative analysis of ultrasound examination, computed tomography, magnetic resonance imaging, and surgical data for the spread of primary and secondary orbital tumors showed the high significance of sonography in identifying invasion of the muscular apparatus, blood vessels, and optic nerve. CT had an advantage in visualizing damage to orbital bone walls. MRI had significant advantages over CT and ultrasound examination methods, both in diagnosing and structurally assessing small-sized tumor tumors and in terms of process spread direction.

2. The use of magnetic resonance imaging with specialized eye protocol, integrating such regimes as DWI (with diffusion coefficient mapping), post-contrast T1-weighted images with fat signal suppression and subtraction, significantly simplifies identification of tumor cellular matrix. Perfusion regimes have auxiliary significance in determining the type, degree of tumor vascularization, and metabolic specificity and may be considered for integration into standardized protocols in the future.

3. When using the MRI method, compared to CT, the absence of radiation exposure allows for magnetic resonance imaging (including using non-contrast angiographic regime) during dynamic observation of patients with orbital tumors.

4. The role of MRI in developing optimal treatment tactics for patients with primary and secondary orbital tumors has been demonstrated, as well as for clarifying the spread of pathological processes to adjacent tissues, the course of orbital bone destruction, and selecting adequate treatment.

**REFERENCES:**

1. Abdel Razek AA, Gaballa G, Elhawarey G, Megahed AS, Hafez M, Nada N. Characterization of pediatric head and neck masses with diffusion-weighted MR imaging. European radiology. 2009 Jan;19:201-8.
2. Aburn NS, Sergott RC. Orbital colour Doppler imaging. Eye. 1993 Sep;7(5):639-47.
3. Ahmed S, Shahid RK, Sison CP, Fuchs A, Mehrotra B. Orbital lymphomas: a clinicopathologic study of a rare disease. The American journal of the medical sciences. 2006 Feb 1;331(2):79-83.
4. Ahmad SM, Esmaeli B. Metastatic tumors of the orbit and ocular adnexa. Curr Opin Ophthalmol 2007;18(5):405-13.
5. Akansel G, Hendrix L, Erickson BA, Demirci A, Papke A, Arslan A, Ciftci E. MRI patterns in orbital malignant lymphoma and atypical lymphocytic infiltrates. European journal of radiology. 2005 Feb 1;53(2):175-81.
6. Albert DM, Jakobiec FA, editors. Principles and practice of ophthalmology. Saunders; 2000.
7. Alker GJ, Leslie EV, Banna MO, Pallie W, Rudin S, Bednarek DR, Oh YS. Computed tomography of the orbit. Critical Reviews in Diagnostic Imaging. 1981 Jan 1;15(1):27-93.
8. Allen RC. Orbital metastases: when to suspect? When to biopsy?. Middle East African Journal of Ophthalmology. 2018 Apr 1;25(2):60-4.
9. Alkatan H, Chaudhry I. Myeloid sarcoma of the orbit. Annals of Saudi Medicine. 2008 Nov 1;28(6):461.
10. Alongi F, Bolognesi A, Gajate AM, Motta M, Landoni C, Berardi G, Alongi P, Gianolli L, Di Muzio N. Inflammatory pseudotumor of mediastinum treated with tomotherapy and monitored with FDG-PET/CT: case report and literature review. Tumori Journal. 2010 Mar;96(2):322-6.
11. Angotti-Neto H, Cunha LP, Oliveira ÂV, Monteiro ML. Mesenchymal chondrosarcoma of the orbit. Ophthalmic Plastic & Reconstructive Surgery. 2006 Sep 1;22(5):378-82.
12. Ansari SA, Mafee MF. Orbital cavernous hemangioma: role of imaging. Neuroimaging Clinics. 2005 Feb 1;15(1):137-58.
13. Atlas SW, editor. Magnetic resonance imaging of the brain and spine. Lippincott Williams & Wilkins; 2009.
14. Ayoub E, Farid A, Yahya C, Meryem H, Youssef LA, Meriem B, Maâroufi M, Badreeddine A. Cavernous hemangioma of the orbit: Case report and a review of the literature. Radiology Case Reports. 2022 Nov 1;17(11):4104-7.

15. Baek CH, Chung MK, Jeong HS, Son YI, Choi J, Kim YD, Choi JY, Kim HJ, Ko YH. The clinical usefulness of 18F-FDG PET/CT for the evaluation of lymph node metastasis in periorbital malignancies. Korean Journal of Radiology. 2009 Feb 1;10(1):1-7.
16. Baker LL, Dillon WP, Hieshima GB, Dowd CF, Frieden IJ. Hemangiomas and vascular maltumors of the head and neck: MR characterization. American journal of neuroradiology. 1993 Mar 1;14(2):307-14.
17. Barnes L, editor. Pathology and genetics of head and neck tumours. IARC; 2005.
18. Becker M, Zaidi H. Imaging in head and neck squamous cell carcinoma: the potential role of PET/MRI. The British journal of radiology. 2014 Apr 1;87(1036):20130677.
19. Becker M, Masterson K, Delavelle J, Viallon M, Vargas MI, Becker CD. Imaging of the optic nerve. European journal of radiology. 2010 May 1;74(2):299-313.
20. Bilaniuk LT. Vascular lesions of the orbit in children. Neuroimaging Clinics. 2005 Feb 1;15(1):107-20.
21. Bisdorff AJ, Mulliken JB, Carrico J, Robertson RL, Burrows PE. Intracranial vascular anomalies in patients with periorbital lymphatic and lymphaticovenous maltumors. American Journal of Neuroradiology. 2007 Feb 1;28(2):335-41.
22. Bisdorff AJ, Mulliken JB, Carrico J, Robertson RL, Burrows PE. Intracranial vascular anomalies in patients with periorbital lymphatic and lymphaticovenous maltumors. American Journal of Neuroradiology. 2008 Feb 1;28(2):342-47.
23. Boitte JP, Traoré J, Boukhet F, Mondié JM, Traoré M, Delbosc B. Adenoid cystic carcinoma of the lacrimal gland in a 14-year-old girl. Journal Francais D'ophtalmologie. 2006 Oct 1;29(8):937-40.
24. Boulos PT, Dumont AS, Mandell JW, Jane JA. Meningiomas of the orbit: contemporary considerations. Neurosurgical focus. 2001 May 1;10(5):1-0.
25. Brush M, Zhang J, Schuetze S, Sires B. Angiosarcoma metastatic to the orbit. Ophthalmic Plastic & Reconstructive Surgery. 2006 Jan 1;22(1):62-4.
26. Cao Y, Tang X, Zan X, Li S. Benign optic nerve gliomas in an adult: A case report. Medicine. 2022 Aug 26;101(34):e30132.
27. Castillo M, Mukherji SK, Wagle NS. Imaging of the pediatric orbit. Neuroimaging Clinics of North America. 2000 Feb 1;10(1):95-116.
28. Cauley KA, Filippi CG. Diffusion-tensor imaging of small nerve bundles:

cranial nerves, peripheral nerves, distal spinal cord, and lumbar nerve roots—clinical applications. American journal of roentgenology. 2013 Aug;201(2):W326-35.
29. Chan-Kai BT, Yen MT. Combined positron emission tomography/computed tomography imaging of orbital lymphoma. American journal of ophthalmology. 2005 Sep 1;140(3):531-3.
30. Chaskes MB, Rabinowitz MR. Orbital schwannoma. Journal of Neurological Surgery Part B: Skull Base. 2020 Aug;81(04):376-80.
31. Chen Z, Zheng XH, Xie BJ, Yuan JJ, Yu HH, Li SH. Study on the growth of orbital volume in individuals at different ages by computed tomography. [Zhonghua yan ke za zhi] Chinese journal of ophthalmology. 2006 Mar 1;42(3):222-5.
32. Chen A, Hwang TN, Phan LT, McCulley TJ, Yoon MK. Long-term management of orbital and systemic reactive lymphoid hyperplasia with rituximab. Middle East African Journal of Ophthalmology. 2012 Oct 1;19(4):432-5.
33. Chung EM, Smirniotopoulos JG, Specht CS, Schroeder JW, Cube R. Pediatric orbit tumors and tumorlike lesions: nonosseous lesions of the extraocular orbit. Radiographics. 2007 Nov;27(6):1777-99.
34. Chung EM, Specht CS, Schroeder JW. Pediatric orbit tumors and tumorlike lesions: neuroepithelial lesions of the ocular globe and optic nerve. Radiographics. 2007 Jul;27(4):1159-86.
35. CHUNG EM, MURPHEY MD, SPECHT CS, CUBE R, SMIRNIOTOPOULOS JG. Pediatric orbit tumors and tumorlike lesions: osseous lesions of the orbit. Radiographics. 2008;28(4):1193-214
36. Chung EM, Murphey MD, Specht CS, Cube R, Smirniotopoulos J. From the archives of the AFIP pediatric orbit tumors and tumorlike lesions: osseous lesions of the orbit. Radiographics. 2008 Jul;28(4):1193-214.
37. Daniels DL, Haughton VM, Naidich TP. Cranial and spinal magnetic resonance imaging: an atlas and guide. Journal of Computer Assisted Tomography. 1988 May 1;12(3):541-2.
38. de Graaf PO, Pouwels PJ, Rodjan F, Moll AC, Imhof SM, Knol DL, Sanchez E, van der Valk P, Castelijns JA. Single-shot turbo spin-echo diffusion-weighted imaging for retinoblastoma: initial experience. American journal of neuroradiology. 2012 Jan 1;33(1):110-8.
39. Deike-Hofmann K, von Lampe P, Eerikaeinen M, Ting S, Schlüter S, Schlemmer HP, Bechrakis NE, Forsting M, Radbruch A. Anterior chamber enhancement predicts optic nerve infiltration in retinoblastoma. European radiology. 2022 Nov;32(11):7354-64.
40. Delmas J, Loustau JM, Martin S, Bourmault L, Adenis JP, Robert PY.

Comparative study of 3 exophthalmometers and computed tomographic biometry. European Journal of Ophthalmology. 2018 Mar;28(2):144-9.
41. Dimaras H, Kimani K, Dimba EA, Gronsdahl P, White A, Chan HS, Gallie BL. Retinoblastoma. The Lancet. 2012 Apr 14;379(9824):1436- 46.
42. Dimitrova G, Kato S. Color Doppler imaging of retinal diseases. Survey of ophthalmology. 2010 May 1;55(3):193-214.
43. Donnelly LF, Adams DM, Bisset III GS. Vascular maltumors and hemangiomas: a practical approach in a multidisciplinary clinic. American Journal of Roentgenology. 2000 Mar;174(3):597-608.
44. Dubois J, Garel L. Imaging and therapeutic approach of hemangiomas and vascular maltumors in the pediatric age group. Pediatric radiology. 1999 Nov;29:879-93.
45. Dunkel IJ, Chan HS, Jubran R, Chantada GL, Goldman S, Chintagumpala M, Khakoo Y, Abramson DH. High-dose chemotherapy with autologous hematopoietic stem cell rescue for stage 4B retinoblastoma. Pediatric Blood & Cancer. 2010 Jul 15;55(1):149-52.
46. Eldesouky MA, Elbakary MA. Clinical and imaging characteristics of orbital metastatic lesions among Egyptian patients. Clinical Ophthalmology. 2015 Sep 10:1683-7.
47. Eldesouky MA, Elbakary MA, Shalaby OE, Shareef MM. Orbital metastasis from hepatocellular carcinoma: report of 6 cases. Ophthalmic Plastic & Reconstructive Surgery. 2014 Jul 1;30(4):e78-82.
48. El-Ghafar AA, ElKhair HA. Evacuation of dermoid cysts before excision. Journal of the Egyptian Ophthalmological Society. 2013 Oct 1;106(4):235-8.
49. Elkhamary SM. Lacrimal gland lesions: Can addition of diffusion-weighted MR imaging improve diagnostic accuracy in characterization?. The Egyptian Journal of Radiology and Nuclear Medicine. 2012 Jun 1;43(2):165-72.
50. Erb-Eigner K, Willerding G, Taupitz M, Hamm B, Asbach P. Diffusion-weighted imaging of ocular melanoma. Investigative radiology. 2013 Oct 1;48(10):702-7.
51. Farazdaghi MK, Katowitz WR, Avery RA. Current treatment of optic nerve gliomas. Current opinion in Ophthalmology. 2019 Sep 1;30(5):356-63.
52. Fatima Z, Ichikawa T, Ishigame K, Motosugi U, Waqar AB, Hori M, Iijima H, Araki T. Orbital masses: the usefulness of diffusion-weighted imaging in lesion categorization. Clinical neuroradiology. 2014 Jun;24:129-34.

53. Ferrario VF, Sforza C, Ciusa V, Dellavia C, Tartaglia GM. The effect of sex and age on facial asymmetry in healthy subjects: a cross-sectional study from adolescence to mid-adulthood. Journal of Oral and Maxillofacial Surgery. 2001 Apr 1;59(4):382-8.
54. Ferrario VF, Sforza C, Colombo A, Schmitz JH, Serrao G. Morphometry of the orbital region: a soft-tissue study from adolescence to mid-adulthood. Plastic and Reconstructive Surgery. 2001 Aug 1;108(2):285-92.
55. Ferreira TA, Jaarsma-Coes MG, Marinkovic M, Verbist B, Verdijk RM, Jager MJ, Luyten GP, Beenakker JW. MR imaging characteristics of uveal melanoma with histopathological validation. Neuroradiology. 2022 Jan;64:171-84.
56. Holland D, Maune S, Kovács G, Behrendt S. Metastic tumors of the orbit: A retrospective study. Orbit. 2003 Jan 1;22(1):15-24.
57. Flanders AE, Espinosa GA, Markiewicz DA, Howell DD. Orbital lymphoma. Role of CT and MRI. Radiologic Clinics of North America. 1987 May 1;25(3):601-13.
58. Font RL, Smith SL, Bryan RG. Malignant epithelial tumors of the lacrimal gland: a clinicopathologic study of 21 cases. Archives of Ophthalmology. 1998 May 1;116(5):613-6.
59. Forbes G. Vascular lesions in the orbit. Neuroimaging Clinics of North America. 1996 Feb 1;6(1):113-22.
60. Foti PV, Travali M, Farina R, Palmucci S, Spatola C, Liardo RL, Milazzotto R, Raffaele L, Salamone V, Caltabiano R, Broggi G. Diagnostic methods and therapeutic options of uveal melanoma with emphasis on MR imaging—Part II: Treatment indications and complications. Insights into imaging. 2021 Dec;12:1-24.
61. Frieden IJ, Reese V, Cohen D. PHACE syndrome: the association of posterior fossa brain maltumors, hemangiomas, arterial anomalies, coarctation of the aorta and cardiac defects, and eye abnormalities. Archives of dermatology. 1996 Mar 1;132(3):307-11.
62. Friedrich RE, Bleckmann V. Adenoid cystic carcinoma of salivary and lacrimal gland origin: localization, classification, clinical pathological correlation, treatment results and long-term follow-up control in 84 patients. Anticancer research. 2003 Mar 1;23(2A):931-40.
63. Fries PD, Char DH, Norman D. MR imaging of orbital cavernous hemangioma. Journal of computer assisted tomography. 1987 May 1;11(3):418-21.
64. Galluzzi P, Hadjistilianou T, Cerase A, De Francesco S, Toti P, Venturi C. Is CT still useful in the study protocol of retinoblastoma?. American

journal of neuroradiology. 2009 Oct 1;30(9):1760-5.
65. Garrity JA. Metastatic carcinomas. Henderson's orbital tumors. New York: Raven Press. 2007:313-26.
66. Garrity JA. Henderson's Orbital Tumors. Lippincott Williams & Wilkins; 2007.
67. Garrity JA. Henderson's Orbital Tumors. Lippincott Williams & Wilkins; 2008.
68. Ginat DT, Mangla R, Yeaney G, Johnson M, Ekholm S. Diffusion-weighted imaging for differentiating benign from malignant skull lesions and correlation with cell density. American Journal of Roentgenology. 2012 Jun;198(6):W597-601.
69. Goh PS, Gi MT, Charlton A, Tan C, Sundar JG, Amrith S. Review of orbital imaging. European journal of radiology. 2008 Jun 1;66(3):387-95.
70. Goldberg RA, Rootman J, Cline RA. Tumors metastatic to the orbit: a changing picture. Survey of ophthalmology. 1990 Jul 1;35(1):1-24.
71. Graaf P, Göricke S, Rodjan F, Galluzzi P, Maeder P, Castelijns J, Brisse H. Guidelines for imaging retinoblastoma: imaging principles and MRI standardization. Pediatric Radiology. 2012 Jan 1;42(1).
72. Greene AK, Burrows PE, Smith L, Mulliken JB. Periorbital lymphatic maltumor: clinical course and management in 42 patients. Plastic and reconstructive surgery. 2005 Jan 1;115(1):22-30.
73. Greenwald MJ, Strauss LC. Treatment of intraocular retinoblastoma with carboplatin and etoposide chemotherapy. Ophthalmology. 1996 Dec 1;103(12):1989-97.
74. Gündüz AK, Yeşiltaş YS, Shields CL. Orbital tumors: A systematic review: Part II. Expert Review of Ophthalmology. 2015 Sep 3;10(5):485-508.
75. Gündüz K, Shields CL, Günalp I, Erden E, Shields JA. Orbital schwannoma: correlation of magnetic resonance imaging and pathologic findings. Graefe's archive for clinical and experimental ophthalmology. 2003 Jul;241:593-7.
76. Gupta M, Rennie IG. Orbital metastasis from a choroidal melanoma. Eye. 2005 Feb;19(2):227-9.
77. Gupta D, Garg P, Mittal A. Suppl-1, M7: Computed Tomography in Craniofacial Fibrous Dysplasia: A Case Series with Review of Literature and Classification Update. The open dentistry journal. 2017;11:384.
78. Gyldensted C, Lester J, Fledelius H. Computed tomography of orbital lesions: A radiological study of 144 cases. Neuroradiology. 1977 Jan;13:141-50.
79. Habermann CR, Arndt C, Graessner J, Diestel L, Petersen KU, Reitmeier

F, Ussmueller JO, Adam G, Jaehne M. Diffusion-weighted echo-planar MR imaging of primary parotid gland tumors: is a prediction of different histologic subtypes possible?. American journal of neuroradiology. 2009 Mar 1;30(3):591-6.

80. Haik BG, Karcioglu ZA, Gordon RA, Pechous BP. Capillary hemangioma (infantile periocular hemangioma). Survey of ophthalmology. 1994 Mar 1;38(5):399-426.
81. Haik BG, Jakobiec FA, Ellsworth RM, Jones IS. Capillary hemangioma of the lids and orbit: an analysis of the clinical features and therapeutic results in 101 cases. Ophthalmology. 1979 May 1;86(5):760-89.
82. Hajda M, Korányi K, Salomváry B, Bajcsay A. Clinical presentation, differential diagnosis and treatment of lacrimal gland tumours. Magyar Onkologia. 2005 May 18;49(1):65-70.
83. Harris GJ, Jakobiec FA. Cavernous hemangioma of the orbit. Journal of neurosurgery. 1979 Aug 1;51(2):219-28.
84. Hassan WM, Bakry MS, Hassan HM, Alfaar AS. Incidence of orbital, conjunctival and lacrimal gland malignant tumors in USA from Surveillance, Epidemiology and End Results, 1973-2009. International journal of ophthalmology. 2016;9(12):1808.
85. Hatton MP, Remulla HD, Tolentino MJ, Rubin PA. Clinical applications of color Doppler imaging in the management of orbital lesions. Ophthalmic Plastic & Reconstructive Surgery. 2002 Nov 1;18(6):462-5.
86. Héran F, Bergès O, Blustajn J, Boucenna M, Charbonneau F, Koskas P, Lafitte F, Nau E, Roux P, Sadik JC, Savatovsky J. Tumor pathology of the orbit. Diagnostic and interventional imaging. 2014 Oct 1;95(10):933-44.
87. Holden R, Damato BE. Preventable delays in the treatment of intraocular melanoma in the UK. Eye. 1996 Jan;10(1):127-9.
88. Hosten N, Schörner W, Zwicker C, Lietz A, Serke S, Huhn D, Felix R. Lymphozytäre Infiltrationen der Orbita in MRT und CT. InRöFo-Fortschritte auf dem Gebiet der Röntgenstrahlen und der bildgebenden Verfahren 1991 Nov (Vol. 155, No. 11, pp. 445-451). © Georg Thieme Verlag Stuttgart· New York.
89. Hou LC, Murphy MA, Tung GA. Primary orbital leiomyosarcoma: a case report with MRI findings. American journal of ophthalmology. 2003 Mar 1;135(3):408-10.
90. Hui KH, Pfeiffer ML, Esmaeli B. Value of positron emission tomography/computed tomography in diagnosis and staging of primary ocular and orbital tumors. Saudi Journal of Ophthalmology. 2012 Oct 1;26(4):365-71.

91. Iannetti G, Valentini V, Rinna C, Ventucci E, Marianetti TM. Ethmoido-orbital tumors: our experience. Journal of Craniofacial Surgery. 2005 Nov 1;16(6):1085-91.
92. Ismail M. Computed Tomographic Evaluation of Orbital Masses (Doctoral dissertation, Rajiv Gandhi University of Health Sciences (India)).
93. Issing PR, Ruh S, Kloss A, Kuske M, Lenarz T. Diagnostik und Therapie lymphoider Tumoren der Orbita. Hno. 1997 Jul;45:545-50.
94. Jacobson DM. Gliomas of the anterior visual pathways. Neurosurgery Clinics of North America. 1999 Oct 1;10(4):683-98.
95. Jacomb-Hood I, Moseley I. Orbital fibroin histiocytoma: CT in 10 cases and a review of radiological findings. Clin. Radiol. 1998;143(2):117.
96. Jiblawi A, Chanbour H, Tayba A, Khayat H, Jiblawi K. Magnetic resonance imaging diagnosis of choroidal melanoma. Cureus. 2021 Jul;13(7).
97. Jung WS, Ahn KJ, Park MR, Kim JY, Choi JJ, Kim BS, Hahn ST. The radiological spectrum of orbital pathologies that involve the lacrimal gland and the lacrimal fossa. Korean Journal of Radiology. 2007 Aug 1;8(4):336-42.
98. Kalapesi, F.B., Garrott, H.M., Moldovan, C., Williams, M., Ramanan, A. and Herbert, H.M., 2013. IgG4 orbital inflammation in a 5-year-old child presenting as an orbital mass. Orbit, 32(2), pp.137-140.
99. Kalender WA. Principles and applications of spiral CT. Nuclear medicine and biology. 1994 Jul 1;21(5):693-9.
100. Kanamalla US. The optic nerve tram-track sign. Radiology. 2003 Jun;227(3):718-9.
101. Karcioglu ZA, Hadjistilianou D, Rozans M, DeFrancesco S. Orbital rhabdomyosarcoma. Cancer Control. 2004 Sep;11(5):328-33.
102. Karim S, Clark RA, Poukens V, Demer JL. Demonstration of systematic variation in human intraorbital optic nerve size by quantitative magnetic resonance imaging and histology. Investigative ophthalmology & visual science. 2004 Apr 1;45(4):1047-51.
103. Katsumata A, Fujishita M, Maeda M, Ariji Y, Ariji E, Langlais RP. 3D-CT evaluation of facial asymmetry. Oral Surgery, Oral Medicine, Oral Pathology, Oral Radiology, and Endodontology. 2005 Feb 1;99(2):212-20.
104. Kapur R, Sepahdari AR, Mafee MF, Putterman AM, Aakalu V, Wendel LJ, Setabutr P. MR imaging of orbital inflammatory syndrome, orbital cellulitis, and orbital lymphoid lesions: the role of diffusion-weighted imaging. American Journal of Neuroradiology. 2009 Jan 1;30(1):64-70.

105. Kavanagh EC, Heran MK, Peleg A, Rootman J. Imaging of the natural history of an orbital capillary hemangioma. Orbit. 2006 Jan 1;25(1):69-72.124. Kincaid M.C. Uveal melanoma. // Cancer control J.- 2008.-5(4).-P.675-703.
106. Kerdoud O, Aloua R, Belem O, Hmoura Z, Slimani F. Dumbbell-shaped dermoid cyst of the orbit: Case report. Advances in Oral and Maxillofacial Surgery. 2021 Jul 1;3:100135.
107. Kingston JE, Hungerford JL, Madreperla SA, Plowman PN. Results of combined chemotherapy and radiotherapy for advanced intraocular retinoblastoma. Archives of Ophthalmology. 1996 Nov 1;114(11):1339-43.
108. Khan MH, Haque S, Yagi K, Takinami S, Khan SH, Ohmori K, Nishioka T. Pattern of local relapse of maxillary sinus carcinoma. Mymensingh Medical Journal: MMJ. 2006 Jul 1;15(2):188-91.
109. Khan SN, Sepahdari AR. Orbital masses: CT and MRI of common vascular lesions, benign tumors, and malignancies. Saudi Journal of Ophthalmology. 2012 Oct 1;26(4):373-83.
110. Kim E, Kim HJ, Kim YD, Woo KI, Lee H, Kim ST. Subconjunctival fat prolapse and dermolipoma of the orbit: differentiation on CT and MR imaging. American journal of neuroradiology. 2011 Mar 1;32(3):465-7.
111. Kodsi SR, Shetlar DJ, Campbell RJ, Garrity JA, Bartley GB. A review of 340 orbital tumors in children during a 60-year period. American journal of ophthalmology. 1994 Feb 1;117(2):177-82.
112. Krantz BA, Dave N, Komatsubara KM, Marr BP, Carvajal RD. Uveal melanoma: epidemiology, etiology, and treatment of primary disease. Clinical ophthalmology. 2017 Jan 31:279-89.
113. Kurli M, Reddy S, Tena LB, Pavlick AC, Finger PT. Whole body positron emission tomography/computed tomography staging of metastatic choroidal melanoma. American journal of ophthalmology. 2005 Aug 1;140(2):193-e1.
114. La Rocca M, Leonardi BF, Lo Greco MC, Marano G, Finocchiaro I, Iudica A, Milazzotto R, Liardo RL, La Monaca VA, Salamone V, Basile A. Radiotherapy of Orbital and Ocular Adnexa Lymphoma: Literature Review and University of Catania Experience. Cancers. 2023 Dec 10;15(24):5782.
115. Lee JS, Lim DW, Lee SH, Oum BS, Kim HJ, Lee HJ. Normative measurements of Korean orbital structures revealed by computerized tomography. Acta Ophthalmologica Scandinavica. 2001 Apr;79(2):197-200.
116. Lee AG, Johnson MC, Policeni BA, Smoker WR. Imaging for neuro-

ophthalmic and orbital disease–a review. Clinical & experimental ophthalmology. 2009 Jan;37(1):30-53.
117. Lemke AJ, Kazi I, Felix R. Magnetic resonance imaging of orbital tumors. European radiology. 2006 Oct;16:2207-19.
118. Lemke AJ, Hosten N, Bornfeld N, Bechrakis NE, Schüler A, Richter M, Stroszczynski C, Felix R. Uveal melanoma: correlation of histopathologic and radiologic findings by using thin-section MR imaging with a surface coil. Radiology. 1999 Mar;210(3):775-83.
119. Lin LK, Andreoli CM, Hatton MP, Rubin PA. Recognizing the protruding eye. Orbit. 2008 Jan 1;27(5):350-5.
120. Lin J, Zhao H, Yang Z, Wang Y, Zhang L. Clinicopathologic characteristics of angioleiomyoma of the eyelids and orbit. [Zhonghua yan ke za Zhi] Chinese Journal of Ophthalmology. 2015 Aug 1;51(8):586-91.
121. Lober RM, Guzman R, Cheshier SH, Fredrick DR, Edwards MS, Yeom KW. Application of diffusion tensor tractography in pediatric optic pathway glioma. Journal of Neurosurgery: Pediatrics. 2012 Oct 1;10(4):273-80.
122. Lope LA, Hutcheson KA, Khademian ZP. Magnetic resonance imaging in the analysis of pediatric orbital tumors: utility of diffusion-weighted imaging. Journal of American Association for Pediatric Ophthalmology and Strabismus. 2010 Jun 1;14(3):257-62.
123. Madabhavi I, Sandeep KS, Lethika RD, Tumbal S, Miskin AT, Sarkar M, Modi M. Intraconal metastasis leading to diagnosis of hepatocellular carcinoma. Middle East Journal of Digestive Diseases. 2020 Jan;12(1):48.
124. Mafee MF, Pai E, Philip B. Rhabdomyosarcoma of the orbit: evaluation with MR imaging and CT. Radiologic Clinics of North America. 1998 Nov 1;36(6):1215-27.
125. Mafee MF, Goodwin J, Dorodi S. Optic nerve sheath meningiomas: role of MR imaging. Radiologic Clinics of North America. 1999 Jan 1;37(1):37-58.
126. Mafee MF, Putterman A, Valvassori GE, Campos M, Capek V. Orbital space-occupying lesions: role of computed tomography and magnetic resonance imaging: an analysis of 145 cases. Radiologic Clinics of North America. 1987 May 1;25(3):529-59.
127. Mafee MF, Edward DP, Koeller KK, Dorodi S. Lacrimal gland tumors and simulating lesions: clinicopathologic and MR imaging features. Radiologic clinics of North America. 1999 Jan 1;37(1):219-39.
128. Mafee MF, Inoue Y, Mafee RF. Ocular and orbital imaging. Neuroimaging Clinics of North America. 1996 May 1;6(2):291-318.

129. Mardin C. Kucule M., Naumann G. Klinish uniwartete maligne Melanome der Uvea //Klin. Mbl. Augenheilk. 2007(1):18-121.
130. Martin M, Zierhut D, Piroth M, Gutwein S, Debus J, Dithmar S. Solitary iris metastasis from breast cancer: Effective local therapy with electron beam irradiation. Der Ophthalmologe. 2006 Jan;103:48-51.
131. McCaffery S, Simon EM, Fischbein NJ, Rowley HA, Shimikawa A, Lin S, O'Brien JM. Three-dimensional high-resolution magnetic resonance imaging of ocular and orbital malignancies. Archives of Ophthalmology. 2002 Jun 1;120(6):747-54.
132. McCartney AC. Pathology of ocular melanomas. British medical bulletin. 1995 Jan 1;51(3):678-93.
133. McCaffery S, Simon EM, Fischbein NJ, Rowley HA, Shimikawa A, Lin S, O'Brien JM. Three-dimensional high-resolution magnetic resonance imaging of ocular and orbital malignancies. Archives of Ophthalmology. 2003 Jun 1;120(6):747-54.
134. Miller NR. Primary tumours of the optic nerve and its sheath. Eye. 2004 Nov;18(11):1026-37.
135. Miller NR. Primary tumours of the optic nerve and its sheath. Eye. 2004 Nov;18(11):10386-48.
136. Miyamoto J, Tatsuzawa K, Owada K, Kawabe T, Sasajima H, Mineura K. Usefulness and limitations of fluorine-18-fluorodeoxyglucose positron emission tomography for the detection of malignancy of orbital tumors. Neurologia medico-chirurgica. 2008;48(11):495-9.
137. Mncube SS, Goodier MD. Normal measurements of the optic nerve, optic nerve sheath and optic chiasm in the adult population. SA Journal of Radiology. 2019;23(1):1-7.
138. Mombaerts I, Ramberg I, Coupland SE, Heegaard S. Diagnosis of orbital mass lesions: clinical, radiological, and pathological recommendations. survey of ophthalmology. 2019 Nov 1;64(6):741-56.
139. Motoori K, Yamamoto S, Ueda T, Nakano K, Muto T, Nagai Y, Ikeda M, Funatsu H, Ito H. Inter-and intratumoral variability in magnetic resonance imaging of pleomorphic adenoma: an attempt to interpret the variable magnetic resonance findings. Journal of computer assisted tomography. 2004 Mar 1;28(2):233-46.
140. Mulliken JB, Glowacki J. Hemangiomas and vascular maltumors in infants and children: a classification based on endothelial characteristics. Plastic and reconstructive surgery. 1982 Mar 1;69(3):412-20.
141. Murdock N, Mahan M, Chou E. Benign orbital tumors.
142. Muzaffar R, Shousha MA, Sarajlic L, Osman MM. Ophthalmologic abnormalities on FDG-PET/CT: a pictorial essay. Cancer Imaging.

2013;13(1):100.
143. Naggara O, Koskas P, Lafitte F, Heran F, Piekarski JD, Meder JF, Berges O. Vascular tumours and maltumor of the orbit. Journal de radiologie. 2006 Jan 1;87(1):17-27.
144. Neubauer H, Evangelista L, Hassold N, Winkler B, Schlegel PG, Köstler H, Hahn D, Beer M. Diffusion-weighted MRI for detection and differentiation of musculoskeletal tumorous and tumor-like lesions in pediatric patients. World journal of pediatrics. 2012 Nov;8:342-9.
145. Newman SA. Orbital surgery: evolution and revolution. Journal of Neurological Surgery Part B: Skull Base. 2021 Feb;82(01):007-19.
146. Nguyen VD, Singh AK, Altmeyer WB, Tantiwongkosi B. Demystifying orbital emergencies: a pictorial review. Radiographics. 2017 May;37(3):947-62.
147. Nilson L.F., Luis P., Deise M.N., Maria T.S. Orbital granulocytic sarcoma: case report. Arq.Bras. Oftalmol. 2005 Nov; 4:26-28.
148. Norregaard JC, Gerner N, Jensen OA, Prause JU. Malignant melanoma of the conjunctiva: occurrence and survival following surgery and radiotherapy in a Danish population. Graefe's archive for clinical and experimental ophthalmology. 1996 Sep;234:569-72.
149. Ohtsuka K, Hashimoto M, Suzuki Y. A review of 244 orbital tumors in Japanese patients during a 21-year period: origins and locations. Japanese journal of ophthalmology. 2005 Jan;49:49-55.
150. Orjuela M, Castaneda VP, Ridaura C, Lecona E, Leal C, Abramson DH, Orlow I, Gerald W, Cordon-Cardo C. Presence of human papilloma virus in tumor tissue from children with retinoblastoma: an alternative mechanism for tumor development. Clinical cancer research. 2000 Oct 1;6(10):4010-6.
151. Olsen TG, Heegaard S. Orbital lymphoma. Survey of ophthalmology. 2019 Jan 1;64(1):45-66.
152. Oohira A, Kubo R. Ocular blood flow defect in gaze-evoked amaurosis. Japanese Journal of Ophthalmology. 1999 Jul 1;43(4):336.
153. Orbit E. Lacrimal System: Basic and Clinical Science Course. American Academy of Ophthalmology The Eye MD Association. 2004;7:331.
154. Ozgen A, Ariyurek M. Normative measurements of orbital structures using CT. AJR. American journal of roentgenology. 1998 Apr;170(4):1093-6.
155. Pakdaman MN, Sepahdari AR, Elkhamary SM. Orbital inflammatory disease: Pictorial review and differential diagnosis. World Journal of Radiology. 2014 Apr 4;6(4):106.
156. Patnana M, Sevrukov AB, Elsayes KM, Viswanathan C, Lubner M,

Menias CO. Inflammatory pseudotumor: the great mimicker. American Journal of Roentgenology. 2012 Mar;198(3):W217-27.
157. Pappas A, Araque JM, Sarup V. Orbital Venous Varices: A Rare Bilateral Asymptomatic Presentation, Cureus. 2018 Sep 14;10(9):e3302.
158. Park WC, White WA, Woog JJ, Garrity JA, Kim YD, Lane J, Witte R, Babovic-Vuksanovic D. The role of high-resolution computed tomography and magnetic resonance imaging in the evaluation of isolated orbital neurofibromas. American journal of ophthalmology. 2006 Sep 1;142(3):456-63.
159. Patel BC, De Jesus O, Margolin E. Optic nerve sheath meningioma.
160. Politi LS, Forghani R, Godi C, Resti AG, Ponzoni M, Bianchi S, Iadanza A, Ambrosi A, Falini A, Ferreri AJ, Curtin HD. Ocular adnexal lymphoma: diffusion-weighted MR imaging for differential diagnosis and therapeutic monitoring. Radiology. 2010 Aug;256(2):565-74.
161. Mirian Getsadze, Sofia Chedia. Study of orbital neoplasms by Magnetic Resonance Imaging procedure. GEORGIA MEDICAL NEWS, ТБИЛИСИ - NEW YORK, SCKOPUS, ISSN 1512-0112, Submission URL, Issue, 10 /335. 2024, p 226-235, https://www.geomednews.com/Articles/2024/10_2024/225-233.pdf ,
162. Mirian Getsadze. Magnetic Resonance Imaging Procedure In The Study Of Neoplasms Of The Eye And Orbit. IOSR Journal of Dentali and Medical Sciences e-ISSN 2275-0853, p-ISSN: 2279-0861, DOI: 10.9790/0853-2309091525, Issue, 23/ 09, 2024,p 15-24 https://www.iosrjournals.org/iosr-jdms/pages/23(9)Series-9.html www.submitpapersnow.com
163. Mirian Getsadze, Results Of The Study Of Brain Metabolism In Patients With Multiple Sclerosis According To H-MRS Data, IOSR Journal of Dentali and Medical Sciences ISSN 2279-0853, p-ISSN: 2279-0861,DOI 10.9790/0853-2208075564, 8, 7, 2023 p55-64
164. Mirian Getsadze, OT FINDNGS IN PATIENTS WITH COVID-19 PNEUMONIA, Issue. Warsaw, POLISH SCIENCE JOURNAL, Issue, 8(53), 2022, p 47-51 https://sciencecentrum.pl/wp-ntent/uploads/2022/11/POLISH%20SCIENCE%20JOURNAL%2053%20%28web%29.pdf
165. Mirian Getsadze, MORPHOMETRIC DATA FROM MRI STUDY IN PATIENTS WITH RRMS, Issue. Warsaw, POLISH SCIENCE JOURNAL, Issue, 5(61), 2023, p 17-21. https://sciencecentrum.pl/wp-content/uploads/2022/09/polish-science-journal-51-web-1.jpg
166. Mirian Getsadze, COMPLEX RADIOLOGICAL DIAGNOSIS OF ORBITAL TUMORS (LITERATURE REVIEW). Issue. Warsaw,

POLISH SCIENCE JOURNAL, Issue, 10(66), 2023 p11-15
https://sciencecentrum.pl/wpcontent/uploads/2023/12/POLISH%20SCIENCE%20JOURNAL%2066%20%28web%29.pdf

167. Mirian Getsadze, DIAGNOSIS OF PRIMARY NEOPLASMS OF THE ORBIT BY THE METHOD OF ULTRASOUND EXAMINATION. POLISH SCIENCE JOURNAL, Warsaw, Issue, 4(70), 2024, p 31-39
https://sciencecentrum.pl/wp-content/uploads/2024/04/POLISH%20SCIENCE%20JOURNAL%2070%20%28web%29.pdf
168. Mirian Getsadze, Study of neoplasms of the eye and orbit by computed tomography method, EXPERIMENTAL AND CLINICAL MEDICCINE, ISSN1512-0392 E-ISSN2667-9736, DOI, GEORGIA, Issue 5, 2024, p 31-35
https://journals.4science.ge/index.php/jecm/issue/view/174/161

**CONTENTS**

**MONOGRAPH**

Mirian Getsadze

# THE ROLE OF MODERN RADIOLOGICAL IMAGING IN THE DIAGNOSIS OF ORBITAL TUMORS

Subscribe to print 05/05/2026. Format 60×90/16.
Edition of 300 copies.
Printed by “iScience” Sp. z o. o.
Warsaw, Poland
08-444, str. Grzybowska, 87
info@sciencecentrum.pl, https://sciencecentrum.pl

This work is devoted to studying the enhancement of diagnostic and differential diagnostic effectiveness of orbital and ocular neoplasms through the complex application of modern instrumental-diagnostic methods.

The monograph discusses the main instrumental methods of research – orbital ultrasonography, computed tomography (CT), and magnetic resonance imaging (MRI) – which make it possible to determine the size and spread of tumors, as well as to assess the soft tissues and bony structures of the orbit.

The monograph is intended for physicians working in the field of radiology, as well as medical Bachelor and Master students.

ISBN 978-83-68188-49-3